A TRIDENT SCHOLAR PROJECT REPORT

NO. 277

DEVELOPMENT OF A SEMI-EMPIRICAL MODEL FOR SEUs IN MODERN DRAMs

UNITED STATES NAVAL ACADEMY
ANNAPOLIS, MARYLAND

REPORT DOCUMENTATION PAGE

Form Approved
OMB No. 074-0188

1. AGENCY USE ONLY (Leave blank)	2. REPORT DATE	3. REPORT TYPE AND DATE COVERED
	8 May 2000	

4. TITLE AND SUBTITLE
Development of a semi-empirical model for SEUs in modern DRAMs

5. FUNDING NUMBERS

6. AUTHOR(S)
Sarlese, Justin A.

7. PERFORMING ORGANIZATION NAME(S) AND ADDRESS(ES)
U.S. Naval Academy
Annapolis, MD

8. PERFORMING ORGANIZATION REPORT NUMBER
USNA Trident Scholar project report no. 277 (2000)

9. SPONSORING/MONITORING AGENCY NAME(S) AND ADDRESS(ES)

10. SPONSORING/MONITORING AGENCY REPORT NUMBER

11. SUPPLEMENTARY NOTES
Accepted by the U.S. Trident Scholar Committee

12a. DISTRIBUTION/AVAILABILITY STATEMENT
This document has been approved for public release; its distribution is UNLIMITED.

12b. DISTRIBUTION CODE

13. ABSTRACT: Studies have found that the passage of a charged particle through a dynamic random access memory (DRAM) can cause a bit flip (1 to 0 or 0 to 1), also referred to as a *single event upset* (SEU). This is more noticeable in newer, denser computer systems which contain much more DRAM memory and, as a result, are more sensitive to radiation. SEUs are also more common at higher altitudes, where the neutron and proton fluxes were found to be as much as several hundred times greater than at sea level. For this reason, IBM, Boeing, the Department of Defense, and other government and commercial organizations have performed numerous studies on the phenomenon aimed at reducing the SEU effect in aircraft, missiles, and satellites which use DRAMs. Many of the previous models developed to characterize the SEU are not applicable to modern high-density chips. This project has developed a new and improved model which applied to the higher density chips and is based on particle energy, particle flux, and SEU cross-section data taken from a wide range of experiments. This study also identifies the nuclear reactions, chip characteristics, and particle environments which affect a DRAM's SEU rate. From this model, the soft error rates (SERs) of various commercial off-the-shelf (COTS) DRAMs were calculated at various altitudes, latitudes, and longitudes. These rates were used to identify which DRAMs were the most and least sensitive to radiation. Those DRAMs with lowest expected SEU rates will be more reliable in aircraft systems while those with the highest expected SEU rates can potentially be used in the development of a smaller lightweight neutron detection system.

14. SUBJECT TERMS
single event upset, soft error rate, atmospheric particle flux, dynamic random access memory

15. NUMBER OF PAGES

16. PRICE CODE

17. SECURITY CLASSIFICATION OF REPORT	18. SECURITY CLASSIFICATION OF THIS PAGE	19. SECURITY CLASSIFICATION OF ABSTRACT	20. LIMITATION OF ABSTRACT

U.S.N.A.---Trident Scholar project report; no. 277 (2000)

DEVELOPMENT OF A SEMI-EMPIRICAL MODEL FOR SEUs IN MODERN DRAMs

by

Midshipman Justin A. Sarlese, Class of 2000
United States Naval Academy
Annapolis, MD

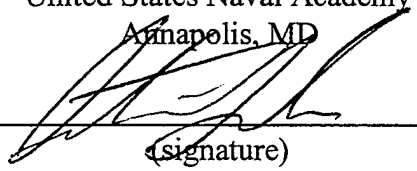

(signature)

Certification of Adviser Approval

Professor Martin E. Nelson
Department of Naval Architecture, Ocean, and Marine Engineering

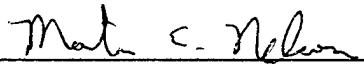

(signature)

Acceptance for the Trident Scholar Committee

Professor Joyce E. Shade
Chair, Trident Scholar Committee

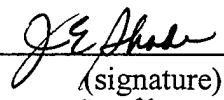

(signature)

8 May 2000

(date)

Abstract

Studies have found that the passage of a charged particle through a dynamic random access memory (DRAM) can cause a bit flip ($1\rightarrow0$ or $0\rightarrow1$), also referred to as a *single event upset* (SEU). This is more noticeable in newer, denser computer systems which contain much more DRAM memory and, as a result, are more sensitive to radiation. SEUs are also more common at higher altitudes, where the neutron and proton fluxes were found to be as much as several hundred times greater than at sea level. For this reason IBM, Boeing, the Department of Defense, and other government and commercial organizations have performed numerous studies on the phenomenon aimed at reducing the SEU effect in aircraft, missiles, and satellites which use DRAMs.

Many of the previous models developed to characterize the SEU are not applicable to modern high density chips. This project has developed a new and improved model which applies to the higher density chips and is based on particle energy, particle flux, and SEU cross-section data taken from a wide range of experiments.

This study also identifies the nuclear reactions, chip characteristics, and particle environments which affect a DRAM's SEU rate. From this model, the soft error rates (SERs) of various commercial off-the-shelf (COTS) DRAMs were calculated at various altitudes, latitudes, and longitudes. These rates were used to identify which DRAMs were the most and least sensitive to radiation. Those DRAMs with the lowest expected SEU rates will be more reliable in aircraft systems while those with the highest expected SEU rates can potentially be used in the development of a smaller lightweight neutron detection system.

Keywords: Single Event Upset, Soft Error Rate, Atmospheric Particle Flux, Dynamic Random Access Memory

Acknowledgments

This trident project consisted mainly of theoretical modeling; consequently, it depended mostly upon the experimental data taken by others and theories previously developed by experts in the field. This project wouldn't have been possible without the assistance and information received from scientists willing to advance the world of knowledge.

Dr. James Ziegler of IBM contributed the experimental data necessary for determining the radiation sensitivity of various COTS DRAMs. His flux model and his one-on-one instructional periods were informative. Visual aids for my Trident presentation were also provided by him. Dr. Art Cambell and Dr. Allan Tylka from NRL also provided valuable information. Their models provided important data and concepts for my modeling. Dr. Petersen from the the University of Colorado also provided me with useful experimental data. Dr. Eugene Normand of Boeing also provided a model which served as a valuable reference. Michael Gibbons provided technical support, constructing the experimental apparatus.

The experimental data provided would not have existed without the resources provided by Triangle University Meson Facility and Harvard Cyclotron Laboratory.

The idea for this project came from my advisor, Professor Martin Nelson whose imagination and ingenuity provided the ideas which got this project going and kept it going. His assistance and scientific advice were very helpful. I learned much from him.

TABLE OF CONTENTS

List of Symbols and Abbreviation

SEU	Single Event Upset
DRAM	Dynamic Random Access Memory
SER	Soft Error Rate (fails/s and fails/hr)
SER_{tested}	Soft Error Rate of an experimentally tested DRAM (fails/s and fails/hr)
$SER_{untested}$	Soft Error Rate of DRAM not experimentally tested(fails/s and fails/hr)
COTS	Commercial-over-the-Shelf
NRL	Naval Research Laboratory
CREME	*Cosmic Ray Effects on Microelectronics*
Φ_{USNA}	USNA Particle Flux Model
dJ/dE	Differential Particle Flux Energy Spectrum (particles/cm^2-MeV-s)
$d\Phi/dE$	Normalized Differential Particle Flux Energy Spectrum (particles/cm^2-MeV-s)
E	Energy (MeV)
$\hat{S}(X,a,b)$	Exponential Step Function as a function of the independent variable X and the fitting parameters a and b
G	Geomagnetic Cutoff (GV)
RIG	Geomagnetic Cutoff at altitude of 20km (GV)
LAT	Geographic Northerly Latitude (°)
LONG	Geographic Easterly Longitude (°)
ALT	Altitude (ft)
P	Atmospheric Pressure (g/cm^2)
Φ	Particle Flux (particles/cm^{2}s and nucleons/cm^{2}s)
F_0	Relative Particle Flux at reference location with respect to New York City (dimensionless)
F	Particle Flux at location of interest (particles/cm^{2}s)
L	Attenuation Factor (g/cm^2)
F_{IBM}	Particle Flux obtained using information from IBM model(particles/cm^{2}s)
Φ_{NRL}	Particle Flux obtained using information from NRL CREME model(particles/cm^{2}s)
Φ_T	Particle Flux obtained from combination of IBM and NRL CREME models(particles/cm^{2}s)

Φ_0	Particle Flux expected to make it to a location based on geomagnetic cutoff (particles/cm^{2}s)
Ω	Solid angle (steradians)
T	Percentage Transmission of particles to a specific location based on atmospheric pressure
S_1	First solar factor based on time of day
S_2	Second Solar Factor based on 11.9 year solar cycle
s	second
m	minute
h	hour
M	month
y	year
A, B, C, D, E, F	DRAM vendors
σ	cross-section (cm^2)
$\sigma_{hv}(E)$	heating value cross-section in silicon for neutrons and protons of energy E (MeVcm^2/atom)
$\sigma_{SEU}(E)$	SEU cross-section for neutrons and protons of energy E (10^{-15}cm^2 fails/bit)
$\sigma'_{SEU}(E)$	Shell's SEU cross-section for neutrons and protons of energy E (10^{-15}cm^2 fails/bit)
$\sigma^{\pi}_{SEU}(E)$	SEU cross-section for pions of energy E (10^{-15}cm^2 fails/bit)
α, β	logarithmic fitting parameters for proton and neutron SEU cross-section spectra
α', β'	logarithmic fitting parameters for pion SEU cross-section spectra
V_{dd}	DRAM operating voltage (V)
f	DRAM operating frequency (MHz)
A′	DRAM surface area (cm^2)
$F(E_i\ E_{i+1})$	Fraction of the total particle flux between energies E_i and E_{i+1}
N	Number of memory bits (bits)
Q	Threshold energy for a nuclear reaction(MeV)
γ	gamma ray
RP	Relative Probability a reaction will occur

Chapter I - Introduction

Years of research and bad experiences have shown that when a heavy charged particle or nucleon (proton or neutron) passes through a computer chip, there is a small possibility it will interact with an atomic nucleus in the chip (usually silicon) and produce charged ions. These ions may physically damage the chip or deposit charge in one of the chip's capacitors or transistors and result in a bit flip ($1 \rightarrow 0$ or $0 \rightarrow 1$). The latter effect is of greater concern, because it happens much more frequently [1]. It is referred to as a *single event upset* (SEU). This project dealt with the study of SEUs in dynamic random access memories (DRAMs), the fastest, densest chips which have more memory bits than any other type of chip in the computer industry and use capacitors to store their memory.

The consequences of an SEU can range from negligible to critical depending upon the electronic system involved and the process the electronic system is carrying out. Some of these consequences are shown below in Table 1.1 [2].

Table 1.1 - The events which can occur in a computer system as a result of an SEU

Possible Consequences of a Single Event Upset
- Nothing
- Cause chip latchup
- Cause chip burnout
- Change information in memory cell
- Change processing in logic system
- Corrupt database
- Cause parity error
- Cause incorrect calculations

For these reasons, SEUs have posed problems for the aircraft, space, defense, communications, and computer industries for years. In 1975, for example, Hughes Aircraft Company published a paper mentioning "anomalies...caused by the unexpected triggering of digital circuits " in a few of their satellite electronic systems. Later studies would conclude that galactic cosmic rays had caused what at that time were referred to as *electronic upsets* and would later be called *SEUs* in the satellite electronic systems [3]. Three years later some Intel engineers published an article mentioning the fact that the new 16Kb chips they was placing in their new long distance phones were only lasting 20 minutes before crashing. Later studies concluded that alpha particles produced in the ceramic chip caps were causing SEUs in the chips and causing them to fail [4]. In 1996 Micron Technology suddenly began having trouble with the chips they were producing. A thorough investigation concluded that the phosphorus used in the chip's aluminum etching process was coming from an old uranium mine. The phosphorus was slightly radioactive, making the aluminum in the chips slightly radioactive and causing SEUs in these chips [5].

Events like these may occur more often in the future, especially in the military and with NASA. This is because these organizations are switching over from the older radiation hardened DRAMs to the newer, commercial-off-the-shelf (COTS) DRAMs which are smaller, faster, and cost less. At the same time, as information systems become more advanced each year, they require more DRAM memory which means they have

more memory bits and, as a result, are more susceptible to SEUs. For this reason, one must now have a basic knowledge and understanding of various DRAMs' susceptibility to SEUs before using them in a radiation environment. This is the case in missiles and aircraft, for example, which operate in areas with particle fluxes up to hundreds of times more intense than sea-level particle fluxes [1] and employ the use of more advanced DRAM systems every couple years.

Many industries have developed models for determining the rates at which SEUs occur, referred to as the *soft error rates* (SERs[1]), for various DRAMs. Unfortunately, many of these models are too case specific to be useful; some of them are not available to the public; and most of them are not applicable to the newer modern DRAMs. The primary objective of this project was to develop a new model which applies to the newer DRAMs, applies to a broader range of cases, and is simple to use. Many of these older models include studies of the electronic systems in a DRAM, but the model developed in this project does not. The model developed here can calculate the SERs of many of the newer 64Mb COTS DRAMs at various locations in the earth's atmosphere at various times and can also be used to compare the SEU susceptibility of different COTS DRAMs, given the SER of a related DRAM.

In order to calculate the SER of a particular DRAM, the particle flux[2] environment of the DRAM must first be known. Thus, a particle flux model for calculating the particle flux at various latitudes, longitudes, altitudes, and times was developed (Chapter II) by combining published models from industry and government. Calculating the SER for a DRAM also requires information on the sensitivity of the DRAM to radiation. In order to determine this, experimental SEU cross-section data on a number of DRAMs from a number of sources was extrapolated and interpolated to determine the SEU cross-sections at various energies for those DRAMs (Chapter III). In order to determine the SERs of a wide range of DRAMs, the relationships between the SERs of experimentally tested DRAMs and the SERs of untested DRAMs must be determined. In order to deal with this, a literature and model search was performed to determine how particular chip characteristics can affect the SER of a DRAM (Chapter IV). The information and equations obtained from these three steps were then combined into a comprehensive model and used to calculate and compare the SERs of various COTS DRAMs at various locations in the world (Chapter V).

Understanding more about what happens in a DRAM when an SEU occurs would be useful to a DRAM developer who intends to reduce the SEU susceptibility. For this reason, a literature search was done in order to determine the major initial nuclear reactions that occur inside a DRAM when it is bombarded with heavy charged particles or nucleons. A few calculations were also made to determine which reactions are the most likely to occur (Chapter VI). Knowing which elements in DRAMs react the most with heavy charged particles or nucleons may be useful for determining which are most responsible for SEUs.

Knowing which DRAMs are the most and the least susceptible to SEUs would

---

[1] Soft Error Rates are usually given in units of fails/hr.

[2] Flux is defined as the number of incident particles/cm^{2}s.

also be useful. The DRAMs with the highest SERs could possibly be used for the development of a smaller, lighter radiation detection system [6]. On the other hand, the DRAMs with the lowest SERs may be safer for aircraft and missile systems. Therefore, the five most susceptible and the five least susceptible DRAMs were determined (Chapter VII). Appendix A gives a flow chart of the project which shows the main steps and their relationship to each other. Finally, the conclusions and recommendations for further study are given in chapter VIII.

CHAPTER II - The Particle Flux Model

Before the SER of a DRAM can be calculated, the particle flux environment of the DRAM must be determined. This project is only concerned with the natural particle environment found in the earth's atmosphere caused by the shower of particles from outer space. Many models have been created to calculate this, but very few have been published and most of them are too specific, tailored for the needs of a particular corporation/institution. The most noteworthy published models are the four created by IBM, Boeing, NASA, and NRL.

IBM's model, *Terrestrial Cosmic Ray Intensities* [7,8], computes the particle[3] fluxes above major cities up to an altitude of approximately 30,000ft. Boeing has developed a model, *Single Event Effects in Avionics* [9], which calculates the low energy neutron flux at 35,000ft. NASA's model, *Altitude and Latitude Variations in Avionics SEU and Atmospheric Neutron Flux* [10], computes the low energy neutron flux up to approximately 50,000 ft. Naval Research Laboratory (NRL) has developed a model, *Cosmic Ray Effects on Microelectronics* (CREME) [11,12,13,14], which calculates the proton and heavy ion fluxes between satellite orbit altitudes and approximately 100,000ft. None of these models by itself has enough information for calculating the particle flux energy spectrum at any location in the earth's atmosphere, at any time. This project developed a newer model for calculating this which from now on will be referred to as the USNA flux model, or Φ_{USNA}, by combining the first and last models together.

A. The Atmospheric Particle Flux

Particle fluxes in the earth's atmosphere exist as the by-product of cosmic rays[4] from the sun and from deep space. These cosmic rays are mainly composed of protons and collide with nitrogen and oxygen in the upper atmosphere, resulting in a cosmic ray shower of electrons, muons[5], neutrons, pions[6], and additional protons [7,8]. Electrons and muons rarely induce SEUs because of their low energy deposition rate per unit pathlength in silicon; therefore, they will be neglected in this study. At very high altitudes, protons are the main source of SEUs. At lower altitudes (60,000 to 40,000ft), as more and more protons are either absorbed or involved in collisions and more pions and neutrons are produced, pions and neutrons become the main source of SEUs. At even lower altitudes (40,000ft to ~sea level), as pions are absorbed into the atmosphere, neutrons become the main source of SEUs. By sea level, most of the showered particles are absorbed and the cosmic ray shower is very small compared to the upper atmosphere. This means the

---

[3] In this case, the word *particle* refers to protons, neutron, pions, electrons, and muons.

[4] Cosmic rays are very energetic nuclei which span the entire periodic table from hydrogen (its nucleus is a proton) to heavy nuclei (i.e. Uranium).

[5] A muon is a subatomic lepton which may be either positively or negatively charged and is produced in pion decay. It can be thought of as either a heavy electron or positron.

[6] A pion is a subatomic hadron which may be positively, negatively, or neutrally charged and has a lifetime of 26ns in Earth's atmosphere.

particle flux depends upon the altitude.

When a charged particle enters the earth's magnetic field it will be slowed down and sometimes directed away from its original course by forces exerted on it as a result of that magnetic field. For this reason, a charged particle must have a certain amount of momentum per unit charge, or geomagnetic rigidity, to reach a certain place in the atmosphere. The amount of momentum it must have to reach that location is referred to as the geomagnetic cutoff of that location [7,8,12]. Any particle which has a geomagnetic rigidity less than the geomagnetic cutoff at a location will be deflected before it can reach that location. In this study, geomagnetic rigidity is expressed in units of gigavolts or GV. This means a location in the atmosphere with a large geomagnetic cutoff will deflect more particles away from the earth, resulting in smaller particle fluxes at that location. It also means the particle flux depends upon the geomagnetic cutoff. This will be discussed and demonstrated in more detail later.

The geomagnetic cutoff at a particular location depends upon the strength and the direction of the earth's magnetic field at that particular location. Near the earth's magnetic poles, the magnetic field is nearly parallel to the direction of incoming cosmic rays, so it will exert less force on the particles. This results in a much lower geomagnetic cutoff near the magnetic poles. On the other hand, near the earth's geomagnetic equator (in a geomagnetic coordinate system the magnetic poles are at a latitude of 90°), the magnetic field is perpendicular to the direction of incoming cosmic rays and will exert greater force on the particles. This results in a higher geomagnetic cutoff [12]. At the same time, the strength of the magnetic field varies at different latitudes, longitudes, and altitudes [7]. The stronger the field, the more force it will exert on incoming cosmic rays, and the higher the geomagnetic cutoff will be at that location. Since the particle flux depends upon the geomagnetic cutoff, it also depends upon latitude and longitude.

The sun is the source of a small fraction of the cosmic rays bombarding the earth. For this reason, the cosmic ray intensities will be at a maximum around 1200 noon when the location of interest is faced towards the sun and at a minimum around midnight when the location of interest is faced away from the sun. Consequently, the time of day will also affect the particle flux. The difference between the noon maximum and the midnight minimum varies from month to month. It will be greatest in June and least in December; therefore, the particle flux will also depend upon the time of year [7].

The sun's solar wind also causes changes in the configuration earth's magnetic field. It proceeds through active and quiet periods in an approximately 10.9 year cycle. During a quiet sun, the solar wind will have very little affect on the earth's magnetic field lines, resulting in larger cosmic ray intensities. On the other hand, during an active sun, there is more solar wind which distorts the earth's magnetic field lines and increases the field's shielding against cosmic rays [7,11]. This results in a decrease in the particle flux. This means the particle flux depends upon the year as well. The changes in the particle flux as a result of the sun will be mentioned in greater detail later. A summary of the variables that the particle flux depends upon is shown in table 2.1.

Table 2.1 - The major variables affecting the particle flux at a specific location

Factors Affecting the Particle Flux at a Particular Location
Latitude - due to change in magnetic field at different latitudes
Longitude - due to change in magnetic field at different longitudes
Altitude - due to change in magnetic field and the amount of atmosphere a particle must pass through at different altitudes
Time - due to change in solar activity over time

B. Determining the Differential Particle Flux Spectrum

In order to simplify the model, it was assumed that the shape of the differential particle flux energy spectrum remained the same regardless of location in the earth's atmosphere. Although it does change a little at higher altitudes, it generally follows the normalized differential particle energy spectrum found in *Terrestial Cosmic Rays* and shown in Figure E.1:

$$d\Phi/dE(\text{particles/cm}^2\text{-MeV-s}) = 211.9e^{Z(E)} \qquad (2.1)$$

Where $Z(E) = -5.2752 - 2.6043 \ln E + .5985 (\ln E)^2 - .08915 (\ln E)^3 + .003694 (\ln E)^4$

such that $$\Phi = \int_E \frac{d\Phi}{dE} dE = 1 \text{ particle} / \text{cm}^2\text{s}$$

and E is the particle energy in MeV. Since the integral of this function over the energy range is normalized to unity, the differential particle flux energy spectrum at a particular location can be obtained by multiplying eq. 2.1 by the total particle flux at that particular location. As a result of this assumption, only the total particle flux at various locations needed to be calculated in order to determine the differential particle flux energy spectra at those locations.

The first step in determining the total particle flux which, as discussed earlier, depends upon latitude, longitude, altitude, and time, was calculating the geomagnetic cutoff at various locations in the world. Geomagnetic cutoff depends upon latitude, longitude, and altitude. In this case, however, the geomagnetic cutoff at an altitude of 20km was determined as a function of latitude and longitude. The next step involved calculating the total particle flux as a function of the altitude and of the 20km geomagnetic cutoff at that particular latitude and longitude. This required the use of both the IBM and NRL CREME Models.

The IBM model had to be analyzed and expanded in order to calculate the particle fluxes over the whole world between sea level and 46,000ft. The NRL model also had to be analyzed and expanded in order to calculate the particle fluxes between 100,000ft and 300,000ft for any geomagnetic cutoff. Then they were extrapolated at altitudes between the 46,000ft and 100,000ft, resulting in a flux equation which calculated the particle flux at a particular latitude, longitude, and altitude. The final step involved the attachment of the solar factors which accounted for the change in particle flux with respect to time.

In some cases, multiple mathematical expressions that were each valid over specific intervals were combined into a single mathematical function, using the following exponential step function shown in Figure E.2:

$$\hat{S}(X,a,b) = [.5 + .5(\tanh((X-a)/b)] \qquad (2.2)$$

where X is the independent variable, a is the X value where the step function rises or falls, and b determines the rate at which the transition between functions occurs and whether the step function rises or falls. For example, if one had a function $Y_1(X)$ which was valid from X= 0 to z, and $Y_2(X)$ which was valid from X = z to infinity, one could create the function $Y_3(X) = \hat{S}(X, a=z, b= -w)Y_1(X) + \hat{S}(X, a=z, b= w)Y_2(X)$ which would now be valid over the range X= 0 to infinity. Additionally, the variable w would be adjusted until a smooth transition between functions is observed.

C. The Geomagnetic Cutoff

As mentioned earlier, the first step in determining the particle flux at various locations is determining the geomagnetic cutoff at various locations as a function of latitude and easterly longitude [11,12]. Geomagnetic cutoff actually depends upon latitude, longitude, and altitude, but in order to simplify Φ_{USNA} it was calculated at 20km at various locations, removing the altitude dependence. IBM's model has a world map which includes geomagnetic cutoff contour lines, each 1GV apart from 1 to 17 GV, that can be referenced in order to determine the geomagnetic cutoff [7, 8]. It is shown in Figure E.3. Unfortunately, this can't be readily used for modeling that requires mathematical expressions.

NRL's model has hundreds of data points for the geomagnetic cutoff at various latitudes and longitudes [11,12], but obtaining an accurate geomagnetic cutoff requires linear interpolation over both the latitude and longitude.

In order to define the geomagnetic cutoff in a single mathematical expression, a fifth order polynomial fit was performed on the NRL CREME Model's data points resulting in the following expression and shown in Figure E.4:

$$\begin{aligned} RIG = \{ & (.130LONG) + (.494e-1LONG) - (.393e-6LAT\,LONG^3) + (.153e-9LAT^3LONG^3) \\ & +(.608e-11LAT^2LONG^4) - (.160e-7LONG^2LAT^3) - (.150e-8LAT^2LONG^3) \\ & -(.960e-14LAT^2LONG^5) + (.106e-8LONG^4LAT) + (.339e-6LAT^3LONG) \\ & +(.428e-4LONG^2LAT) - (.698e-3LAT\,LONG) + (.178e-12LONG^3LAT^4) \\ & -(.696e-15LAT^4LONG^4) + (.292e-6LAT^2LONG^2) - (.364e-4LAT^2LONG) \\ & -(.343e-10LAT^5LONG) - (.410e-19LAT^5LONG^5) + (.110e-17LAT^4LONG^5) \\ & -(.369e-10LONG^2LAT^4) + (.462e-8LAT^4LONG) - (.143e-13LONG^3LAT^5) \\ & -(.776e-12LONG^5LAT) + (13.5) + (.448e-12LAT^3LONG^4) - (.537e-2LAT^2) \\ & +(.381e-15LAT^3LONG^5) + (.444e-16LONG^4LAT^5) + (.143e-11LONG^2LAT^5) \\ & -(.603e-4LAT^3) + (.534e-6LAT^4) + (.637e-8LAT^5) - (.333e-3LONG^2) \\ & +(.159e-5LONG^3) - (.728e-8LONG^4) + (.125e-10LONG^5) \} \end{aligned} \qquad (2.3)$$

where RIG is the 20km geomagnetic cutoff in GV, LAT is the northerly latitude in degrees, and LONG is the easterly longitude in degrees. The accuracy of various points in this expression as well as the accuracy of general trends in this formula were tested using the IBM model's world map. The function was found to be accurate (standard error < 10%), except near the poles (|latitude| > 70°) where the geomagnetic cutoff actually drops to zero.

D. The IBM model

After determining the geomagnetic cutoff at a specific latitude and easterly longitude, the particle flux had to be determined as a function of the 20km geomagnetic cutoff and altitude. At lower altitudes, the IBM model was found to be useful for this purpose. The IBM model is based upon the linear attenuation[7] of particles between 30,000ft. and sea level and determines particle fluxes based on latitude, longitude, altitude, and time [8]. It calculates the particle fluxes near large cities for protons, neutrons, pions, as well as for electrons, and muons which have been neglected in Φ_{USNA}.

In order to understand the IBM model and create an easy method for calculating particle fluxes at low altitudes, a spreadsheet was created based on assumptions and equations presented in the IBM model. This spreadsheet expanded the IBM model up to the Pfotzer[8] point and over the rest of the earth's surface.

The expansion of the IBM model is based upon two underlying concepts. First, locations in the world with the same geomagnetic cutoff will have similar if not identical particle fluxes at the same time, and, second, as particles come closer to the earth's surface they will pass through more atmosphere [7]. As a result of the second concept, fluxes at different altitudes were compared using the atmospheric pressure[9] at those altitudes where, from [8]:

$$\text{Atmospheric Pressure}\left(\frac{g}{cm^2}\right) = P = \begin{cases} 1033 - .03648ALT + 4.26\cdot10^{-7}ALT & \text{if } ALT \le 30{,}000ft \\ 1033e^{(-ALT/22678)} & \text{if } ALT > 30{,}000ft \end{cases} \quad (2.4)$$

Here ALT is the altitude in feet and P is the atmospheric pressure in g/cm^2. It simplifies the model however, to use the exponential step function mentioned earlier (eq. 2.2) to obtain a single equation for the atmospheric pressure:

$$P = \left\{ \begin{array}{c} [.5+.5\tanh(\frac{ALT-30{,}000}{-3000})](1033 - .03648ALT + 4.26\cdot10^{-7}ALT) + \\ [.5+.5\tanh(\frac{ALT-30{,}000}{3000})][1033e^{(-ALT/22678)}] \end{array} \right\} \quad (2.4b)$$

[7] Linear attenuation is the absorption of incident particles as they pass through a substance.

[8] The Pfotzer point is the altitude where the total particle flux reaches a maximum, at ~46,000ft.

[9] The quantity used is actually the *atmospheric density-length*, referred to as the atmospheric pressure by scientists in the field of radiation technology.

The spreadsheet makes calculations for a location of interest based on a simple two step process, using published data points for cities with known geomagnetic cutoffs, altitudes, and relative particle fluxes (relative to New York City's sea level flux) [8]. First, based on the geomagnetic cutoff entered for the location of interest, it finds a city with a nearly equal cutoff, as well as the relative particle flux and the altitude at that city. Then, based on the altitude entered for the location of interest, it will calculate the particle flux by accounting for the difference between the atmospheric pressures of the other city and the location of interest in the following equation:

$$F = [.0142\text{nuc./cm}^2\text{s}] \cdot F_0 e^{\left(\frac{P_0 - P_1}{L}\right)} \quad (2.5)$$

where F is the flux at the location of interest in nucleons/cm^{2}s, F_0 is the relative particle flux of the other city, .0142nuc./cm^{2}s is the sea level particle flux in New York City, P_0 is the atmospheric pressure at the altitude of other city in g/cm^2, P_1 is atmospheric pressure at the altitude of the location of interest in g/cm^2, and L is the attenuation factor which will vary from 100 to 160 g/cm^2 depending upon the particle and altitude [8].

Some of the results of this spreadsheet are seen in Figures E.5, E.6, and E.7, which show particle flux calculations over Annapolis or USNA. Notice in Figure E.5 that the neutron flux is greater than the proton and pion fluxes by two and three orders of magnitude, respectively, at sea level. At the Pfotzer point, however, the neutron flux is only one and two orders of magnitude greater than the proton and pion fluxes, respectively. Figure E.6 shows the particle flux vs. the geomagnetic cutoff at both sea level and the Pfotzer point. The Pfotzer point flux is about 300 times greater than the sea level flux, and the geomagnetic cutoff causes the flux to vary by a factor of 2 around the world. Figure E.7 shows the differential particle flux energy spectra for neutrons, protons, and pion in Annapolis, using eq. 2.1 for the shape of the differential particle flux energy spectra.

The IBM model is useful for calculating low altitude particle fluxes and can be integrated into a particle flux model valid at all locations. For this reason, a mathematical function describing the low altitude particle flux was developed using the IBM model. This mathematical function, obtained through a fourth order polynomial fit, calculates the sum of the neutron and proton fluxes at various places in the lower atmosphere based on the 20km geomagnetic cutoff and the altitude at the location of interest. Since pions likely constitute a small portion of the total particle flux, they were neglected in this function. The mathematical function is given by equation 2.6 and is shown in Figure E.8:

$$\Phi(ALT, RIG) = .0142\left\{\begin{array}{l}[(.376e-7ALT^2)+(.145e-1RIG)+(.286e-3ALT)-(.192e-4RIG^4)\\ -(.107e-1RIG^2)+(.796e-3RIG^3)+(.498e-11ALT^3)-(.806e-16ALT^4)\\ +(1.02)+(.879e-5RIG\ ALT)-(.286e-19RIG^4ALT^4)-(.822e-13RIG^2ALT^3)\\ +(.159e-8RIG^2ALT^2)-(.452e-8ALT^2RIG)-(.170e-7RIG^4ALT)\\ -(.288e-16RIG^2ALT^4)+(.158e-17RIG^3ALT^4)-(.190e-9ALT^2RIG^3)\\ +(.177e-15ALT^4RIG)-(.699e-12ALT^3RIG)+(.186e-13RIG^3ALT^3)\\ -(.729e-15ALT^3RIG^4)-(.612e-5RIG^2ALT)+(.581e-6RIG^3ALT)\\ +(.644e-11ALT^2RIG^4)\end{array}\right\} \quad (2.6)$$

where Φ is the total particle flux in nucleons/cm^{2}s, RIG is the 20km geomagnetic cutoff at the location of interest in GV, and ALT is the altitude at the location of interest in ft.

When graphed at higher altitudes, an error was observed in eq.2.6. As the geomagnetic cutoff decreases for a specific altitude, the particle flux should increase, but the particle flux in this function decreases as the geomagnetic cutoff falls below 4.5GV. In order to minimize eq. 2.6's inaccuracy, this error was corrected by using the exponential step function (eq. 2.2) to keep eq. 2.6 constant below a cutoff of 4.5GV. This was done by substituting a cutoff of 4.5GV into equation 2.6 in order to obtain a polynomial function for flux in terms of altitude. The result is eq. 2.7 which is shown in Figure E.9:

$$\Phi(ALT, RIG = 4.5) = .0142\left\{\begin{array}{l}.938+(.247e-3ALT)+(.349e-7ALT^2)+\\ (.157e-11ALT^3)+(.265e-15ALT^4)\end{array}\right\} \quad (2.7)$$

Then the exponential step function was used to keep the flux equal to eq. 2.7 when RIG < 4.5GV and equal to eq. 2.6 when RIG > 4.5GV. This is shown in Figure E.10 and represented by equation 2.8:

$$\Phi_{IBM}(ALT,RIG) = \hat{s}(RIG,4.5,1)(\text{eq. } 2.6) + \hat{s}(RIG,4.5,-1)(\text{eq. } 2.7) =$$

$$.0142\left\{\begin{array}{l}(.5+.5\tanh(RIG-4.5))[(.376e-7ALT^2)+(.145e-1RIG)+(.286e-3ALT)\\ -(.192e-4RIG^4)-(.107e-1RIG^2)+(.796e-3RIG^3)+(.498e-11ALT^3)\\ -(.806e-16ALT^4)+(1.02)+(.879e-5RIG\,ALT)-(.286e-19RIG^4ALT^4)\\ -(.822e-13RIG^2ALT^3)+(.159e-8RIG^2ALT^2)-(.452e-8ALT^2RIG)\\ -(.170e-7RIG^4ALT)-(.288e-16RIG^2ALT^4)+(.158e-17RIG^3ALT^4)\\ -(.190e-9ALT^2RIG^3)+(.177e-15ALT^4RIG)-(.699e-12ALT^3RIG)\\ +(.186e-13RIG^3ALT^3)-(.729e-15ALT^3RIG^4)-(.612e-5RIG^2ALT)\\ +(.581e-6RIG^3ALT)+(.644e-11ALT^2RIG^4)]+(.5-.5\tanh(RIG-4.5))[.938\\ +(.247e-3ALT)+(.349e-7ALT^2)+(.157e-11ALT^3)+(.265e-15ALT^4)]\end{array}\right\} \quad (2.8)$$

where Φ_{IBM} is the neutron and proton flux in nucleons/cm^{2}s at a desired location with an altitude of ALT in feet and a 20km cutoff of RIG in GV.

Eq.2.8, Φ_{IBM}, is the mathematical function for the IBM flux model. Below the Pfotzer point this expression is within 20% of the flux values shown in reference [8], and it is within 10% of these values below 10,000 ft. However, eq.2.8's flux values grow up to four orders of magnitude too high above the Pfotzer point. For flux values at higher altitudes, a mathematical function for the NRL CREME Model was developed.

E. The NRL CREME Model

The best source of information for determining the particle flux at higher altitudes as a function of geomagnetic cutoff and altitude is the NRL CREME Model. CREME is based on the galactic particle flux showering the earth and can be used to calculate the particle flux for protons, alpha particles, and numerous heavy nuclei. CREME also has information about the South American anomaly[10], but that was not included in this study. It determines the particle fluxes experienced by low orbiting satellites which pass through different altitudes and different geomagnetic cutoffs in the course of a full orbit.

In order to simplify Φ_{USNA}, only proton flux information was extracted from *CREME*, since the incident proton flux is an order of magnitude greater than the flux of the second most important particle and orders of magnitude greater than the flux of most heavy nuclei. It was also assumed that all protons showering the earth had a trajectory directly perpendicular to the earth's surface. This means all calculations assumed the worst case scenario, in which the largest possible percentage of incident particles made it to a specific location in the atmosphere.

---

[10]There is an unusually large flux of protons above South America, but these protons are at altitudes too high to be relevant to this project.

CREME is based upon the theory that only a certain number of the particles incident to the earth's atmosphere are capable of making it to a specific location based on the geomagnetic cutoff at that location. Of those particles, only a small percentage will actually make it because of the solid angle blocked by the earth and the absorption of particles as they pass through the atmosphere [15].

The first step undertaken was determining the flux of particles expected to make it to a location with a specific cutoff. Data from the *CREME '96* website [16] was extracted, analyzed, and combined in order to obtain the expected particle flux based on the cutoff at the location of interest. Then a polynomial fit was used to create a mathematical function for the expected flux based on the cutoff, resulting in the following equation, shown in Figure E.11:

$$\Phi_0(G) = 4010 + 1590G + 267G^2 - 22.3G^3 + .902G^4 - .0141G^5 \quad (2.9)$$

where Φ_0 is the flux of particles, in nucleons/steradian-cm^{2}s, capable of making it to a location in the atmosphere with a geomagnetic cutoff of G which is in GV. Here G is the geomagnetic cutoff at the latitude, longitude, and altitude of the desired location, different from RIG which is the geomagnetic cutoff at an altitude of 20km and the latitude and longitude of the desired location. Since the earth stands in the way of some of the galactic particles heading towards the location of interest, only a portion of Φ_0 will actually make it to that location. This is accounted for in CREME by introducing a solid angle formula which calculates the number of steradians of solid angle not blocked by the earth and is given by equation 2.10 [15], shown in Figure E.12:

$$\Omega(ALT) = 4\pi\left\{.5+.5\frac{\left((.209e8+ALT)^2-(.438e15)\right)^{.5}}{.209e8+ALT}\right\} \quad (2.10)$$

where Ω is the solid angle in steradians and ALT is the altitude in ft. The last item to consider is the fraction of the initial particles left after passing through the atmosphere to reach the location of interest [15]. Using more data points extracted from other data on the *CREME '96* website, an exponential fit was made to determine the fraction of particle flux transmission as a function of atmospheric pressure, valid from P = 0 to 1033g/cm^2:

$$T(P) = e^{-.110P+.0245} \quad (2.11)$$

where T is the fraction of particles which make it down to the location of interest with atmospheric pressure, P, which is in g/cm^2. Eq. 2.11 is plotted in Figure E.13.

In order to make eqs. 2.9 and 2.11 compatible with Φ_{USNA}, they need to be functions of the 20km cutoff, or RIG, and the altitude, or ALT, just like Φ_{IBM}. Equation 2.09 is a function of the cutoff at the location of interest, not the 20km cutoff. Because the cutoff at a specific location is inversely proportional to the square of the distance from the center of the earth [9], the two parameters (G and RIG) can be related by the following equation [11]:

$$G = RIG\left(\frac{2.10E7}{ALT + 2.09E7}\right)^2 \quad (2.12)$$

where G is the cutoff in GV at the desired location; RIG is the 20km cutoff at the desired location in GV; ALT is the altitude at the desired location in ft, 2.09E7 is the earth's radius in ft; and 2.10E7 is the sum of the earth's radius and 20km, in ft. Equation 2.11 is a function of atmospheric pressure and the relationship between the altitude, ALT, and the atmospheric pressure is found in equation 2.4b. Therefore, the flux calculated from *CREME* is found by 1) substituting equation 2.12 into equation 2.9, 2) substituting equation 2.4b into equation 2.11, and 3) multiplying this result by equation 2.10. Figure E.14 shows the result of this process and is expressed mathematically by eq.2.13:

$$\Phi_{NRL} = \Omega(ALT)\, T(P = \text{eq. } 2.4b)\, \Phi_0(G = \text{eq. } 2.12) =$$

$$\frac{\pi}{2500}\left[.5+.5\frac{\left((.209e8+ALT)^2-(.438e15)\right)^{.5}}{.209e8+ALT}\right]*$$

$$\left[+4010-.670e18\frac{RIG}{(.209e8+ALT)^2}+.520e32\frac{RIG^2}{(.209e8+ALT)^4}-.191e46\frac{RIG^3}{(.209e8+ALT)^6}+.341e59\frac{RIG^4}{(.209e8+ALT)^8}-.236e72\frac{RIG^5}{(.209e8+ALT)^{10}}\right]* \quad (2.13)$$

$$e^{\left[(-.00549(1033-.0365ALT+.426e-6ALT^2)(-\tanh(\frac{ALT}{3000}-10)+1)\right.}$$
$$\left.-5.67e^{(\frac{-ALT}{22700})}(\tanh(\frac{ALT}{3000}-10)+1)+.0245\right]$$

where Φ_{NRL} is the particle flux in nucleons/cm^{2}s at a location with an altitude of ALT, in feet and a 20km cutoff of RIG, in GV.

Eq. 2.13, Φ_{NRL}, is the mathematical expression for the particle flux at various locations based on the relationships found in the NRL CREME Model and is accurate in calculating the particle flux in nucleons/cm^{2}s at altitudes above 100km. However, the flux from eq.2.13 is too low at lower altitudes because the NRL CREME Model doesn't consider the buildup of particles from cosmic ray interactions[11] with the earth's atmosphere.

F. Combination of the NRL and IBM Models

In order to calculate the particle flux at any location based on the 20km geomagnetic cutoff and the altitude, Φ_{IBM} and Φ_{NRL} needed to be combined into a single

[11] As incident protons penetrate deeper into the earth's atmosphere, a higher percentage will collide with nitrogen and oxygen, resulting in a cascade of secondary particles which reach a maximum flux at the Pfotzer point.

mathematical expression. This was difficult due to the lack of useful particle flux data between the Pfotzer point and 100,000ft.

Figure E.15 shows the difference between the two models, in this case over Annapolis and also compares their results to the results of the NASA and Boeing models. The IBM and NRL CREME Models include particles with energies up to approximately 10GeV, whereas the NASA and Boeing models only include particles with energies up to 10MeV. For this reason, the IBM and NRL CREME Models should have values three to five times higher than the values found in the latter two models. The IBM data in this figure remains three to five times higher than the NASA and Boeing data, but the NRL data, which drops below the NASA and Boeing data, is much too low in this altitude range.

In order to combine both models smoothly, three conditions were imposed. The first condition was that the particle flux be a maximum at the Pfotzer point, or 46,000ft. The second condition was that the Pfotzer point particle flux be 300 times the sea level particle flux. The third condition was that the flux monotonically decrease after the Pfotzer point [17]. A variety of step functions (eq.2.2) were then tested until a mathematical expression which most closely satisfied these three assumptions was found.

The final expression which most closely fits these assumptions is shown here:

$$\Phi_T = \hat{S}(ALT, 35000, 15000)\Phi_{NRL} + \hat{S}(ALT, 35000, -15000)\Phi_{IBM} \qquad (2.14)$$

where Φ_T is the total neutron and proton particle flux in nucleons/cm^{2}s. This is plotted in Figure E.16, where it can be seen that the mathematical expression does have two minor errors. In the 0 to 1 GV cutoff range, the flux decreases after the Pfotzer point, then increases at higher altitudes. At the same time, the flux values are negative in the 17 GV[12] range near the Pfotzer point. Errors such as these are expected at the extreme edges of a mathematical expression like eq.2.14.

The values in eq.2.14 are consistent below the Pfotzer point [8] and above 100,000 ft [16]. Eq.2.14's accuracy between these altitudes can't be proven because most of the experimental data available in this altitude range is either unreliable or does not include adequate latitude, longitude, altitude, or time information to go with the flux values. The exponential step functions used to create Φ_T, however, are simple enough for future researchers to easily refit Φ_{NRL} and Φ_{IBM} more accurately when better experimental data is obtained in the future.

G. The Solar Factors

None of the previous equations account for the changes in particle flux which occur over time. In fact, eq.2.14 itself only calculates the average daily flux during a quiet sun. In order to account for these changes over time, two unitless solar factors were created for correcting eq.2.14 based on the time of day, year, and solar cycle.

The first solar factor, S_1, accounts for the change in incident particles from the

---

[12]Note that 17 GV is near the geomagnetic cutoff maximum.

sun. Because a small fraction of the incident cosmic rays come from the sun, the particle flux decreases at night and increases around noon. The average particle flux is observed at 6 a.m. and at 6 p.m., while the noon and midnight particle fluxes deviate from this by .45% in December and .60% in June [8]. The easiest way of accounting for this effect is through a cosine function which oscillates between 1.006 and .994 in June and between 1.0045 and .9955 in December. This information is available in reference [8] and can be expressed by eq. 2.15 below:

$$S_1 = 1 - A_s \cos[(2\pi/24)\cdot(h + m/60)]$$

$$A_s = .00525 + .00075\cos[(2\pi/12)(M-6)] \qquad (2.15)$$

where h is the hour of the day (from 1-24); m is the minute of the hour; and M is the month of the year. A plot of S_1 is shown in Figure E.17.

The second solar factor, S_2, accounts for the effect of the solar cycles. During a quiet sun, the solar wind will have a very small effect on the particle flux. During an active sun, however, an increase in the solar wind will cause a distortion in the earth's magnetic field, increasing its shielding against cosmic rays. This will result in a 25% decrease in the average daily particle flux. The sun proceeds through these active and quiet periods in 10.9 year cycles [8]. The simplest method for accounting for the solar cycles is through a sine function which oscillates between 1 and .75 over an 10.9 year period. The information is available in reference [8] and is expressed by eq.2.16 below:

$$S_2 = .875 + .125\sin\{[2\pi/10.9][y + ((M-1)/12) - 1960.5]\} \qquad (2.16)$$

where y is the year, M is the month of the year, and 1960.5 (June 1960) is a time when the observed particle flux was 87.5 % of the particle flux observed during a quiet sun. A plot of S_2 is shown in Figure E.18.

H. The New Flux Model, Φ_{USNA}

Φ_{USNA} was developed using data, concepts and relations found in IBM's and NRL's particle flux models. The information obtained from these models was combined, analyzed, and placed into mathematical functions which can be used to determine the total neutron and proton particle flux at a location based on latitude, easterly longitude, altitude, date, and time. It replaces raw data and lookup tables with equations which can be used in a simple computer model, but are not recommended for calculations by hand.

In order to use Φ_{USNA} to calculate the proton and neutron particle flux, the following four steps must be followed:

1) Calculate RIG (the 20km geomagnetic cutoff) based on LAT (the northerly latitude) and LONG (easterly longitude), using equation 2.3.

2) Calculate the Φ_T (proton and neutron particle flux) based on the RIG (20km

geomagnetic cutoff) and ALT (the altitude) using equations 2.14, 2.13, and 2.8.

3) Calculate S_1 and S_2 (the solar factors) based on h(the hour), M (the month), and y(the year), using equations 2.15 and 2.16.

4) Take the product of the particle flux, calculated in step 2, and the solar factors, calculated in step 3.

Typical results of this process are given in Chapter 5. Φ_{USNA} is important for determining the particle flux environment of a DRAM, however it must be combined with DRAM cross-sections, which are discussed in the next chapter, in order to calculate SERs.

CHAPTER III - The SEU Cross-Sections

In order to calculate the SERs for various COTS DRAMs, their susceptibility to SEUs must also be determined. For this reason, the SEU cross-sections[13] for various DRAMs at various energies was determined based on experimental data taken before this project began.

A. The Experimental Cross-Section Data[14]

The experimental SEU cross-section data used in this project was taken by scientists from IBM, the University of Colorado, and USNA [11]. The experiments were conducted at the Triangle University Meson Facility in Vancouver, the Harvard Cyclotron Laboratory, the National Institute of Standards and Technology in Gaithersburg Maryland, and at USNA. The data obtained includes neutron cross-sections for thermal and 14MeV neutrons as well as cross-sections for protons of energies ranging from 50 to 148 MeV. Pion data were also taken for both positively and negatively charged pions with energies ranging from 40 to 240 MeV.

Experimental runs were performed on 16- and 64-Mb DRAMs from 11 different vendors. However, there were only neutron and proton cross-section data for 6 of the vendors that covered all experimental conditions. These six vendors include IBM, Fujitsu, NEC, Micron, Hitachi, and Toshiba. In order to refrain from altering the reputation of any of these vendors and because the experimental data was limited, they shall be referred to as Vendors A, B, C, D, E, and F, not respectively, during the rest of this report. There was only enough useful pion cross-section data for 5 of these vendors. Graphs of the cross-section data used in this project can be seen in Figures E.19 and E.20 which show a typical variation of two to three orders of magnitude in cross-sections among vendors.

B. The Neutron and Proton Data

In the field of radiation hardened technology, it is commonly assumed that incident protons will have the same effect on COTS DRAMs as incident neutrons, if their energies are equal [17]. Therefore, the neutron and proton data were handled together in order to anayze the SEU cross-sections for both particles from thermal energies (.025eV) up to 1000 MeV[15]. The data were separated into three separate energy bins and the cross-sections over each energy bin were determined using three different mathematical methods. In order to have a continuous SEU cross-section, a mathematical fit was applied to the discrete experimental data. The first energy range included cross-sections

---

[13] An SEU cross-section is a measure of the probability that an incident particle with a specific kinetic energy will cause an SEU, in units of $10^{-15}cm^2$ fails/bit.

[14] This cross-section data is based on chips which didn't have error correction codes.

[15] Above 1000MeV very few particles exist, as shown in Figure E.1

for 4.2 to 14 MeV protons and neutrons[16]. Since there were very little SEU cross-section data in this energy interval, the SEU cross-sections in this interval were obtained by looking at the heating value cross-sections in silicon for particles of these energies. This approach was useful because the heating value cross-sections (see Figure E.21) give the amount of energy a particle with an incoming energy will deposit as it passes through a substance, and studies have shown [18] that it has the same functionality relationship as the observed SEU cross-section for other DRAMs. Based on data obtained from Shell [19], the heating value was found to be related to the SEU cross-section for his DRAMs by the following linear function:

$$\sigma'_{SEU}(E) = -.8137 + 11.4665 \cdot \sigma_{hv}(E) \qquad (3.1)$$

where σ_{hv} is the heating value cross-section in MeVcm^2/atom at energy E and σ'_{SEU} is the SEU cross-section calculated by Shell for the DRAMs tested. The cross-sections calculated by Shell needed to be scaled for particular vendors. This was handled by multiplying σ'_{SEU} by the 14MeV neutron cross-section obtained for a particular vendor and dividing it by the average 14MeV neutron cross-section obtained by Shell, which was $21.5 \cdot 10^{-15}$cm^2 fails/bit:

$$\sigma_{SEU}(E) = \left[\sigma_{SEU}(14MeV) / 21.5 \cdot 10^{-15}\right] \cdot [-.8137 + 11.4665 \cdot \sigma_{hv}(E)] \qquad (3.2)$$

where σ_{SEU}(14MeV) is the SEU cross-section of a particular vendor's DRAM for 14 MeV neutrons or protons and σ_{SEU}(E) is the SEU cross-section in cm^2 fails/bit of the same DRAM for neutron and protons of energy E.

The next energy range included cross-sections for 14 to 148 MeV protons and neutrons. Since there were more data available within this energy interval, the SEU cross sections were simply found by logarithmically fitting the data for each vendor:

$$\sigma_{SEU}(E) = \log^{-1}\{\alpha \cdot \log(E) + \beta\} \qquad (3.3)$$

where α and β vary by vendor. The α and β coefficients are given in Table E.22 in Appendix E.

The last interval dealt with SEU cross-sections for 150 to 1000MeV protons and neutrons. The accuracy in this energy interval was less important because the atmosphere contains very few particles in this energy range. A constant cross-section, equal to the cross-section at 150 MeV, was assumed for energies above 150 MeV. Thus, in this energy range:

$$\sigma_{SEU}(\text{Energy}) = \text{Constant} = \sigma_{SEU}(150MeV) \qquad (3.4)$$

---

[16]The cross-sections were taken to be zero below 4.2 MeV because the (n,α) reaction in silicon, the primary material in DRAMs, has a threshold energy of 4.2 MeV.

Eqs. 3.2, 3.3, and 3.4 were then used to obtain the SEU cross-section energy spectra. The neutron and proton cross-section spectra for the six vendors are shown in Figure E.23, which is a log-log plot of σ_{SEU} versus particle energy. The fluctuations in the cross-sections below 10 MeV are due to the fluctuations in the heating value cross-sections in this range.

C. The Pion Data

Even though pions were not included in Φ_{USNA}, in the final SEU model, or in the final SER calculations, the pion SEU cross-sections were still calculated. This was done because the pion cross-sections are higher than the neutron and proton cross-sections, making it important to assess their possible effect on the SERs of COTS DRAMs. This was also done so that future researchers who are able to determine the pion flux at various locations in the world accurately can use these cross-sections to make more accurate SER calculations.

Research has shown that pions with energies below 20MeV don't play a role in SEUs [20]. Consequently, the pion cross-sections were calculated for energies ranging from 20 to 1000MeV. Research has also shown that positively charged pions usually have the same effect on DRAMs as negatively charged pions [20]; therefore, the data for both types of pions was combined into a single set of data. The cross-section calculations were broken up into two energy ranges. The first energy range, which encompassed all the data points, included cross-sections for 20 to 280MeV pions. The SEU cross-sections were determined using logarithmic fits to the data points of each vendor:

$$\sigma^{\pi}_{SEU}(E) = \alpha' \cdot \log(E) + \beta' \qquad (3.5)$$

where σ^{π}_{SEU} is the pion SEU cross-section at energy E, while α' and β' vary with vendor. The α' and β' coefficients are given in Table E.24.

The second energy range included cross-sections for 280 to 1000MeV pions. Experimental research [20] has shown that pion cross sections generally remain constant in this energy range [20]; therefore, it was assumed that the cross-sections would remain constant after 280MeV:

$$\sigma^{\pi}_{SEU}(\text{Energy}) = \text{Constant} = \sigma^{\pi}_{SEU}(280\text{MeV}) \qquad (3.6)$$

These equations were then used to obtain the SEU cross-section spectrum. The pion cross-section spectra for the five vendors are shown in Figure E.25. By comparing the σ_{SEU} in Figure E.23 with σ^{π}_{SEU} in Figure E.25, it was found that vendors with higher neutron and protons SEU cross-sections had higher pion SEU cross-sections.

CHAPTER IV - DRAM Characteristics Affecting the SER - Rules of Thumb

There is enough information presented in chapters II and III to calculate the SERs for the experimentally tested DRAMs. The primary objective of this project, however, was to calculate the SERs for both tested and untested COTS DRAMs at various locations in the earth's atmosphere. In order to account for the difference between the SER of an untested DRAM from a particular vendor and the SER of the tested DRAM for that same vendor, a scaling factor was created. This scaling factor was based on use of rules of thumb for DRAM operating parameters and was used to calculate the SER for an untested DRAM based on the SER for an experimentally tested DRAM from the same vendor, manufactured during the same time period.

In order to determine which DRAM operating parameters affect the SER, a literature search was conducted. Four well known SER models, produced by Boeing [9], NASA [10], Los Alamos National Laboratory [16], and NRL [11], were found. They are presented in Appendix B and reveal important DRAM characteristic information. From these models, 3 factors were found to be important in scaling DRAM SERs.

From all four models, it was inferred that the SER is directly proportional to the surface area (A′) of the DRAM. This is because a DRAM with a larger surface area will be bombarded by more atmospheric particles which will cause more SEUs. Thus, a chip's surface area was chosen as the first scaling factor.

The third and fourth models indicate that the SER is directly related to Q_{crit}, the minimum amount of charge required to cause an SEU. Q_{crit} isn't a DRAM operating parameter, but it is related to a DRAM's operating voltage (V_{dd}). Some research [21] has found the SER to be proportional to the exponent of negative one times the operating voltage. This is not always the case, but it was used as a rule of thumb in this project. Some scientists believe this is the case because a DRAM with a smaller operating voltage will have capacitors which hold less charge. A capacitor which holds less charge is more susceptible to ions produced by incident particles. Thus, a chip's operating voltage expressed as an exponent ($e^{-V_{dd}}$) was chosen as the second scaling factor.

Other research [14] has shown that the SER can, in some cases, be directly proportional to a DRAM's operating frequency (f). This is not always the case, but it was also used as a rule of thumb in this project. Some scientists believe this is the case because a DRAM system is more sensitive to an SEU during the charge up phase in each AC cycle. A DRAM with a higher frequency will have more charge up phases in a shorter amount of time. Thus, chip frequency was chosen as the third characteristic affecting SERs.

These three relationships were used to create a scaling factor which predicts the SER for an untested DRAM based on the SER of a tested DRAM manufactured by the same vendor in the same time period:

$$SER_{UNTESTED} = SER_{TESTED} \cdot \frac{(A'fe^{-V_{dd}})_{UNTESTED}}{(A'fe^{-V_{dd}})_{TESTED}} \qquad (4.1)$$

where $SER_{UNTESTED}$ is the soft error rate of the untested DRAM in fails/s; SER_{TESTED} is the

soft error rate of the tested DRAM; and A′, f, and V_{dd} are the operating frequency (MHz), surface area (cm^2), and operating voltage (V) of the tested and untested DRAMs. These three operating parameters were found for 118 DRAMs manufactured by Vendors A through F in the past five years [21-31]. The scaling factors for them are shown in Appendix C. They vary by a factor of 3.1, ranging in value from .70 to 2.2.

CHAPTER V - Calculation of the Soft Error Rates

Once a DRAM's particle environment has been calculated, its sensitivity to those particles fluxes determined, and its scaling factor evaluated, the SER for that DRAM at that location can then be calculated.

A. The SER Calculation Procedure

In order to calculate the soft error rate of a DRAM, information about the particle flux environment (CH. II) must first be combined with the DRAM's SEU cross-section spectrum (CH. III). Both the first and second models in Appendix B show that the product of the differential particle flux spectrum and the cross-section spectrum must be integrated over the energy range to find the SER. Since the product of the cross-section spectrum and the particle flux spectrum can't be directly integrated, a summation was used instead. This process is given in eq. 5.1 below:

$$\text{SER / bit} = \int_E \sigma_{SEU}(E)\cdot(dJ/dE)\cdot dE \approx \sum_i \left\{\sigma_{SEU}(E_i)\cdot\frac{dJ}{dE}(E_i)\cdot\Delta E\right\} \qquad (5.1)$$

where SER/bit is the soft error rate of a tested DRAM, per bit, in units of fails/s-bit; dJ/dE (E_i), explained below, is the differential particle flux spectrum in particles/cm^2-MeV-s at the ith Energy; $\sigma_{SEU}(E_i)$ is the cross-section at the ith Energy in fails-cm^2/bit; and ΔE is the difference in energy between E_i and E_{i+1} in MeV. The integral and sum are over the energy range E = 4.2 to 1000 MeV.

Now, the differential particle flux spectrum, dJ/dE, is equal to the product of the normalized differential particle flux spectrum (eq. 2.1), the total particle flux (eq. 2.14), and the solar factors (eq. 2.15 and eq. 2.15). Therefore, the fraction of the total particle flux found in various energy ranges, or energy "bins," was determined and the SER per bit was calculated in the following manner:

$$\text{SER / bit} \approx \sum_i \left\{\sigma_{SEU}(E_i)\cdot\frac{dJ}{dE}(E_i)\cdot\Delta E\right\} \approx \sum_i \left\{\sigma_{SEU}(E_{i+\frac{1}{2}})\cdot S_1S_2\cdot\Phi_T\cdot F(E_i,E_{i+1})\right\}$$

$$= S_1S_2\Phi_T\sum_i \left\{\sigma_{SEU}(E_{i+\frac{1}{2}})\cdot F(E_i,E_{i+1})\right\} \qquad (5.2)$$

where $F(E_i\ E_{i+1})$ is the fraction of the total particle flux between energies E_i and E_{i+1} (based on eq.2.1; $\sigma_{SEU}(E_{i+1/2})$ is the SEU cross-section at energy $E_{i+1/2}$, for a particular vendor; and S_1 and S_2 are the solar factors. Thus, the SER/bit was found through the following procedure:

1) The flux of particles in a certain energy bin was determined from the product of the total particle flux, Φ_T (eq.2.14), and the fraction of the total particle flux in that energy bin, $F(E_i\ E_{i+1})$.

2) The SER/bit contribution from particles in that energy bin was then calculated by

taking the product of the flux obtained in step 1 and the SEU cross-section at the energy in the center of that bin ($\sigma_{SEU}(E_{i+1/2})$)

3) Last, the total SER/bit was found by summing the SER/bit contribution from each energy bin and multiplying this result by the solar factors (S_1 and S_2).

The summation term in equation 5.2 was determined for the experimentally tested DRAM of each vendor and is found in Table E.26. In selecting the number of energy bins to use, more bins were used at lower energies since the σ_{SEU} had a greater energy dependence and fewer bins were used at higher energies.

In order to determine the SER of a DRAM system, one must calculate the product of the SER per bit (in eq.5.2), the number of bits in the DRAM system, and the scaling factor (in eq.4.1). This results in the following equation;

$$SER(fails/s) = NS_1S_2\Phi_T\{\sum_i \sigma_{SEU}(E_{i+\frac{1}{2}}, Vendor)F(E_i, E_{i+1})\}\frac{(fA'e^{-V_{dd}})_{untested}}{(fA'e^{-V_{dd}})_{tested}} \quad (5.3)$$

where

N is the number of bits in the DRAM system
Φ_T is the total particle flux from eq. 2.14, in nucleons/cm^{2}s
$F(E_i\ E_{i+1})$ is the fraction of the total particle flux between energies E_i and E_{i+1},
$\sigma_{SEU}(E_{i+1/2})$ is the SEU cross-section at energy $E_{i+1/2}$, for a particular vendor, in fails-cm^2/bit
S_1 and S_2 are the solar factors, from eqs. 2.15 and 2.16
f is the operating frequency of the DRAM in MHz
A′ is the surface area of the DRAM in cm^2
V_{dd} is the operating voltage of the DRAM in V

B. The SER Calculations

The SERs were calculated for 118 of the 64Mb-DRAMs manufactured by vendors A through F in the last five years. The process for calculating the SER is summarized in Appendix F. The amount of SEUs calculated per second in a 64-Mb DRAM was found to be very small, on the order of 10^{-7} to 10^{-9} fails/s. At the same time, most modern computer systems contain many 64-Mb DRAMs; therefore, it was found to be more relevant to calculate the SERs for a 100Gb DRAM system in units of fails/hour.

This was calculated at various altitudes above Annapolis to determine the effect altitude has on the SER. SERs were also calculated at sea level and at the Pfotzer point over the magnetic poles, Bombay, Los Angeles, London, and Moscow in order to determine the effect geomagnetic cutoff has on the SER. The magnetic pole and Bombay were chosen because they are expected to have the highest and lowest particle fluxes in the world, respectively. Los Angeles, London, and Moscow were chosen because they have lots of air traffic and are strategically important. The calculated geomagnetic cutoffs, particle fluxes, and SERs are tabulated in Tables C.1 through C.6 in Appendix C for these cities, altitudes, and DRAMs.

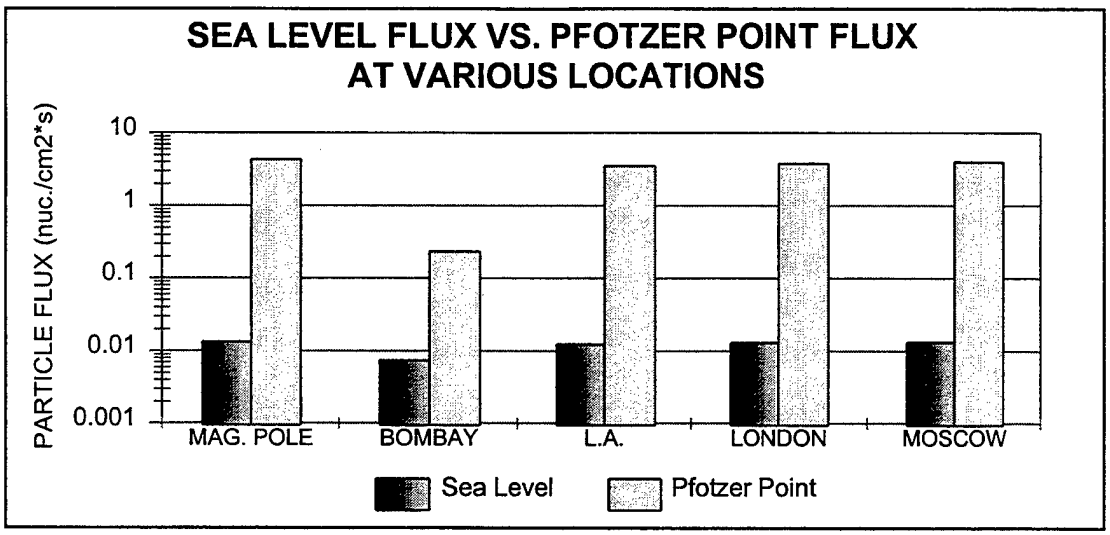

Figure 5.1 - A comparison of the sea level and Pfotzer point fluxes at various locations.

The particle fluxes are compared in Figure 5.1 at these five world locations. This Figure shows that the Pfotzer point flux is typically two and a half orders of magnitude greater than the sea level particle flux in areas of low cutoff (i.e., the magnetic poles). On the other hand, the Pfotzer point flux is typically one and a half orders of magnitude greater than the sea level flux in areas of high cutoff (i.e., Bombay). It also shows that the geomagnetic cutoff causes the particle flux to vary by a factor of 2 at sea level and a factor of 20 at the Pfotzer point. This is different from Figure E.6 which treats altitude and geomagnetic cutoff as independent variables, with the variation in flux caused by one variable remaining the same regardless of the value of the other variable. Figure 5.1 also

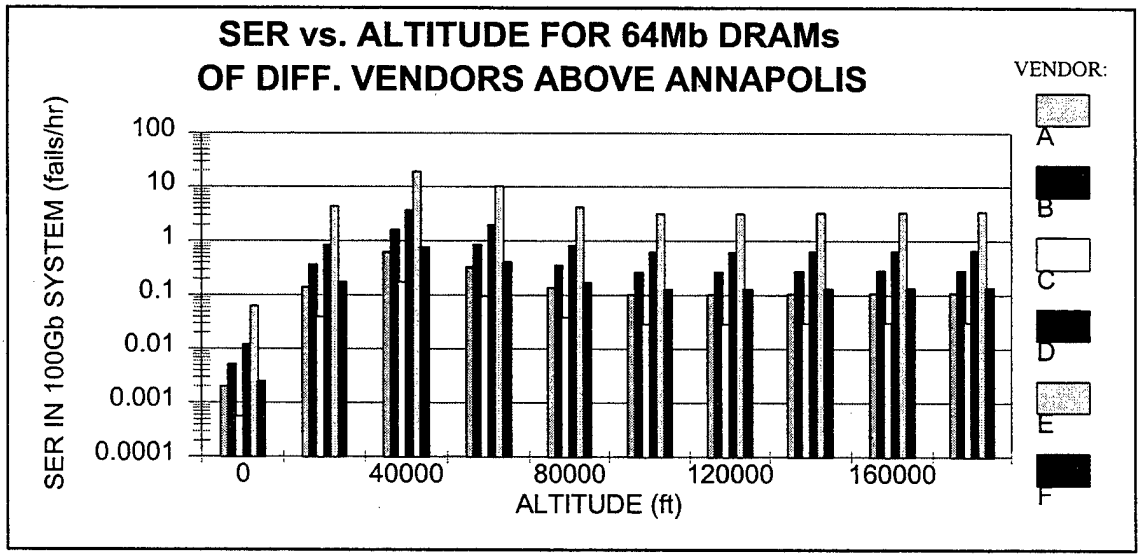

Figure 5.2 - The calculated SERs in a 100 Gb system for the six experimentally tested DRAMs at various altitudes over Annapolis.

shows the flux values over the entire world vary by a factor of 600, with the particle flux ranging from .007 to 4 nucleons /cm^{2}s.

The calculated SERs above Annapolis for the experimentally tested DRAMs of each vendor are shown in Figure 5.2. This Figure shows a variation of two and a half orders of magnitude between the sea level SER and the Pfotzer point SER. It also shows a variation of two orders of magnitude between the SERs for each vendors. Together, these make up an overall SER variation of 4 and a half orders of magnitude, with SERs varying from .00039 to 20 fails per hour for a 100Gb system with 64Mb DRAMs.

Figure 5.3 compares the calculated SERs for the experimentally tested DRAMs of each vendor at the Pfotzer point and at sea level, above the magnetic poles, Bombay, Los Angeles, London, and Moscow. The same variations observed in Figures 5.1 and 5.2 can be seen in Figure 5.3. It can also be seen in this figure, however, that the SERs for the experimentally tested DRAMs at different locations in the world vary by an overall factor of approximately 65,000, ranging from .00031 to 20 fails/hour for a 100Gb system with 64Mb DRAMs.

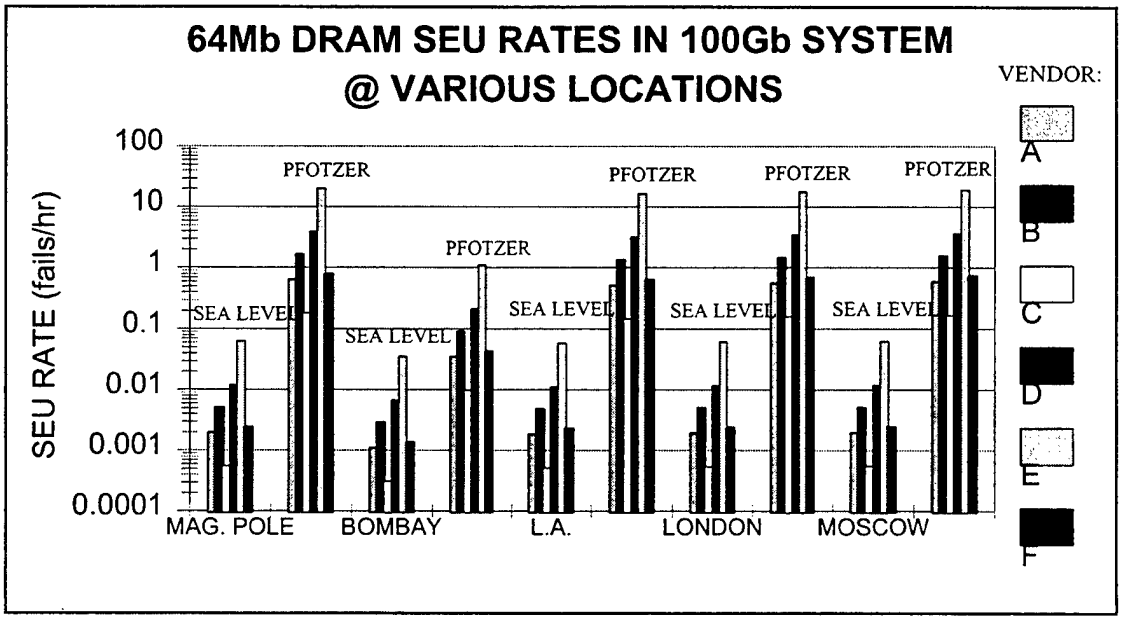

Figure 5.3 - The calculated SERs in a 100 Gb system for the six experimentally tested DRAMs at both sea level and the Pfotzer point at different locations in the world.

Figure 5.4 compares the calculated SERs of each DRAM manufactured by the same vendor. The SERs, on the average, only vary by a factor of 1.5 within the same vendor, which is a minor variation. Overall, the SERs for all 118 DRAMs over all parts of the world vary by a factor of approximately 95,000, with SERs ranging from .00022 to 21 fails/hour.

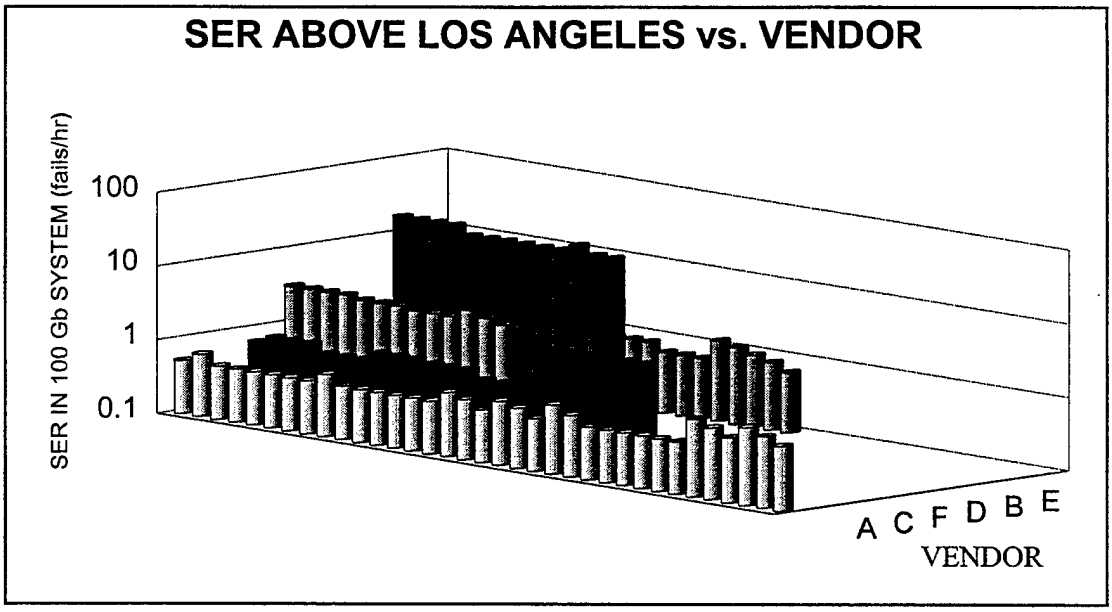

Figure 5.4 - The calculated SERs in a 100 Gb system for the DRAMs of each vendor, at the Pfotzer point above Los Angeles.

CHAPTER VI - The Major Nuclear Reactions

Part of understanding the SEU is understanding the initial nuclear reactions which can cause it. Future researchers may be able to develop better SEU models based on information known about the nuclear reactions which lead to them. DRAM developers may be able to reduce SERs if they know which isotopes in the DRAM are the most responsible for causing them. Scientists may have an easier time studying the SEU if they already know which reactions they need to study.

A. Neutron Nuclear Reactions in a DRAM

A literature search was conducted in order to determine the initial nuclear reactions most commonly associated with SEUs. Most of the nuclear reactions found were neutron induced. This is because neutrons are more prevalent below the Pfotzer point and because nuclear reactions producing a gamma ray usually have a smaller threshold energy. When a neutron comes in contact with a DRAM, it may react with the silicon in the DRAM through one of the following reactions [18]:

$$n + {}^{28}Si \rightarrow {}^{25}Mg + {}^{4}He \qquad Q = -2.65\ MeV^{17} \qquad (6.1)$$
$$n + {}^{28}Si \rightarrow {}^{28}Al + p + \gamma \qquad Q = -3.86\ MeV \qquad (6.2)$$
$$n + {}^{29}Si \rightarrow {}^{29}Al + p + .94\gamma \qquad Q = -67.92\ MeV \qquad (6.3)$$
$$n + {}^{30}Si \rightarrow {}^{30}Al + p + .61\gamma \qquad Q = -7.76\ MeV \qquad (6.4)$$
$$n + {}^{30}Si \rightarrow {}^{27}Mg + {}^{4}He + .7\gamma \qquad Q = -4.21\ MeV \qquad (6.5)$$

The incoming neutron may also react with any aluminum or boron found in the DRAMs:

$$n + {}^{27}Al \rightarrow {}^{27}Mg + p + .7\gamma \qquad Q = -1.83\ MeV \qquad (6.6)$$
$$n + {}^{10}B \rightarrow {}^{7}Li + {}^{4}He + .94\gamma \qquad Q = 2.79\ MeV \qquad (6.7)$$

The products of these nuclear reactions will cause SEUs by producing electron-hole pairs through ionization, but the processes involved in that are beyond the scope of this project.

B. The Most Common Reactions

When determining the most common reactions, one must consider the shape of the normalized differential particle flux spectrum shown in Figure E.1. There are more particles at lower energies than there are at higher energies. One must also consider that DRAMs have more silicon than aluminum or boron.

In order to determine the relative probability that a reaction will occur, it was assumed that the relative probability of each nuclear reaction occurring was directly proportional to the reaction rate, which is calculated in a manner similar to the SER calculation. Therefore, a summation similar to that found in equation 5.1 was used:

---

[17] A negative Q indicates an endothermic reaction requiring the incident particle to have energy greater than Q, while a positive Q indicates an exothermic reaction which requires an incident particle of very little energy and produces energy.

$$RP \;\alpha\; \int_E \sigma(E)\cdot(d\Phi/dE)\cdot dE \approx \sum_i \left\{\sigma(E_i)\cdot F(E_i, E_{i+1})\right\} \qquad (6.8)$$

where $\sigma(E_i)$ is the reaction cross-section at energy E_i from [33], $F(E_i, E_{i+1})$ is the fraction of the particle flux spectrum between energies E_i, and E_{i+1} based on the normalized differential flux spectrum, and RP is the relative probability that the reaction will occur. RP doesn't account for the amount of the reactant present.

With this summation, the relative probabilities (normalized so RP for the ^{27}Al reaction = 1) for the ^{27}Al (eq. 6.6), ^{30}Si (eqs. 6.4 & 6.5), ^{28}Si (eqs. 6.1 & 6.2), and ^{29}Si (eq. 6.3) reactions were found to be 1, 0.7, 0.6, and 0.3, respectively. Because these factors are small when compared to the amount of ^{28}Si present in a DRAM, which makes up over 92% of the natural silicon [32], the ^{28}Si reactions (eqs. 6.1 & 6.2) must be the most common reactions. Since reaction 6.1 has a smaller threshold energy, it must be the most common reaction.

Since the natural abundances of ^{29}Si and ^{30}Si in natural silicon are 4.7% and 3.1%, respectively, the ^{29}Si (eq. 6.3) and ^{30}Si (eqs. 6.4 & 6.5) reactions are the next most likely reactions to occur. Because the relative probability for the ^{30}Si reactions is double that for the ^{29}Si reaction, the next most common reactions must be the ^{30}Si reactions (eqs. 6.4 & 6.5). Since reaction 6.5 requires less energy than reaction 6.4, it is more likely to occur and is the next most common reaction.

DRAMs have much less aluminum than silicon; therefore, the ^{27}Al reaction (eq. 6.6) was considered the least common reaction.

The relative occurrence of the ^{10}B reaction (eq. 6.7) is difficult to assess. The ^{10}B reaction (eq. 6.8) requires no incident neutron energy to occur, so it might be a common reaction. However, the amount of ^{10}B in a DRAM varies widely among vendors, making it difficult to assess the importance of this reaction.

In order to summarize this section, the reactions are listed below from most common to least common in table 6.1, except for the ^{10}B reaction.

Ranking	Reaction	Q-value (MeV)
1	$n + {}^{28}Si \rightarrow {}^{25}Mg + {}^{4}He$	- 2.65
2	$n + {}^{28}Si \rightarrow {}^{28}Al + p + \gamma$	- 3.86
3	$n + {}^{30}Si \rightarrow {}^{27}Mg + {}^{4}He + .7\gamma$	- 4.21
4	$n + {}^{30}Si \rightarrow {}^{30}Al + p + .61\gamma$	- 7.76
5	$n + {}^{29}Si \rightarrow {}^{29}Al + p + .94\gamma$	- 67.92
6	$n + {}^{27}Al \rightarrow {}^{27}Mg + p + .7\gamma$	- 1.83

table 6.1 - The six most common initial reactions in a DRAM based on relative abundance and the relative probability (eq.6.10)

It is recognized that the linear energy transfer (LET) of the products produced in these reactions play an important role in producing SEUs. However, it was beyond the scope of this project to calculate the LET of the reaction products.

C. Experimentation

Many of these reactions produce positively charged ions which cause ionization in the DRAM substrate material leading to a buildup of charge in a DRAM's capacitors. But what about the alpha particles (^{4}He) produced in some of these reactions? Is it possible that alpha particles produced in nuclear reactions induce SEUs in the new DRAMs? In order to answer this question an experiment was prepared involving an alpha source (^{241}Am) and a DRAM placed in a vacuum chamber. The vacuum chamber was needed because of the short range of alpha particles in air. Due to equipment problems, the experiment was unsuccessful; nevertheless, it is important to discuss this experiment briefly for future researchers.

The setup for the experiment can be seen in Appendix D. As it shows, the vacuum chamber had a photomultiplier tube placed at the end connected to a high voltage source and to a preamp which was attached to an amplifier and an Analog-to-Digital converter. If the alpha particles emitted by the source reacted with any material in the DRAM, photons would be emitted and detected by the photomultiplier tube. This would indicate the production of fluorescence via alpha reactions.

This is important because many of the nuclear reactions listed above produce alpha particles. If alpha particles turn out to be an important source of fluorescence, the reactions which produce them may play a larger role in the occurrence of SEUs in the new DRAMs. This is because silicon based microchips are known to be light sensitive.

This is especially important in many of the newer DRAMs lined with borosilicate glass which contains ^{10}B. Since the ^{10}B reaction (eq. 6.7) is exothermic, it can easily be induced. If it turns out the alpha particles produced in the other initial nuclear reactions are causing fluorescence in the borosilicate glass, it would make ^{10}B a key player in SEU production.

CHAPTER VII - The Noteworthy DRAMs

A DRAM which is much less sensitive to radiation might be more reliable at aircraft altitudes. For this reason, one objective of this project was to determine the five DRAMs least sensitive to the atmospheric particle flux. There were nine found to have the same, and lowest, sensitivity; therefore, all nine are included in Table 7.1. Also included are the product of their vendor sum and their scaling factor. This was calculated from the data in Tables C.1 through C.6.

Table 7.1 - The 9 least sensitive DRAMs and the product of their vendor sum (sum in eq. 5.2) and scaling factor (eq. 4.1).

The 9 least sensitive DRAMs from Vendor C		
$\{\sum_i \sigma_{SEU}(E_{i+½}, \text{Vender})F(E_i, E_{i+1})\}\frac{(fAe^{-V_{dd}})_{untested}}{(fAe^{-V_{dd}})_{tested}}$ $= .0593 \cdot 10^{-15}$fails-cm^2/bit		
XXX0364164-10	XXX0364404-10	XXX0364804-10
XXX0364164-260	XXX0364404-260	XXX0364804-260
XXX0364164-360	XXX0364404-360	XXX0364804-360

On the other hand, a DRAM which is much more sensitive to radiation might be useful in a new radiation detection system. Such a radiation detection system would be lighter, simpler, and smaller. This would be useful in fields such as health physics and nuclear weapons detection. For these reasons, another objective of this project was to determine the five DRAMs most sensitive to neutrons and protons. These five DRAMs are found in table 7.2, with the product of their vendor sum and their scaling factors.

Table 7.1 - The 5 most sensitive DRAMs and the product of their vendor sum (sum in eq. 5.2) and scaling factors (eq. 4.1).

Vendor	DRAM	$\{\sum_i \sigma_{SEU}(E_{i+½}, \text{Vender})F(E_i, E_{i+1})\}\frac{(fAe^{-V_{dd}})_{untested}}{(fAe^{-V_{dd}})_{tested}}$ in 10^{-15}fails-cm^2/bit
E	XXX4564323G5-A80	9.64
E	XXX4564441G5-A80	9.54
E	XXX4564441G5-A10	9.54
E	XXX4564441G5-A10B	9.54
E	XXX4564841G5-A80	9.54

The sensitivity of the most sensitive DRAMs differs from the sensitivity of the least sensitive DRAMs by a factor of 160.

Chapter VIII - Conclusions and Recommended Future Research

Each year many industries and institutions employ the use of more advanced DRAM systems. This necessitates the need for better understanding the SEU and for better methods for calculating the SER. For these reasons, the primary objective of this project was to develop a model which simply and effectively calculated the SERs of various COTS DRAMs at various locations in the earth's atmosphere. Based on information obtained from IBM and NRL, a new particle flux model, Φ_{USNA}, was created for determining the differential particle flux spectrum. This model was combined with experimental data obtained from USNA, IBM, and the University of Colorado, as well as with relationships obtained from published literature in order to calculate the SERs for 118 COTS DRAMs. The particle fluxes in the earth's atmosphere were found to vary by a factor of 600 (CH 5) while the sensitivity of the 64Mb DRAMs was found to vary by a factor of 160 (CH.6). The SERs for a 100Gb system with 64Mb DRAMs located in the earth's atmosphere were found to vary by a factor of 95,000 (CH.5).

The secondary objective of this project was to determine which initial nuclear reactions are most closely related to the SEU. The most common nuclear reactions were determined, but their direct relationships to SEUs were not determined. Another secondary objective of this project was determining which DRAMs yielded the highest and lowest SEU rates. These were successfully determined through theoretical calculations based on experimental data.

Since most of the work and the calculations in this project are based upon theoretical modeling, some of the calculations made may not be valid in a real world situation. There was a small amount of information available for testing the results, but it is recommended that more research be performed by those who have the time, resources, and facilities to test the results of this project.

The particle fluxes determined between the Pfotzer point and 100,000ft are fairly uncertain. For this reason, it would benefit members of the aircraft and defense industries to perform flight experiments to determine the particle flux levels in this altitude range. Another uncertainty is the SER of these DRAMs. Since there is presently no laboratory particle beam which can be used to simulate the atmospheric particle flux spectrum over a wide range of energies, it would benefit anyone who uses DRAMs to perform flight experiments at the Pfotzer point and ground experiments at sea level near Bombay and near the magnetic poles. In order to obtain at least 100 SEUs for a counting error of approximately 10%, 100Gb of the most sensitive DRAMs (Vendor E) should be tested for 10 hours during the Pfotzer point flight experiments and for 1000 hours during the sea level ground experiments. During the flight experiments the number of SEUs, the altitude, the plane's location, and the flight duration should be recorded.

Regardless of how accurate the calculations in this model are found to be, the mathematical methods of evaluating the particle flux, the SERs, and the most common nuclear reactions should still be considered valid methods which can be employed in future SEU models. Those with more time, resources, and facilities available to them to study the SEU should take advantage of these in order to keep developing more accurate models for each set of new DRAMs. DRAMs will keep changing and so will the SEUs which cause some of them to fail from time to time. This is why it is very important for

the Navy to stay on the cutting edge of SEU research, constantly using new methods to determine what causes it, to predict it, and then to prevent it.

Document and Internet References

[1] Joseph Melinger, *Single Event Effects in Avionics* presentation, NRL Radiation Effects Group, Washington, DC.

[2] Eugene Normand, *Single Event Upset and Latchup Measurements in Avionics Devices Using the WNR Neutron Beam and a New Neutron-Induced Latchup Model*, Boeing Defense & Space Group Document, Seattle, WA, 1994.

[3] D. Binder, E. C. Smith, and A. B. Holman, *Satellite Anomalies From Galactic Cosmic Rays*, IEEE Trans. Nucl. Sci., Vol. 22, No.6, December 1975.

[4] Steven Hershberger and Dirk Hanson, *Widen Effort to Control Alpha Particles in 16Ks*, Electronics News, August 28, 1978.

[5] J. F. Ziegler (IBM), personal conversations, February, 1999.

[6] J. L. Davis, *Use of Computer Memeory Chips as the Basis for a Digital Albedo Neutron Dosimeter*, Health Physics, vol.49, no.2, pp 259-265, 1985.

[7] J. F. Ziegler, *Terrestrial Cosmic Ray Intensities*, IBM Journal of Research and Development, Vol. 42, No. 1, January 1998.

[8] J. F. Ziegler, *Terrestrial Cosmic Rays*, IBM Journal of Research and Development, Vol. 40, No. 1, January 1996.

[9] Eugene Normand, *Single Event Effects in Avionics*, Boeing Defense & Space Group Document, Seattle, WA, 1995.

[10] E. Normand and T. J. Baker, *Altitude and Latitude Variations in Avionics SEU and Atmospheric Neutron Flux*, IEEE Trans. Nucl. Sci., Vol. 40, 1484, 1993.

[11] J. H. Adams Jr., R. Silberberg, and C. H. Tsao, Cosmic Ray Effects on Microelectronics: Part I, The Near-Earth Particle Environment, NRL Memorandum Report 4885, August 25, 1981.

[12] J. H. Adams Jr., J. R. Letaw, and D. F. Smart, Cosmic Ray Effects on Microelectronics: Part II, The Geomagnetic Cutoff Effects, NRL Memorandum Report 5099, May 26, 1983.

[13] C. H. Tsao, R. Silberberg, J. H. Adams Jr., and J. R. Letaw, Cosmic Ray Effects on Microelectronics: Part III, Propagation of Cosmic Rays in the Atmosphere, NRL Memorandum Report 5402, August 9, 1984.

[14] J. H. Adams Jr., R. Silberberg, and C. H. Tsao, Cosmic Ray Effects on Microelectronics: Part IV,, NRL Memorandum Report 5901, December 31, 1986.

[15] A. Tylka (NRL), personal conversation, NRL, November, 1999.

[16] *Cosmic Ray Effects on Microelectronics* '96, web page

http://crsp3.nrl.navy.mil/creme96/, Naval Research Laboratory, October 1999.

[17] J. F. Ziegler (IBM), personal conversations, October to January, 1999.

[18] Y. Tosaka, S.Satoh, etal., *Measurements and Analysis of Neutron-Reaction-Induced Charges in a Silicon Surface Region*, IEEE Trans. Nucl. Sci., 1997.

[19] James D. Shell, *Radiation Induced Single Event Upsets of Dynamic and Static RAM Memory Devices*, U.S. Naval Academy Division of Engineering and Weapons, Annapolis, MD, Summer 1995.

[20] G. J. Hofman, R. J. Peterson, etal., *Light Hadron induced SER and scaling relations for 16Mb and 64Mb dRAMs*, IEEE Trans. Nucl. Sci., 1999.

[21] Neil Cohen, T.S. Sriram, etal., *Soft Error Considerations for Deep-Submicron CMOS Circuit Applications*, IEEE Trans. Nucl. Sci., 1999.

[22] Hitachi Semiconductor, web page http://semiconductor.hitachi.com/search/tree/, September 1999.

[23] Micron Technology Inc., web page http://www.micron.com/, September 1999.

[24] Hyundai Electronic America, web page http://www.hea.com/hean2/docs/prodhome.htm, September 1999.

[25] Texas Instruments, web page http://www.ti.com/sc/docs/eedesign.htm, September 1999.

[26] Toshiba America Electronics Components, web page http://www.toshiba.com/taec/, September 1999.

[27] Samsung Semiconductor, web page http://www.usa.samsungsemi.com/, September 1999.

[28] NEC Electronic Inc., web page http://www.necel.com/, September 1999.

[29] IBM, web page, web page http://www.chips.ibm.com/products/memory/, September 1999.

[30] OKI Semiconductor Communicator, web page http://www.okisemi.com/, September 1999.

[31] Fujitsu, web page http://www.fujitsu.com/, September 1999.

[32] Mitsubishi Semiconductors, web page http://www.mitsubishichips.com/, September 1999.

[33] Jonghwa Chang, *Table of the Nuclides*, web page http://www.dne.bnl.gov/CoN/, Brookhaven National Laboratory, Brookhaven NY, September 1999.

Appendix A - Trident Project Flow Chart

The following is a flow chart showing the main steps involved in the project and their relationships to one another. Included with the steps are the chapters which discuss them.

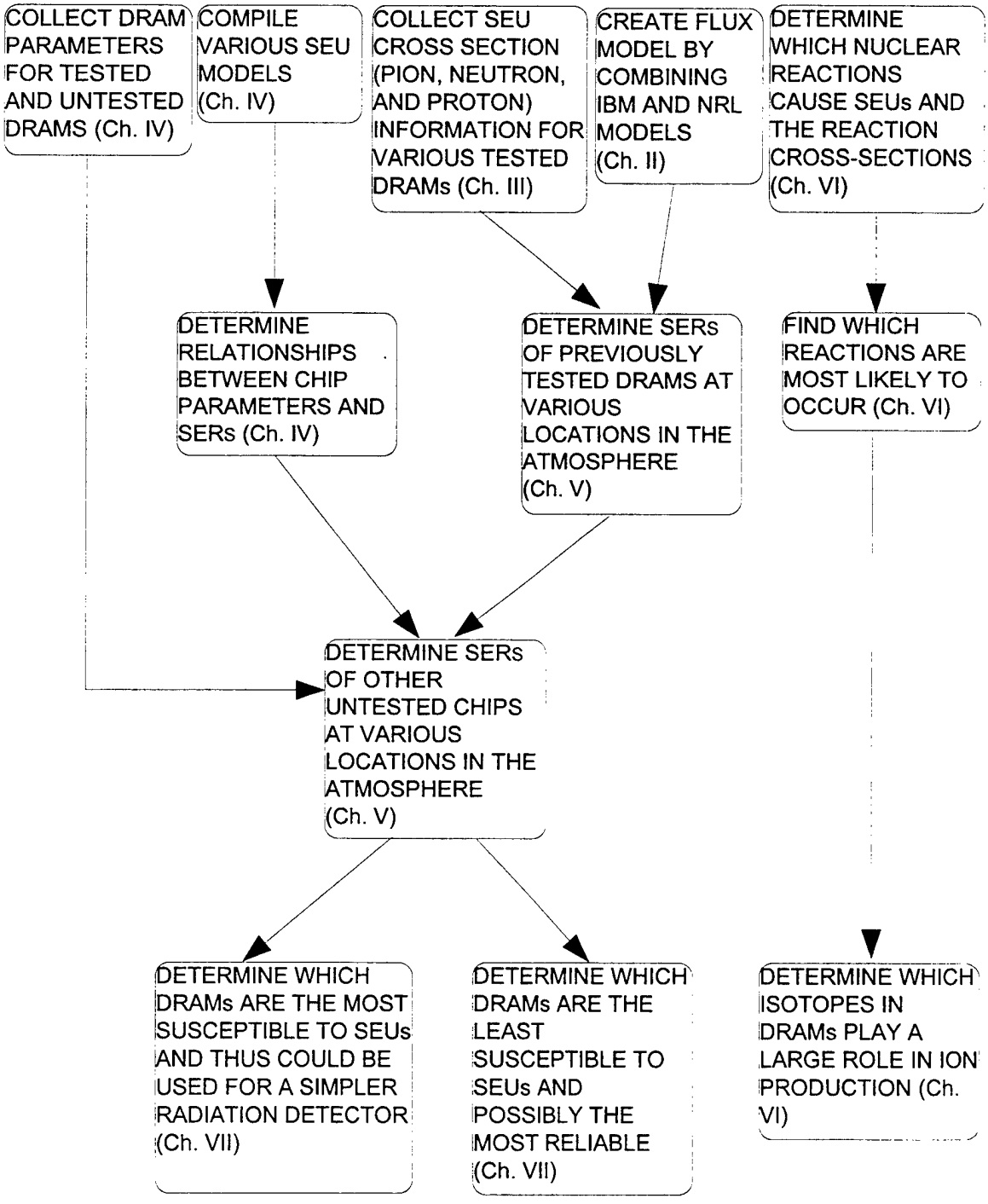

Appendix B - SEU models

The following SEU models were used to determine the COTS DRAM characteristics which affect the SER. They are discussed in chapter IV.

I. *Single Event Effects in Avionics* by Eugene Normand (Boeing) [9]

A.

$$\text{Upset Rate} = \int \sigma_{nseu}(E) \cdot (dN/dE) \cdot dE$$

where σ_{nseu} = Neutron-induced SEU cross-section in 10^{-15}cm^{2}fails/bit
(dN /dE) = Atmospheric differential neutron flux in neut./cm^{2}sMeV

B.

$$\text{Upset Rate} = C \sum_i \Delta V_i \int_E BGR(E, E_{ri}) \cdot (dJ/dE) \cdot dE$$

where C = ion collection efficiency (usually ~ .5)
ΔV_i = ith sensitive volume
E_{ri} = ith recoil energy, MeV
BGR(E, E_{ri}) = burst generation rate, cm^2/μm^3, probability that particle of Energy E will produce recoils of energy $\geq E_{ri}$
dJ/dE = neutron/proton differential flux

and $\Delta V_i = t\,\Delta\sigma_i$, μm^3
where t = chip sensitive thickness, μm
$\Delta\sigma_i = \sigma_i - \sigma_{i-1}$
σ_i = heavy ion SEU cross-section for the ith portion of the curve obtained when using the Weibull distribution, cm^2

and $E_{ri} = t \cdot .23 \cdot LET_i$
where LET_i = representative Linear Energy Transfer (the amount of energy a particle deposits per distance traveled) for ith portion of the LET curve, MeVcm^2/mg

II. *Altitude and Latitude Variations in Avionics SEU and Atmospheric Neutron Flux* by E. Normand and T.J. Baker (NASA) [10]

A.

$$\text{Upset Rate} = C \sum_i \Delta V_i \int_E BGR(E, E_{ri}) \cdot (dN/dE) \cdot dE$$

where the parameters are the same as defined above

B.

$$\text{Upset Rate} = C\sum_{i=1}^{N} t[\sigma(L_{i+1}) - \sigma(L_i)]\int_{E} BGR(E, E_{ri}) \cdot (dN/dE) \cdot dE$$

where $Eri = .23t \cdot (L_{i+1} + L_i)/2$, and L_i is the same as LET_i explained in part 1B.

III. *Measurement and Analysis of Neutron-Reaction-Induced Charges in a Silicon Surface Region* by Y. Tosaka, S. Satoh, etal. (Los Alamos National Laboratory) [18]

$$\text{Upset Rate}(Q_c) = IS(Q_c) \cdot \text{neutron } \Phi \cdot \text{sensitive volume} \cdot C$$

where Q_c = critical charge, fC
sensitive volume = sensitive area · depth of junction, μm^3
IS = charge collection spectra in burst generation rate units, $cm^2/\mu m^3$

IV. *Cosmic Ray Effects on Microelectronics, Part IV*, by James H. Adams Jr. [11]

$$N_e = 22.5\pi A Q_{crit} \int_{22.5Q_{crit}/P_{max}}^{L_{max}} D[p(\ell)]F(L)/L^2 \cdot dL$$

where A = surface area of the sensitive volume, m^2
Q_{crit} = minimum charge required for upset, pC
$L_{max} = 1.05 \cdot 10^5$ MeVcm^2/g, the highest LET any stopping ion can deliver
P_{max} = the largest diameter of the sensitive volume, g/cm^2
L = LET in MeVcm^2/g
F(L) = the integral LET spectrum in particles/m^2-ster-sec
$D[p(\ell)]$ = the differential path length distribution in the sensitive volume of each memory cell in cm^2/g
$p(\ell) = 22.5Q_{crit}/L$ = the path length over which an ion of LET, L, will produce a charge Q_{crit} in pCg/MeVcm^2

Appendix C - Particle Flux and SER Calculations for COTS DRAMS

The following six tables show the calculated particle fluxes and calculated SERs for the 118 COTS DRAMs at various locations and altitudes. The box at the top of each table shows the latitude (degrees), easterly longitude (degrees), altitude (ft), 20km cutoff (GV), and calculated particle flux (nuc./cm^{2}s) for each location of interest (explained in CH. II). The left side of the larger, lower box shows the COTS DRAMs, their vendors, their vendor sums (fails-cm^2/bit), and their scaling factors (explained in CH. III and CH. IV). The first two or three letters in the DRAM model numbers have been replaced by X's to conceal the vendors. The rest of the larger, lower box has the SERs (fails/hr) expected in a 100Gb system consisting of the DRAM found on the left when that system is at the location of interest in the above box (explained in CH. V).

Table C.1 contains flux and SER calculations for DRAMs from vendors A, B, and C over Annapolis from sea level up to 120,000ft.

Table C.2 contains flux and SER calculations for DRAMs from vendors C, D, E, and F over Annapolis from sea level up to 120,000ft.

Table C.3 contains flux and SER calculations for DRAMs from vendors A, B, and C over Annapolis from 140,000ft. up to 180,000ft., as well as over the magnetic poles and Bombay at both sea level and the Pfotzer point (46,000 ft).

Table C.4 contains flux and SER calculations for DRAMs from vendors C, D, E, and F over Annapolis from 140,000ft. up to 180,000ft., as well as over the magnetic poles and Bombay at both sea level and the Pfotzer point (46,000 ft).

Table C.5 contains flux and SER calculations for DRAMs from vendors A, B, and C over Los Angeles, London, and Moscow at both sea level and the Pfotzer point (46,000 ft).

Table C.6 contains flux and SER calculations for DRAMs from vendors C, D, E, and F over Los Angeles, London, and Moscow at both sea level and the Pfotzer point (46,000 ft).

table C.1 - Calculated SERs in a 100 Gb system over Annapolis with DRAMs from vendors A,B, and C (fails/hr)

Point #	1	2	3	4	5	6	7
Description	ANNAPOLIS	ANNAPOLIS	ANNAPOLIS	ANNAPOLIS	ANNAPOLIS	ANNAPOLIS	ANNAPOLIS
Latitude (N)	39	39	39	39	39	39	39
Longitude (E)	283.5	283.5	283.5	283.5	283.5	283.5	283.5
Altitude (ft)	0	20000	40000	60000	80000	100000	120000
Cutoff (GV)	3.3	3.3	3.3	3.3	3.3	3.3	3.3
Φ_T(nuc/cm2s)	1.33E-02	9.38E-01	4.13E+00	2.21E+00	9.13E-01	6.83E-01	6.82E-01

	DRAMS	Vendor Sum	Scaling Factor	SER	SER	SER	SER	SER	SER	SER
A	XX81164442A-10	3.03E-16	1.00E+00	1.99E-03	1.41E-01	6.19E-01	3.30E-01	1.37E-01	1.02E-01	1.02E-01
	XX81F64842D-75	3.03E-16	1.33E+00	2.64E-03	1.87E-01	8.24E-01	4.40E-01	1.82E-01	1.36E-01	1.36E-01
	XX81F64842D-102	3.03E-16	1.00E+00	1.99E-03	1.41E-01	6.19E-01	3.30E-01	1.37E-01	1.02E-01	1.02E-01
	XX81F64842D-102L	3.03E-16	1.00E+00	1.99E-03	1.41E-01	6.19E-01	3.30E-01	1.37E-01	1.02E-01	1.02E-01
	XX81F64842C-102	3.03E-16	1.00E+00	1.99E-03	1.41E-01	6.19E-01	3.30E-01	1.37E-01	1.02E-01	1.02E-01
	XX81F64842C-103	3.03E-16	1.00E+00	1.99E-03	1.41E-01	6.19E-01	3.30E-01	1.37E-01	1.02E-01	1.02E-01
	XX81F64842C-102L	3.03E-16	1.00E+00	1.99E-03	1.41E-01	6.19E-01	3.30E-01	1.37E-01	1.02E-01	1.02E-01
	XX81F64842C-103L	3.03E-16	1.00E+00	1.99E-03	1.41E-01	6.19E-01	3.30E-01	1.37E-01	1.02E-01	1.02E-01
	XX81F64442D-75	3.03E-16	1.33E+00	2.64E-03	1.87E-01	8.24E-01	4.40E-01	1.82E-01	1.36E-01	1.36E-01
	XX81F64442D-102	3.03E-16	1.00E+00	1.99E-03	1.41E-01	6.19E-01	3.30E-01	1.37E-01	1.02E-01	1.02E-01
	XX81F64442D-102L	3.03E-16	1.00E+00	1.99E-03	1.41E-01	6.19E-01	3.30E-01	1.37E-01	1.02E-01	1.02E-01
	XX81F64442C-102	3.03E-16	1.00E+00	1.99E-03	1.41E-01	6.19E-01	3.30E-01	1.37E-01	1.02E-01	1.02E-01
	XX81F64442C-103	3.03E-16	1.00E+00	1.99E-03	1.41E-01	6.19E-01	3.30E-01	1.37E-01	1.02E-01	1.02E-01
	XX81F64442C-102L	3.03E-16	1.00E+00	1.99E-03	1.41E-01	6.19E-01	3.30E-01	1.37E-01	1.02E-01	1.02E-01
	XX81F64442C-103L	3.03E-16	1.00E+00	1.99E-03	1.41E-01	6.19E-01	3.30E-01	1.37E-01	1.02E-01	1.02E-01
	XX81F643242B-70	3.03E-16	1.43E+00	2.84E-03	2.01E-01	8.85E-01	4.73E-01	1.96E-01	1.46E-01	1.46E-01
	XX81F643242B-80	3.03E-16	1.25E+00	2.48E-03	1.76E-01	7.74E-01	4.13E-01	1.71E-01	1.28E-01	1.28E-01
	XX81F643242B-10	3.03E-16	1.00E+00	1.99E-03	1.41E-01	6.19E-01	3.30E-01	1.37E-01	1.02E-01	1.02E-01
	XX81F643242B-70L	3.03E-16	1.43E+00	2.84E-03	2.01E-01	8.85E-01	4.73E-01	1.96E-01	1.46E-01	1.46E-01
	XX81F643242B-80L	3.03E-16	1.25E+00	2.48E-03	1.76E-01	7.74E-01	4.13E-01	1.71E-01	1.28E-01	1.28E-01
	XX81F643242B-10L	3.03E-16	1.00E+00	1.99E-03	1.41E-01	6.19E-01	3.30E-01	1.37E-01	1.02E-01	1.02E-01
	XX81F643242B-60	3.03E-16	1.67E+00	3.32E-03	2.35E-01	1.03E+00	5.52E-01	2.29E-01	1.71E-01	1.71E-01
	XX81F641642D-75	3.03E-16	1.33E+00	2.64E-03	1.87E-01	8.24E-01	4.40E-01	1.82E-01	1.36E-01	1.36E-01
	XX81F641642D-102	3.03E-16	1.00E+00	1.99E-03	1.41E-01	6.19E-01	3.30E-01	1.37E-01	1.02E-01	1.02E-01
	XX81F641642D-102L	3.03E-16	1.00E+00	1.99E-03	1.41E-01	6.19E-01	3.30E-01	1.37E-01	1.02E-01	1.02E-01
	XX81F641642C-102	3.03E-16	1.00E+00	1.99E-03	1.41E-01	6.19E-01	3.30E-01	1.37E-01	1.02E-01	1.02E-01
	XX81F641642C-103	3.03E-16	1.00E+00	1.99E-03	1.41E-01	6.19E-01	3.30E-01	1.37E-01	1.02E-01	1.02E-01
	XX81F641642C-102L	3.03E-16	1.00E+00	1.99E-03	1.41E-01	6.19E-01	3.30E-01	1.37E-01	1.02E-01	1.02E-01
	XX81F641642C-103	3.03E-16	1.00E+00	1.99E-03	1.41E-01	6.19E-01	3.30E-01	1.37E-01	1.02E-01	1.02E-01
	XX811L643242B-12	3.03E-16	2.23E+00	4.42E-03	3.13E-01	1.38E+00	7.35E-01	3.05E-01	2.28E-01	2.28E-01
	XX811L643242B-10	3.03E-16	1.87E+00	3.71E-03	2.63E-01	1.16E+00	6.18E-01	2.56E-01	1.91E-01	1.91E-01
	XX811L643242B-15	3.03E-16	1.49E+00	2.96E-03	2.10E-01	9.23E-01	4.93E-01	2.04E-01	1.53E-01	1.52E-01
	XX811L643242B-10L	3.03E-16	2.23E+00	4.42E-03	3.13E-01	1.38E+00	7.35E-01	3.05E-01	2.28E-01	2.28E-01
	XX811L643242B-12L	3.03E-16	1.87E+00	3.71E-03	2.63E-01	1.16E+00	6.18E-01	2.56E-01	1.91E-01	1.91E-01
	XX811L643242B-15L	3.03E-16	1.49E+00	2.96E-03	2.10E-01	9.23E-01	4.93E-01	2.04E-01	1.53E-01	1.52E-01
B	XX-5165805AJ6	7.92E-16	1.00E+00	5.19E-03	3.68E-01	1.62E+00	8.64E-01	3.58E-01	2.67E-01	2.67E-01
	XX5264165D	7.92E-16	1.11E+00	5.78E-03	4.09E-01	1.80E+00	9.62E-01	3.98E-01	2.98E-01	2.98E-01
	XX5264805D	7.92E-16	1.11E+00	5.78E-03	4.09E-01	1.80E+00	9.62E-01	3.98E-01	2.98E-01	2.98E-01
	XX5264405D	7.92E-16	1.11E+00	5.78E-03	4.09E-01	1.80E+00	9.62E-01	3.98E-01	2.98E-01	2.98E-01
	XX5264165D-A60	7.92E-16	8.91E-01	4.62E-03	3.27E-01	1.44E+00	7.70E-01	3.19E-01	2.38E-01	2.38E-01
	XX5264805D-A60	7.92E-16	8.91E-01	4.62E-03	3.27E-01	1.44E+00	7.70E-01	3.19E-01	2.38E-01	2.38E-01
	XX5264405D-A60	7.92E-16	8.91E-01	4.62E-03	3.27E-01	1.44E+00	7.70E-01	3.19E-01	2.38E-01	2.38E-01
	XX5264165D-B60	7.92E-16	8.91E-01	4.62E-03	3.27E-01	1.44E+00	7.70E-01	3.19E-01	2.38E-01	2.38E-01
	XX5264805D-B60	7.92E-16	8.91E-01	4.62E-03	3.27E-01	1.44E+00	7.70E-01	3.19E-01	2.38E-01	2.38E-01
	XX5264405D-B60	7.92E-16	8.91E-01	4.62E-03	3.27E-01	1.44E+00	7.70E-01	3.19E-01	2.38E-01	2.38E-01
	XX5264165F-75	7.92E-16	1.18E+00	6.15E-03	4.36E-01	1.92E+00	1.02E+00	4.24E-01	3.17E-01	3.17E-01
	XX5264805F-75	7.92E-16	1.18E+00	6.15E-03	4.36E-01	1.92E+00	1.02E+00	4.24E-01	3.17E-01	3.17E-01
	XX5264405F-75	7.92E-16	1.18E+00	6.15E-03	4.36E-01	1.92E+00	1.02E+00	4.24E-01	3.17E-01	3.17E-01
	XX5264165F-A60	7.92E-16	8.91E-01	4.62E-03	3.27E-01	1.44E+00	7.70E-01	3.19E-01	2.38E-01	2.38E-01
	XX5264805F-A60	7.92E-16	8.91E-01	4.62E-03	3.27E-01	1.44E+00	7.70E-01	3.19E-01	2.38E-01	2.38E-01
	XX5264405F-A60	7.92E-16	8.91E-01	4.62E-03	3.27E-01	1.44E+00	7.70E-01	3.19E-01	2.38E-01	2.38E-01
	XX5264165F-B60	7.92E-16	8.91E-01	4.62E-03	3.27E-01	1.44E+00	7.70E-01	3.19E-01	2.38E-01	2.38E-01
	XX5264805F-B60	7.92E-16	8.91E-01	4.62E-03	3.27E-01	1.44E+00	7.70E-01	3.19E-01	2.38E-01	2.38E-01
	XX5264405F-B60	7.92E-16	8.91E-01	4.62E-03	3.27E-01	1.44E+00	7.70E-01	3.19E-01	2.38E-01	2.38E-01
C	Comercial Product	8.49E-17	1.00E+00	5.56E-04	3.94E-02	1.73E-01	9.26E-02	3.83E-02	2.87E-02	2.86E-02
	XXX0364404-68	8.49E-17	1.05E+00	5.83E-04	4.13E-02	1.82E-01	9.71E-02	4.02E-02	3.01E-02	3.00E-02
	XXX0364404-75A	8.49E-17	9.30E-01	5.17E-04	3.66E-02	1.61E-01	8.61E-02	3.57E-02	2.67E-02	2.66E-02
	XXX0364404-260	8.49E-17	6.99E-01	3.89E-04	2.75E-02	1.21E-01	6.47E-02	2.68E-02	2.00E-02	2.00E-02

table C.2 - Calculated SERs in a 100 Gb system over Annapolis with DRAMs from vendors C, D, E, and F (fails/hr)

Point #	1	2	3	4	5	6	7
Description	ANNAPOLIS	ANNAPOLIS	ANNAPOLIS	ANNAPOLIS	ANNAPOLIS	ANNAPOLIS	ANNAPOLIS
Latitude (N)	39	39	39	39	39	39	39
Longitude (E)	283.5	283.5	283.5	283.5	283.5	283.5	283.5
Altitude (ft)	0	20000	40000	60000	80000	100000	120000
Cutoff (GV)	3.3	3.3	3.3	3.3	3.3	3.3	3.3
Φ_T(nuc/cm2s)	1.33E-02	9.38E-01	4.13E+00	2.21E+00	9.13E-01	6.83E-01	6.82E-01

	DRAMS	Vendor Sum	Scaling Factor	SER	SER	SER	SER	SER	SER	SER
C	XXX0364404-360	8.49E-17	6.99E-01	3.89E-04	2.75E-02	1.21E-01	6.47E-02	2.68E-02	2.00E-02	2.00E-02
	XXX0364404-10	8.49E-17	6.99E-01	3.89E-04	2.75E-02	1.21E-01	6.47E-02	2.68E-02	2.00E-02	2.00E-02
	XXX0364804-68	8.49E-17	1.05E+00	5.83E-04	4.13E-02	1.82E-01	9.71E-02	4.02E-02	3.01E-02	3.00E-02
	XXX0364804-75A	8.49E-17	9.30E-01	5.17E-04	3.66E-02	1.61E-01	8.61E-02	3.57E-02	2.67E-02	2.66E-02
	XXX0364804-260	8.49E-17	6.99E-01	3.89E-04	2.75E-02	1.21E-01	6.47E-02	2.68E-02	2.00E-02	2.00E-02
	XXX0364804-360	8.49E-17	6.99E-01	3.89E-04	2.75E-02	1.21E-01	6.47E-02	2.68E-02	2.00E-02	2.00E-02
	XXX0364804-10	8.49E-17	6.99E-01	3.89E-04	2.75E-02	1.21E-01	6.47E-02	2.68E-02	2.00E-02	2.00E-02
	XXX0364164-68	8.49E-17	1.05E+00	5.83E-04	4.13E-02	1.82E-01	9.71E-02	4.02E-02	3.01E-02	3.00E-02
	XXX0364164-75A	8.49E-17	9.30E-01	5.17E-04	3.66E-02	1.61E-01	8.61E-02	3.57E-02	2.67E-02	2.66E-02
	XXX0364164-260	8.49E-17	6.99E-01	3.89E-04	2.75E-02	1.21E-01	6.47E-02	2.68E-02	2.00E-02	2.00E-02
	XXX0364164-360	8.49E-17	6.99E-01	3.89E-04	2.75E-02	1.21E-01	6.47E-02	2.68E-02	2.00E-02	2.00E-02
	XXX0364164-10	8.49E-17	6.99E-01	3.89E-04	2.75E-02	1.21E-01	6.47E-02	2.68E-02	2.00E-02	2.00E-02
D	XX48LC16M4A2TG	1.84E-15	1.00E+00	1.20E-02	8.52E-01	3.75E+00	2.00E+00	8.29E-01	6.20E-01	6.19E-01
	XX48LC16M4A2TG-7G	1.84E-15	1.00E+00	1.20E-02	8.52E-01	3.75E+00	2.00E+00	8.29E-01	6.20E-01	6.19E-01
	XX48LC8M8A2TG-7G	1.84E-15	1.00E+00	1.20E-02	8.52E-01	3.75E+00	2.00E+00	8.29E-01	6.20E-01	6.19E-01
	XX48LC4M16A2TG-7G	1.84E-15	1.00E+00	1.20E-02	8.52E-01	3.75E+00	2.00E+00	8.29E-01	6.20E-01	6.19E-01
	XX48LC16M4A2TG-75	1.84E-15	9.30E-01	1.12E-02	7.92E-01	3.49E+00	1.86E+00	7.71E-01	5.76E-01	5.76E-01
	XX48LC8M8A2TG-75	1.84E-15	9.30E-01	1.12E-02	7.92E-01	3.49E+00	1.86E+00	7.71E-01	5.76E-01	5.76E-01
	XX48LC4M16A2TG-75	1.84E-15	9.30E-01	1.12E-02	7.92E-01	3.49E+00	1.86E+00	7.71E-01	5.76E-01	5.76E-01
	XX48LC16M4A2TG-8E	1.84E-15	8.74E-01	1.05E-02	7.45E-01	3.28E+00	1.75E+00	7.25E-01	5.42E-01	5.42E-01
	XX48LC8M8A2TG-8E	1.84E-15	8.74E-01	1.05E-02	7.45E-01	3.28E+00	1.75E+00	7.25E-01	5.42E-01	5.42E-01
	XX48LC4M16A2TG-8E	1.84E-15	8.74E-01	1.05E-02	7.45E-01	3.28E+00	1.75E+00	7.25E-01	5.42E-01	5.42E-01
	XX48LC2M32B2TG-6	1.84E-15	1.16E+00	1.40E-02	9.89E-01	4.35E+00	2.32E+00	9.63E-01	7.19E-01	7.19E-01
	XX48LC2M32B2TG-7	1.84E-15	1.00E+00	1.20E-02	8.52E-01	3.75E+00	2.00E+00	8.29E-01	6.20E-01	6.19E-01
	XX48LC2M32B2TG-8	1.84E-15	8.74E-01	1.05E-02	7.45E-01	3.28E+00	1.75E+00	7.25E-01	5.42E-01	5.42E-01
E	X456444IGS	9.54E-15	1.00E+00	6.25E-02	4.43E+00	1.95E+01	1.04E+01	4.31E+00	3.22E+00	3.22E+00
	XXX4564441G5-A80	9.54E-15	1.00E+00	6.25E-02	4.43E+00	1.95E+01	1.04E+01	4.31E+00	3.22E+00	3.22E+00
	XXX4564441G5-A10	9.54E-15	1.00E+00	6.25E-02	4.43E+00	1.95E+01	1.04E+01	4.31E+00	3.22E+00	3.22E+00
	XXX4564441G5-A10B	9.54E-15	1.00E+00	6.25E-02	4.43E+00	1.95E+01	1.04E+01	4.31E+00	3.22E+00	3.22E+00
	XXX4564841G5-A80	9.54E-15	8.00E-01	5.00E-02	3.54E+00	1.56E+01	8.32E+00	3.45E+00	2.58E+00	2.58E+00
	XXX4564841G5-A10	9.54E-15	8.00E-01	5.00E-02	3.54E+00	1.56E+01	8.32E+00	3.45E+00	2.58E+00	2.58E+00
	XXX4564841G5-A10B	9.54E-15	8.00E-01	5.00E-02	3.54E+00	1.56E+01	8.32E+00	3.45E+00	2.58E+00	2.58E+00
	XXX4564163G5-A80	9.54E-15	8.00E-01	5.00E-02	3.54E+00	1.56E+01	8.32E+00	3.45E+00	2.58E+00	2.58E+00
	XXX4564163G5-A10	9.54E-15	8.00E-01	5.00E-02	3.54E+00	1.56E+01	8.32E+00	3.45E+00	2.58E+00	2.58E+00
	XXX4564163G5-A10B	9.54E-15	8.00E-01	5.00E-02	3.54E+00	1.56E+01	8.32E+00	3.45E+00	2.58E+00	2.58E+00
	XXX4564323G5-A80	9.54E-15	1.01E+00	6.32E-02	4.48E+00	1.97E+01	1.05E+01	4.36E+00	3.26E+00	3.26E+00
	XXX4564323G5-A10	9.54E-15	8.09E-01	5.06E-02	3.58E+00	1.58E+01	8.42E+00	3.49E+00	2.61E+00	2.60E+00
	XXX4564323G5-A10B	9.54E-15	8.09E-01	5.06E-02	3.58E+00	1.58E+01	8.42E+00	3.49E+00	2.61E+00	2.60E+00
F	XX-59S6404FT-10	3.82E-16	1.00E+00	2.50E-03	1.77E-01	7.80E-01	4.16E-01	1.72E-01	1.29E-01	1.29E-01
	XX59S6416BF-80	3.82E-16	1.25E+00	3.13E-03	2.21E-01	9.75E-01	5.20E-01	2.16E-01	1.61E-01	1.61E-01
	XX59S6408BF-80	3.82E-16	1.25E+00	3.13E-03	2.21E-01	9.75E-01	5.20E-01	2.16E-01	1.61E-01	1.61E-01
	XX59S6404BF-80	3.82E-16	1.25E+00	3.13E-03	2.21E-01	9.75E-01	5.20E-01	2.16E-01	1.61E-01	1.61E-01
	XX59S6416BF-10	3.82E-16	1.00E+00	2.50E-03	1.77E-01	7.80E-01	4.16E-01	1.72E-01	1.29E-01	1.29E-01
	XX59S6408BF-10	3.82E-16	1.00E+00	2.50E-03	1.77E-01	7.80E-01	4.16E-01	1.72E-01	1.29E-01	1.29E-01
	XX59S6404BF-10	3.82E-16	1.00E+00	2.50E-03	1.77E-01	7.80E-01	4.16E-01	1.72E-01	1.29E-01	1.29E-01
	XX59S6416CF-75	3.82E-16	1.33E+00	3.33E-03	2.36E-01	1.04E+00	5.54E-01	2.29E-01	1.71E-01	1.71E-01
	XX59S6408CF-75	3.82E-16	1.33E+00	3.33E-03	2.36E-01	1.04E+00	5.54E-01	2.29E-01	1.71E-01	1.71E-01
	XX59S6404CF-75	3.82E-16	1.33E+00	3.33E-03	2.36E-01	1.04E+00	5.54E-01	2.29E-01	1.71E-01	1.71E-01
	XX59S6416CF-80	3.82E-16	1.25E+00	3.13E-03	2.21E-01	9.75E-01	5.20E-01	2.16E-01	1.61E-01	1.61E-01
	XX59S6408CF-80	3.82E-16	1.25E+00	3.13E-03	2.21E-01	9.75E-01	5.20E-01	2.16E-01	1.61E-01	1.61E-01
	XX59S6404CF-80	3.82E-16	1.25E+00	3.13E-03	2.21E-01	9.75E-01	5.20E-01	2.16E-01	1.61E-01	1.61E-01
	XX59S6416CF-10	3.82E-16	1.00E+00	2.50E-03	1.77E-01	7.80E-01	4.16E-01	1.72E-01	1.29E-01	1.29E-01
	XX59S6408CF-10	3.82E-16	1.00E+00	2.50E-03	1.77E-01	7.80E-01	4.16E-01	1.72E-01	1.29E-01	1.29E-01
	XX59S6404CF-10	3.82E-16	1.00E+00	2.50E-03	1.77E-01	7.80E-01	4.16E-01	1.72E-01	1.29E-01	1.29E-01
	XX59S6432CFT-54	3.82E-16	1.85E+00	4.63E-03	3.28E-01	1.44E+00	7.71E-01	3.19E-01	2.39E-01	2.39E-01
	XX59S6432CFT-60	3.82E-16	1.67E+00	4.17E-03	2.95E-01	1.30E+00	6.94E-01	2.87E-01	2.15E-01	2.15E-01
	XX59S6432CFT-70	3.82E-16	1.43E+00	3.57E-03	2.53E-01	1.11E+00	5.95E-01	2.46E-01	1.84E-01	1.84E-01
	XX59S6432CFT-80	3.82E-16	1.25E+00	3.13E-03	2.21E-01	9.75E-01	5.20E-01	2.16E-01	1.61E-01	1.61E-01
	XX59S6432CFT-10	3.82E-16	1.00E+00	2.50E-03	1.77E-01	7.80E-01	4.16E-01	1.72E-01	1.29E-01	1.29E-01

table C.3 - Calculated SERs in a 100 Gb system over Annapolis, the magnetic poles, and BOMBAY with DRAMs from Vendors A, B, and C (fails/hr)

Point #	8	9	10	11	12	13	14
Description	ANNAPOLIS	ANNAPOLIS	ANNAPOLIS	MAG. POLE	MAG. POLE	BOMBAY	BOMBAY
Latitude (N)	39	39	39	90	90	19	19
Longitude (E)	283.5	283.5	283.5	N/A	N/A	72.8	72.8
Altitude (ft)	140000	160000	180000	0	46,000	0	46,000
Cutoff (GV)	3.3	3.3	3.3	0	0	16.3	16.3
Φ_T(nuc/cm2s)	7.04E-01	7.20E-01	7.30E-01	1.32E-02	4.29E+00	7.37E-03	2.33E-01

	DRAMS	Vendor Sum	Scaling Factor	SER	SER	SER	SER	SER	SER	SER
A	XX81164442A-10	3.03E-16	1.00E+00	1.05E-01	1.08E-01	1.09E-01	1.98E-03	6.43E-01	1.10E-03	3.50E-02
	XX81F64842D-75	3.03E-16	1.33E+00	1.40E-01	1.43E-01	1.46E-01	2.63E-03	8.56E-01	1.47E-03	4.65E-02
	XX81F64842D-102	3.03E-16	1.00E+00	1.05E-01	1.08E-01	1.09E-01	1.98E-03	6.43E-01	1.10E-03	3.50E-02
	XX81F64842D-102L	3.03E-16	1.00E+00	1.05E-01	1.08E-01	1.09E-01	1.98E-03	6.43E-01	1.10E-03	3.50E-02
	XX81F64842C-102	3.03E-16	1.00E+00	1.05E-01	1.08E-01	1.09E-01	1.98E-03	6.43E-01	1.10E-03	3.50E-02
	XX81F64842C-103	3.03E-16	1.00E+00	1.05E-01	1.08E-01	1.09E-01	1.98E-03	6.43E-01	1.10E-03	3.50E-02
	XX81F64842C-102L	3.03E-16	1.00E+00	1.05E-01	1.08E-01	1.09E-01	1.98E-03	6.43E-01	1.10E-03	3.50E-02
	XX81F64842C-103L	3.03E-16	1.00E+00	1.05E-01	1.08E-01	1.09E-01	1.98E-03	6.43E-01	1.10E-03	3.50E-02
	XX81F64442D-75	3.03E-16	1.33E+00	1.40E-01	1.43E-01	1.46E-01	2.63E-03	8.56E-01	1.47E-03	4.65E-02
	XX81F64442D-102	3.03E-16	1.00E+00	1.05E-01	1.08E-01	1.09E-01	1.98E-03	6.43E-01	1.10E-03	3.50E-02
	XX81F64442D-102L	3.03E-16	1.00E+00	1.05E-01	1.08E-01	1.09E-01	1.98E-03	6.43E-01	1.10E-03	3.50E-02
	XX81F64442C-102	3.03E-16	1.00E+00	1.05E-01	1.08E-01	1.09E-01	1.98E-03	6.43E-01	1.10E-03	3.50E-02
	XX81F64442C-103	3.03E-16	1.00E+00	1.05E-01	1.08E-01	1.09E-01	1.98E-03	6.43E-01	1.10E-03	3.50E-02
	XX81F64442C-102L	3.03E-16	1.00E+00	1.05E-01	1.08E-01	1.09E-01	1.98E-03	6.43E-01	1.10E-03	3.50E-02
	XX81F64442C-103L	3.03E-16	1.00E+00	1.05E-01	1.08E-01	1.09E-01	1.98E-03	6.43E-01	1.10E-03	3.50E-02
	XX81F643242B-70	3.03E-16	1.43E+00	1.51E-01	1.54E-01	1.56E-01	2.83E-03	9.20E-01	1.58E-03	5.00E-02
	XX81F643242B-80	3.03E-16	1.25E+00	1.32E-01	1.35E-01	1.37E-01	2.47E-03	8.04E-01	1.38E-03	4.37E-02
	XX81F643242B-10	3.03E-16	1.00E+00	1.05E-01	1.08E-01	1.09E-01	1.98E-03	6.43E-01	1.10E-03	3.50E-02
	XX81F643242B-70L	3.03E-16	1.43E+00	1.51E-01	1.54E-01	1.56E-01	2.83E-03	9.20E-01	1.58E-03	5.00E-02
	XX81F643242B-80L	3.03E-16	1.25E+00	1.32E-01	1.35E-01	1.37E-01	2.47E-03	8.04E-01	1.38E-03	4.37E-02
	XX81F643242B-10L	3.03E-16	1.00E+00	1.05E-01	1.08E-01	1.09E-01	1.98E-03	6.43E-01	1.10E-03	3.50E-02
	XX81F643242B-60	3.03E-16	1.67E+00	1.76E-01	1.80E-01	1.83E-01	3.30E-03	1.07E+00	1.85E-03	5.84E-02
	XX81F641642D-75	3.03E-16	1.33E+00	1.40E-01	1.43E-01	1.46E-01	2.63E-03	8.56E-01	1.47E-03	4.65E-02
	XX81F641642D-102	3.03E-16	1.00E+00	1.05E-01	1.08E-01	1.09E-01	1.98E-03	6.43E-01	1.10E-03	3.50E-02
	XX81F641642D-102L	3.03E-16	1.00E+00	1.05E-01	1.08E-01	1.09E-01	1.98E-03	6.43E-01	1.10E-03	3.50E-02
	XX81F641642C-102	3.03E-16	1.00E+00	1.05E-01	1.08E-01	1.09E-01	1.98E-03	6.43E-01	1.10E-03	3.50E-02
	XX81F641642C-103	3.03E-16	1.00E+00	1.05E-01	1.08E-01	1.09E-01	1.98E-03	6.43E-01	1.10E-03	3.50E-02
	XX81F641642C-102L	3.03E-16	1.00E+00	1.05E-01	1.08E-01	1.09E-01	1.98E-03	6.43E-01	1.10E-03	3.50E-02
	XX81F641642C-103	3.03E-16	1.00E+00	1.05E-01	1.08E-01	1.09E-01	1.98E-03	6.43E-01	1.10E-03	3.50E-02
	XX811L643242B-12	3.03E-16	2.23E+00	2.35E-01	2.40E-01	2.44E-01	4.40E-03	1.43E+00	2.46E-03	7.78E-02
	XX811L643242B-10	3.03E-16	1.87E+00	1.97E-01	2.02E-01	2.05E-01	3.70E-03	1.20E+00	2.07E-03	6.54E-02
	XX811L643242B-15	3.03E-16	1.49E+00	1.57E-01	1.61E-01	1.63E-01	2.95E-03	9.59E-01	1.65E-03	5.21E-02
	XX811L643242B-10L	3.03E-16	2.23E+00	2.35E-01	2.40E-01	2.44E-01	4.40E-03	1.43E+00	2.46E-03	7.78E-02
	XX811L643242B-12L	3.03E-16	1.87E+00	1.97E-01	2.02E-01	2.05E-01	3.70E-03	1.20E+00	2.07E-03	6.54E-02
	XX811L643242B-15L	3.03E-16	1.49E+00	1.57E-01	1.61E-01	1.63E-01	2.95E-03	9.59E-01	1.65E-03	5.21E-02
B	XX-5165805AJ6	7.92E-16	1.00E+00	2.76E-01	2.82E-01	2.86E-01	5.17E-03	1.68E+00	2.89E-03	9.14E-02
	XX5264165D	7.92E-16	1.11E+00	3.07E-01	3.14E-01	3.19E-01	5.76E-03	1.87E+00	3.22E-03	1.02E-01
	XX5264805D	7.92E-16	1.11E+00	3.07E-01	3.14E-01	3.19E-01	5.76E-03	1.87E+00	3.22E-03	1.02E-01
	XX5264405D	7.92E-16	1.11E+00	3.07E-01	3.14E-01	3.19E-01	5.76E-03	1.87E+00	3.22E-03	1.02E-01
	XX5264165D-A60	7.92E-16	8.91E-01	2.46E-01	2.51E-01	2.55E-01	4.61E-03	1.50E+00	2.57E-03	8.14E-02
	XX5264805D-A60	7.92E-16	8.91E-01	2.46E-01	2.51E-01	2.55E-01	4.61E-03	1.50E+00	2.57E-03	8.14E-02
	XX5264405D-A60	7.92E-16	8.91E-01	2.46E-01	2.51E-01	2.55E-01	4.61E-03	1.50E+00	2.57E-03	8.14E-02
	XX5264165D-B60	7.92E-16	8.91E-01	2.46E-01	2.51E-01	2.55E-01	4.61E-03	1.50E+00	2.57E-03	8.14E-02
	XX5264805D-B60	7.92E-16	8.91E-01	2.46E-01	2.51E-01	2.55E-01	4.61E-03	1.50E+00	2.57E-03	8.14E-02
	XX5264405D-B60	7.92E-16	8.91E-01	2.46E-01	2.51E-01	2.55E-01	4.61E-03	1.50E+00	2.57E-03	8.14E-02
	XX5264165F-75	7.92E-16	1.18E+00	3.27E-01	3.34E-01	3.39E-01	6.13E-03	1.99E+00	3.42E-03	1.08E-01
	XX5264805F-75	7.92E-16	1.18E+00	3.27E-01	3.34E-01	3.39E-01	6.13E-03	1.99E+00	3.42E-03	1.08E-01
	XX5264405F-75	7.92E-16	1.18E+00	3.27E-01	3.34E-01	3.39E-01	6.13E-03	1.99E+00	3.42E-03	1.08E-01
	XX5264165F-A60	7.92E-16	8.91E-01	2.46E-01	2.51E-01	2.55E-01	4.61E-03	1.50E+00	2.57E-03	8.14E-02
	XX5264805F-A60	7.92E-16	8.91E-01	2.46E-01	2.51E-01	2.55E-01	4.61E-03	1.50E+00	2.57E-03	8.14E-02
	XX5264405F-A60	7.92E-16	8.91E-01	2.46E-01	2.51E-01	2.55E-01	4.61E-03	1.50E+00	2.57E-03	8.14E-02
	XX5264165F-B60	7.92E-16	8.91E-01	2.46E-01	2.51E-01	2.55E-01	4.61E-03	1.50E+00	2.57E-03	8.14E-02
	XX5264805F-B60	7.92E-16	8.91E-01	2.46E-01	2.51E-01	2.55E-01	4.61E-03	1.50E+00	2.57E-03	8.14E-02
	XX5264405F-B60	7.92E-16	8.91E-01	2.46E-01	2.51E-01	2.55E-01	4.61E-03	1.50E+00	2.57E-03	8.14E-02
C	Comercial Product	8.49E-17	1.00E+00	2.95E-02	3.02E-02	3.07E-02	5.54E-04	1.80E-01	3.09E-04	9.79E-03
	XXX0364404-68	8.49E-17	1.05E+00	3.10E-02	3.17E-02	3.22E-02	5.81E-04	1.89E-01	3.25E-04	1.03E-02
	XXX0364404-75A	8.49E-17	9.30E-01	2.75E-02	2.81E-02	2.85E-02	5.15E-04	1.68E-01	2.88E-04	9.11E-03
	XXX0364404-260	8.49E-17	6.99E-01	2.07E-02	2.11E-02	2.14E-02	3.88E-04	1.26E-01	2.16E-04	6.85E-03

table C.4 - Calculated SERs in a 100 Gb system over Annapolis, the magnetic poles, and BOMBA with DRAMs from vendors C, D, E, and F (fails/hr)

Point #	8	9	10	11	12	13	14
Description	ANNAPOLIS	ANNAPOLIS	ANNAPOLIS	MAG. POLE	MAG. POLE	BOMBAY	BOMBAY
Latitude (N)	39	39	39	90	90	19	19
Longitude (E)	283.5	283.5	283.5	N/A	N/A	72.8	72.8
Altitude (ft)	140000	160000	180000	0	46,000	0	46,000
Cutoff (GV)	3.3	3.3	3.3	0	0	16.3	16.3
Φ_T(nuc/cm2s)	7.04E-01	7.20E-01	7.30E-01	1.32E-02	4.29E+00	7.37E-03	2.33E-01

	DRAMS	Vendor Sum	Scaling Factor	SER	SER	SER	SER	SER	SER	SER
C	XXX0364404-360	8.49E-17	6.99E-01	2.07E-02	2.11E-02	2.14E-02	3.88E-04	1.26E-01	2.16E-04	6.85E-03
	XXX0364404-10	8.49E-17	6.99E-01	2.07E-02	2.11E-02	2.14E-02	3.88E-04	1.26E-01	2.16E-04	6.85E-03
	XXX0364804-68	8.49E-17	1.05E+00	3.10E-02	3.17E-02	3.22E-02	5.81E-04	1.89E-01	3.25E-04	1.03E-02
	XXX0364804-75A	8.49E-17	9.30E-01	2.75E-02	2.81E-02	2.85E-02	5.15E-04	1.68E-01	2.88E-04	9.11E-03
	XXX0364804-260	8.49E-17	6.99E-01	2.07E-02	2.11E-02	2.14E-02	3.88E-04	1.26E-01	2.16E-04	6.85E-03
	XXX0364804-360	8.49E-17	6.99E-01	2.07E-02	2.11E-02	2.14E-02	3.88E-04	1.26E-01	2.16E-04	6.85E-03
	XXX0364804-10	8.49E-17	6.99E-01	2.07E-02	2.11E-02	2.14E-02	3.88E-04	1.26E-01	2.16E-04	6.85E-03
	XXX0364164-68	8.49E-17	1.05E+00	3.10E-02	3.17E-02	3.22E-02	5.81E-04	1.89E-01	3.25E-04	1.03E-02
	XXX0364164-75A	8.49E-17	9.30E-01	2.75E-02	2.81E-02	2.85E-02	5.15E-04	1.68E-01	2.88E-04	9.11E-03
	XXX0364164-260	8.49E-17	6.99E-01	2.07E-02	2.11E-02	2.14E-02	3.88E-04	1.26E-01	2.16E-04	6.85E-03
	XXX0364164-360	8.49E-17	6.99E-01	2.07E-02	2.11E-02	2.14E-02	3.88E-04	1.26E-01	2.16E-04	6.85E-03
	XXX0364164-10	8.49E-17	6.99E-01	2.07E-02	2.11E-02	2.14E-02	3.88E-04	1.26E-01	2.16E-04	6.85E-03
D	XX48LC16M4A2TG	1.84E-15	1.00E+00	6.39E-01	6.53E-01	6.63E-01	1.20E-02	3.90E+00	6.69E-03	2.12E-01
	XX48LC16M4A2TG-7G	1.84E-15	1.00E+00	6.39E-01	6.53E-01	6.63E-01	1.20E-02	3.90E+00	6.69E-03	2.12E-01
	XX48LC8M8A2TG-7G	1.84E-15	1.00E+00	6.39E-01	6.53E-01	6.63E-01	1.20E-02	3.90E+00	6.69E-03	2.12E-01
	XX48LC4M16A2TG-7G	1.84E-15	1.00E+00	6.39E-01	6.53E-01	6.63E-01	1.20E-02	3.90E+00	6.69E-03	2.12E-01
	XX48LC16M4A2TG-75	1.84E-15	9.30E-01	5.94E-01	6.08E-01	6.17E-01	1.11E-02	3.63E+00	6.23E-03	1.97E-01
	XX48LC8M8A2TG-75	1.84E-15	9.30E-01	5.94E-01	6.08E-01	6.17E-01	1.11E-02	3.63E+00	6.23E-03	1.97E-01
	XX48LC4M16A2TG-75	1.84E-15	9.30E-01	5.94E-01	6.08E-01	6.17E-01	1.11E-02	3.63E+00	6.23E-03	1.97E-01
	XX48LC16M4A2TG-8E	1.84E-15	8.74E-01	5.59E-01	5.71E-01	5.80E-01	1.05E-02	3.41E+00	5.85E-03	1.85E-01
	XX48LC8M8A2TG-8E	1.84E-15	8.74E-01	5.59E-01	5.71E-01	5.80E-01	1.05E-02	3.41E+00	5.85E-03	1.85E-01
	XX48LC4M16A2TG-8E	1.84E-15	8.74E-01	5.59E-01	5.71E-01	5.80E-01	1.05E-02	3.41E+00	5.85E-03	1.85E-01
	XX48LC2M32B2TG-6	1.84E-15	1.16E+00	7.42E-01	7.58E-01	7.70E-01	1.39E-02	4.53E+00	7.77E-03	2.46E-01
	XX48LC2M32B2TG-7	1.84E-15	1.00E+00	6.39E-01	6.53E-01	6.63E-01	1.20E-02	3.90E+00	6.69E-03	2.12E-01
	XX48LC2M32B2TG-8	1.84E-15	8.74E-01	5.59E-01	5.71E-01	5.80E-01	1.05E-02	3.41E+00	5.85E-03	1.85E-01
E	X456444IGS	9.54E-15	1.00E+00	3.32E+00	3.39E+00	3.45E+00	6.23E-02	2.03E+01	3.48E-02	1.10E+00
	XXX4564441G5-A80	9.54E-15	1.00E+00	3.32E+00	3.39E+00	3.45E+00	6.23E-02	2.03E+01	3.48E-02	1.10E+00
	XXX4564441G5-A10	9.54E-15	1.00E+00	3.32E+00	3.39E+00	3.45E+00	6.23E-02	2.03E+01	3.48E-02	1.10E+00
	XXX4564441G5-A10B	9.54E-15	1.00E+00	3.32E+00	3.39E+00	3.45E+00	6.23E-02	2.03E+01	3.48E-02	1.10E+00
	XXX4564841G5-A80	9.54E-15	8.00E-01	2.66E+00	2.72E+00	2.76E+00	4.98E-02	1.62E+01	2.78E-02	8.81E-01
	XXX4564841G5-A10	9.54E-15	8.00E-01	2.66E+00	2.72E+00	2.76E+00	4.98E-02	1.62E+01	2.78E-02	8.81E-01
	XXX4564841G5-A10B	9.54E-15	8.00E-01	2.66E+00	2.72E+00	2.76E+00	4.98E-02	1.62E+01	2.78E-02	8.81E-01
	XXX4564163G5-A80	9.54E-15	8.00E-01	2.66E+00	2.72E+00	2.76E+00	4.98E-02	1.62E+01	2.78E-02	8.81E-01
	XXX4564163G5-A10	9.54E-15	8.00E-01	2.66E+00	2.72E+00	2.76E+00	4.98E-02	1.62E+01	2.78E-02	8.81E-01
	XXX4564163G5-A10B	9.54E-15	8.00E-01	2.66E+00	2.72E+00	2.76E+00	4.98E-02	1.62E+01	2.78E-02	8.81E-01
	XXX4564323G5-A80	9.54E-15	1.01E+00	3.36E+00	3.43E+00	3.48E+00	6.30E-02	2.05E+01	3.52E-02	1.11E+00
	XXX4564323G5-A10	9.54E-15	8.09E-01	2.69E+00	2.75E+00	2.79E+00	5.04E-02	1.64E+01	2.81E-02	8.91E-01
	XXX4564323G5-A10B	9.54E-15	8.09E-01	2.69E+00	2.75E+00	2.79E+00	5.04E-02	1.64E+01	2.81E-02	8.91E-01
F	XX-59S6404FT-10	3.82E-16	1.00E+00	1.33E-01	1.36E-01	1.38E-01	2.49E-03	8.11E-01	1.39E-03	4.40E-02
	XX59S6416BF-80	3.82E-16	1.25E+00	1.66E-01	1.70E-01	1.72E-01	3.12E-03	1.01E+00	1.74E-03	5.51E-02
	XX59S6408BF-80	3.82E-16	1.25E+00	1.66E-01	1.70E-01	1.72E-01	3.12E-03	1.01E+00	1.74E-03	5.51E-02
	XX59S6404BF-80	3.82E-16	1.25E+00	1.66E-01	1.70E-01	1.72E-01	3.12E-03	1.01E+00	1.74E-03	5.51E-02
	XX59S6416BF-10	3.82E-16	1.00E+00	1.33E-01	1.36E-01	1.38E-01	2.49E-03	8.11E-01	1.39E-03	4.40E-02
	XX59S6408BF-10	3.82E-16	1.00E+00	1.33E-01	1.36E-01	1.38E-01	2.49E-03	8.11E-01	1.39E-03	4.40E-02
	XX59S6404BF-10	3.82E-16	1.00E+00	1.33E-01	1.36E-01	1.38E-01	2.49E-03	8.11E-01	1.39E-03	4.40E-02
	XX59S6416CF-75	3.82E-16	1.33E+00	1.77E-01	1.81E-01	1.83E-01	3.31E-03	1.08E+00	1.85E-03	5.86E-02
	XX59S6408CF-75	3.82E-16	1.33E+00	1.77E-01	1.81E-01	1.83E-01	3.31E-03	1.08E+00	1.85E-03	5.86E-02
	XX59S6404CF-75	3.82E-16	1.33E+00	1.77E-01	1.81E-01	1.83E-01	3.31E-03	1.08E+00	1.85E-03	5.86E-02
	XX59S6416CF-80	3.82E-16	1.25E+00	1.66E-01	1.70E-01	1.72E-01	3.12E-03	1.01E+00	1.74E-03	5.51E-02
	XX59S6408CF-80	3.82E-16	1.25E+00	1.66E-01	1.70E-01	1.72E-01	3.12E-03	1.01E+00	1.74E-03	5.51E-02
	XX59S6404CF-80	3.82E-16	1.25E+00	1.66E-01	1.70E-01	1.72E-01	3.12E-03	1.01E+00	1.74E-03	5.51E-02
	XX59S6416CF-10	3.82E-16	1.00E+00	1.33E-01	1.36E-01	1.38E-01	2.49E-03	8.11E-01	1.39E-03	4.40E-02
	XX59S6408CF-10	3.82E-16	1.00E+00	1.33E-01	1.36E-01	1.38E-01	2.49E-03	8.11E-01	1.39E-03	4.40E-02
	XX59S6404CF-10	3.82E-16	1.00E+00	1.33E-01	1.36E-01	1.38E-01	2.49E-03	8.11E-01	1.39E-03	4.40E-02
	XX59S6432CFT-54	3.82E-16	1.85E+00	2.46E-01	2.52E-01	2.55E-01	4.62E-03	1.50E+00	2.58E-03	8.16E-02
	XX59S6432CFT-60	3.82E-16	1.67E+00	2.21E-01	2.26E-01	2.30E-01	4.15E-03	1.35E+00	2.32E-03	7.34E-02
	XX59S6432CFT-70	3.82E-16	1.43E+00	1.90E-01	1.94E-01	1.97E-01	3.56E-03	1.16E+00	1.99E-03	6.29E-02
	XX59S6432CFT-80	3.82E-16	1.25E+00	1.66E-01	1.70E-01	1.72E-01	3.12E-03	1.01E+00	1.74E-03	5.51E-02
	XX59S6432CFT-10	3.82E-16	1.00E+00	1.33E-01	1.36E-01	1.38E-01	2.49E-03	8.11E-01	1.39E-03	4.40E-02

table C.5 - Calculated SERs in a 100 Gb system over Los Angeles, London, and Moscow with DRAMs from Vendors A, B, and C (fails/hr)

Point #	15	16	17	18	19	20
Description	L.A.	L.A.	LONDON	LONDON	MOSCOW	MOSCOW
Latitude (N)	34	34	51.5	51.5	55.75	55.75
Longitude (E)	241.8	241.8	359.4	359.4	37.6	37.6
Altitude (ft)	0	46,000	0	46,000	0	46,000
Cutoff (GV)	6	6	5.1	5.1	2.1	2.1
Φ_T(nuc/cm2s)	1.24E-02	3.49E+00	1.29E-02	3.77E+00	1.32E-02	4.00E+00

	DRAMS	Vendor Sum	Scaling Factor	SER	SER	SER	SER	SER	SER
A	XX81164442A-10	3.03E-16	1.00E+00	1.85E-03	5.23E-01	1.94E-03	5.66E-01	1.98E-03	5.99E-01
	XX81F64842D-75	3.03E-16	1.33E+00	2.46E-03	6.96E-01	2.58E-03	7.52E-01	2.63E-03	7.97E-01
	XX81F64842D-102	3.03E-16	1.00E+00	1.85E-03	5.23E-01	1.94E-03	5.66E-01	1.98E-03	5.99E-01
	XX81F64842D-102L	3.03E-16	1.00E+00	1.85E-03	5.23E-01	1.94E-03	5.66E-01	1.98E-03	5.99E-01
	XX81F64842C-102	3.03E-16	1.00E+00	1.85E-03	5.23E-01	1.94E-03	5.66E-01	1.98E-03	5.99E-01
	XX81F64842C-103	3.03E-16	1.00E+00	1.85E-03	5.23E-01	1.94E-03	5.66E-01	1.98E-03	5.99E-01
	XX81F64842C-102L	3.03E-16	1.00E+00	1.85E-03	5.23E-01	1.94E-03	5.66E-01	1.98E-03	5.99E-01
	XX81F64842C-103L	3.03E-16	1.00E+00	1.85E-03	5.23E-01	1.94E-03	5.66E-01	1.98E-03	5.99E-01
	XX81F64442D-75	3.03E-16	1.33E+00	2.46E-03	6.96E-01	2.58E-03	7.52E-01	2.63E-03	7.97E-01
	XX81F64442D-102	3.03E-16	1.00E+00	1.85E-03	5.23E-01	1.94E-03	5.66E-01	1.98E-03	5.99E-01
	XX81F64442D-102L	3.03E-16	1.00E+00	1.85E-03	5.23E-01	1.94E-03	5.66E-01	1.98E-03	5.99E-01
	XX81F64442C-102	3.03E-16	1.00E+00	1.85E-03	5.23E-01	1.94E-03	5.66E-01	1.98E-03	5.99E-01
	XX81F64442C-103	3.03E-16	1.00E+00	1.85E-03	5.23E-01	1.94E-03	5.66E-01	1.98E-03	5.99E-01
	XX81F64442C-102L	3.03E-16	1.00E+00	1.85E-03	5.23E-01	1.94E-03	5.66E-01	1.98E-03	5.99E-01
	XX81F64442C-103L	3.03E-16	1.00E+00	1.85E-03	5.23E-01	1.94E-03	5.66E-01	1.98E-03	5.99E-01
	XX81F643242B-70	3.03E-16	1.43E+00	2.65E-03	7.48E-01	2.77E-03	8.09E-01	2.83E-03	8.56E-01
	XX81F643242B-80	3.03E-16	1.25E+00	2.31E-03	6.54E-01	2.42E-03	7.07E-01	2.47E-03	7.49E-01
	XX81F643242B-10	3.03E-16	1.00E+00	1.85E-03	5.23E-01	1.94E-03	5.66E-01	1.98E-03	5.99E-01
	XX81F643242B-70L	3.03E-16	1.43E+00	2.65E-03	7.48E-01	2.77E-03	8.09E-01	2.83E-03	8.56E-01
	XX81F643242B-80L	3.03E-16	1.25E+00	2.31E-03	6.54E-01	2.42E-03	7.07E-01	2.47E-03	7.49E-01
	XX81F643242B-10L	3.03E-16	1.00E+00	1.85E-03	5.23E-01	1.94E-03	5.66E-01	1.98E-03	5.99E-01
	XX81F643242B-60	3.03E-16	1.67E+00	3.09E-03	8.74E-01	3.24E-03	9.45E-01	3.31E-03	1.00E+00
	XX81F641642D-75	3.03E-16	1.33E+00	2.46E-03	6.96E-01	2.58E-03	7.52E-01	2.63E-03	7.97E-01
	XX81F641642D-102	3.03E-16	1.00E+00	1.85E-03	5.23E-01	1.94E-03	5.66E-01	1.98E-03	5.99E-01
	XX81F641642D-102L	3.03E-16	1.00E+00	1.85E-03	5.23E-01	1.94E-03	5.66E-01	1.98E-03	5.99E-01
	XX81F641642C-102	3.03E-16	1.00E+00	1.85E-03	5.23E-01	1.94E-03	5.66E-01	1.98E-03	5.99E-01
	XX81F641642C-103	3.03E-16	1.00E+00	1.85E-03	5.23E-01	1.94E-03	5.66E-01	1.98E-03	5.99E-01
	XX81F641642C-102L	3.03E-16	1.00E+00	1.85E-03	5.23E-01	1.94E-03	5.66E-01	1.98E-03	5.99E-01
	XX81F641642C-103	3.03E-16	1.00E+00	1.85E-03	5.23E-01	1.94E-03	5.66E-01	1.98E-03	5.99E-01
	XX811L643242B-12	3.03E-16	2.23E+00	4.12E-03	1.16E+00	4.31E-03	1.26E+00	4.41E-03	1.33E+00
	XX811L643242B-10	3.03E-16	1.87E+00	3.46E-03	9.78E-01	3.62E-03	1.06E+00	3.70E-03	1.12E+00
	XX811L643242B-15	3.03E-16	1.49E+00	2.76E-03	7.80E-01	2.89E-03	8.43E-01	2.95E-03	8.93E-01
	XX811L643242B-10L	3.03E-16	2.23E+00	4.12E-03	1.16E+00	4.31E-03	1.26E+00	4.41E-03	1.33E+00
	XX811L643242B-12L	3.03E-16	1.87E+00	3.46E-03	9.78E-01	3.62E-03	1.06E+00	3.70E-03	1.12E+00
	XX811L643242B-15L	3.03E-16	1.49E+00	2.76E-03	7.80E-01	2.89E-03	8.43E-01	2.95E-03	8.93E-01
B	XX-5165805AJ6	7.92E-16	1.00E+00	4.84E-03	1.37E+00	5.07E-03	1.48E+00	5.17E-03	1.57E+00
	XX5264165D	7.92E-16	1.11E+00	5.39E-03	1.52E+00	5.64E-03	1.65E+00	5.76E-03	1.74E+00
	XX5264805D	7.92E-16	1.11E+00	5.39E-03	1.52E+00	5.64E-03	1.65E+00	5.76E-03	1.74E+00
	XX5264405D	7.92E-16	1.11E+00	5.39E-03	1.52E+00	5.64E-03	1.65E+00	5.76E-03	1.74E+00
	XX5264165D-A60	7.92E-16	8.91E-01	4.31E-03	1.22E+00	4.51E-03	1.32E+00	4.61E-03	1.39E+00
	XX5264805D-A60	7.92E-16	8.91E-01	4.31E-03	1.22E+00	4.51E-03	1.32E+00	4.61E-03	1.39E+00
	XX5264405D-A60	7.92E-16	8.91E-01	4.31E-03	1.22E+00	4.51E-03	1.32E+00	4.61E-03	1.39E+00
	XX5264165D-B60	7.92E-16	8.91E-01	4.31E-03	1.22E+00	4.51E-03	1.32E+00	4.61E-03	1.39E+00
	XX5264805D-B60	7.92E-16	8.91E-01	4.31E-03	1.22E+00	4.51E-03	1.32E+00	4.61E-03	1.39E+00
	XX5264405D-B60	7.92E-16	8.91E-01	4.31E-03	1.22E+00	4.51E-03	1.32E+00	4.61E-03	1.39E+00
	XX5264165F-75	7.92E-16	1.18E+00	5.73E-03	1.62E+00	6.00E-03	1.75E+00	6.13E-03	1.85E+00
	XX5264805F-75	7.92E-16	1.18E+00	5.73E-03	1.62E+00	6.00E-03	1.75E+00	6.13E-03	1.85E+00
	XX5264405F-75	7.92E-16	1.18E+00	5.73E-03	1.62E+00	6.00E-03	1.75E+00	6.13E-03	1.85E+00
	XX5264165F-A60	7.92E-16	8.91E-01	4.31E-03	1.22E+00	4.51E-03	1.32E+00	4.61E-03	1.39E+00
	XX5264805F-A60	7.92E-16	8.91E-01	4.31E-03	1.22E+00	4.51E-03	1.32E+00	4.61E-03	1.39E+00
	XX5264405F-A60	7.92E-16	8.91E-01	4.31E-03	1.22E+00	4.51E-03	1.32E+00	4.61E-03	1.39E+00
	XX5264165F-B60	7.92E-16	8.91E-01	4.31E-03	1.22E+00	4.51E-03	1.32E+00	4.61E-03	1.39E+00
	XX5264805F-B60	7.92E-16	8.91E-01	4.31E-03	1.22E+00	4.51E-03	1.32E+00	4.61E-03	1.39E+00
	XX5264405F-B60	7.92E-16	8.91E-01	4.31E-03	1.22E+00	4.51E-03	1.32E+00	4.61E-03	1.39E+00
C	Comercial Product	8.49E-17	1.00E+00	5.18E-04	1.47E-01	5.43E-04	1.58E-01	5.55E-04	1.68E-01
	XXX0364404-68	8.49E-17	1.05E+00	5.44E-04	1.54E-01	5.70E-04	1.66E-01	5.82E-04	1.76E-01
	XXX0364404-75A	8.49E-17	9.30E-01	4.82E-04	1.36E-01	5.05E-04	1.47E-01	5.16E-04	1.56E-01
	XXX0364404-260	8.49E-17	6.99E-01	3.63E-04	1.03E-01	3.80E-04	1.11E-01	3.88E-04	1.17E-01

table C.6 - Calculated SERs in a 100 Gb system over Los Angeles, London, and Moscow with DRAMs from Vendors C, D, E, and F (fails/hr)

Point #	15	16	17	18	19	20
Description	L.A.	L.A.	LONDON	LONDON	MOSCOW	MOSCOW
Latitude (N)	34	34	51.5	51.5	55.75	55.75
Longitude (E)	241.8	241.8	359.4	359.4	37.6	37.6
Altitude (ft)	0	46,000	0	46,000	0	46,000
Cutoff (GV)	6	6	5.1	5.1	2.1	2.1
Φr(nuc/cm2s)	1.24E-02	3.49E+00	1.29E-02	3.77E+00	1.32E-02	4.00E+00

	DRAMS	Vendor Sum	Scaling Factor	SER	SER	SER	SER	SER	SER
C	XXX0364404-360	8.49E-17	6.99E-01	3.63E-04	1.03E-01	3.80E-04	1.11E-01	3.88E-04	1.17E-01
	XXX0364404-10	8.49E-17	6.99E-01	3.63E-04	1.03E-01	3.80E-04	1.11E-01	3.88E-04	1.17E-01
	XXX0364804-68	8.49E-17	1.05E+00	5.44E-04	1.54E-01	5.70E-04	1.66E-01	5.82E-04	1.76E-01
	XXX0364804-75A	8.49E-17	9.30E-01	4.82E-04	1.36E-01	5.05E-04	1.47E-01	5.16E-04	1.56E-01
	XXX0364804-260	8.49E-17	6.99E-01	3.63E-04	1.03E-01	3.80E-04	1.11E-01	3.88E-04	1.17E-01
	XXX0364804-360	8.49E-17	6.99E-01	3.63E-04	1.03E-01	3.80E-04	1.11E-01	3.88E-04	1.17E-01
	XXX0364804-10	8.49E-17	6.99E-01	3.63E-04	1.03E-01	3.80E-04	1.11E-01	3.88E-04	1.17E-01
	XXX0364164-68	8.49E-17	1.05E+00	5.44E-04	1.54E-01	5.70E-04	1.66E-01	5.82E-04	1.76E-01
	XXX0364164-75A	8.49E-17	9.30E-01	4.82E-04	1.36E-01	5.05E-04	1.47E-01	5.16E-04	1.56E-01
	XXX0364164-260	8.49E-17	6.99E-01	3.63E-04	1.03E-01	3.80E-04	1.11E-01	3.88E-04	1.17E-01
	XXX0364164-360	8.49E-17	6.99E-01	3.63E-04	1.03E-01	3.80E-04	1.11E-01	3.88E-04	1.17E-01
	XXX0364164-10	8.49E-17	6.99E-01	3.63E-04	1.03E-01	3.80E-04	1.11E-01	3.88E-04	1.17E-01
D	XX48LC16M4A2TG	1.84E-15	1.00E+00	1.12E-02	3.17E+00	1.17E-02	3.43E+00	1.20E-02	3.63E+00
	XX48LC16M4A2TG-7G	1.84E-15	1.00E+00	1.12E-02	3.17E+00	1.17E-02	3.43E+00	1.20E-02	3.63E+00
	XX48LC8M8A2TG-7G	1.84E-15	1.00E+00	1.12E-02	3.17E+00	1.17E-02	3.43E+00	1.20E-02	3.63E+00
	XX48LC4M16A2TG-7G	1.84E-15	1.00E+00	1.12E-02	3.17E+00	1.17E-02	3.43E+00	1.20E-02	3.63E+00
	XX48LC16M4A2TG-75	1.84E-15	9.30E-01	1.04E-02	2.95E+00	1.09E-02	3.19E+00	1.12E-02	3.37E+00
	XX48LC8M8A2TG-75	1.84E-15	9.30E-01	1.04E-02	2.95E+00	1.09E-02	3.19E+00	1.12E-02	3.37E+00
	XX48LC4M16A2TG-75	1.84E-15	9.30E-01	1.04E-02	2.95E+00	1.09E-02	3.19E+00	1.12E-02	3.37E+00
	XX48LC16M4A2TG-8E	1.84E-15	8.74E-01	9.80E-03	2.77E+00	1.03E-02	3.00E+00	1.05E-02	3.17E+00
	XX48LC8M8A2TG-8E	1.84E-15	8.74E-01	9.80E-03	2.77E+00	1.03E-02	3.00E+00	1.05E-02	3.17E+00
	XX48LC4M16A2TG-8E	1.84E-15	8.74E-01	9.80E-03	2.77E+00	1.03E-02	3.00E+00	1.05E-02	3.17E+00
	XX48LC2M32B2TG-6	1.84E-15	1.16E+00	1.30E-02	3.68E+00	1.36E-02	3.98E+00	1.39E-02	4.21E+00
	XX48LC2M32B2TG-7	1.84E-15	1.00E+00	1.12E-02	3.17E+00	1.17E-02	3.43E+00	1.20E-02	3.63E+00
	XX48LC2M32B2TG-8	1.84E-15	8.74E-01	9.80E-03	2.77E+00	1.03E-02	3.00E+00	1.05E-02	3.17E+00
E	D456444IGS	9.54E-15	1.00E+00	5.83E-02	1.65E+01	6.10E-02	1.78E+01	6.23E-02	1.89E+01
	XXX4564441G5-A80	9.54E-15	1.00E+00	5.83E-02	1.65E+01	6.10E-02	1.78E+01	6.23E-02	1.89E+01
	XXX4564441G5-A10	9.54E-15	1.00E+00	5.83E-02	1.65E+01	6.10E-02	1.78E+01	6.23E-02	1.89E+01
	XXX4564441G5-A10B	9.54E-15	1.00E+00	5.83E-02	1.65E+01	6.10E-02	1.78E+01	6.23E-02	1.89E+01
	XXX4564841G5-A80	9.54E-15	8.00E-01	4.66E-02	1.32E+01	4.88E-02	1.42E+01	4.99E-02	1.51E+01
	XXX4564841G5-A10	9.54E-15	8.00E-01	4.66E-02	1.32E+01	4.88E-02	1.42E+01	4.99E-02	1.51E+01
	XXX4564841G5-A10B	9.54E-15	8.00E-01	4.66E-02	1.32E+01	4.88E-02	1.42E+01	4.99E-02	1.51E+01
	XXX4564163G5-A80	9.54E-15	8.00E-01	4.66E-02	1.32E+01	4.88E-02	1.42E+01	4.99E-02	1.51E+01
	XXX4564163G5-A10	9.54E-15	8.00E-01	4.66E-02	1.32E+01	4.88E-02	1.42E+01	4.99E-02	1.51E+01
	XXX4564163G5-A10B	9.54E-15	8.00E-01	4.66E-02	1.32E+01	4.88E-02	1.42E+01	4.99E-02	1.51E+01
	XXX4564323G5-A80	9.54E-15	1.01E+00	5.89E-02	1.67E+01	6.17E-02	1.80E+01	6.30E-02	1.91E+01
	XXX4564323G5-A10	9.54E-15	8.09E-01	4.71E-02	1.33E+01	4.94E-02	1.44E+01	5.04E-02	1.53E+01
	XXX4564323G5-A10B	9.54E-15	8.09E-01	4.71E-02	1.33E+01	4.94E-02	1.44E+01	5.04E-02	1.53E+01
F	XX-59S6404FT-10	3.82E-16	1.00E+00	2.33E-03	6.59E-01	2.44E-03	7.13E-01	2.49E-03	7.54E-01
	XX59S6416BF-80	3.82E-16	1.25E+00	2.91E-03	8.24E-01	3.05E-03	8.91E-01	3.12E-03	9.43E-01
	XX59S6408BF-80	3.82E-16	1.25E+00	2.91E-03	8.24E-01	3.05E-03	8.91E-01	3.12E-03	9.43E-01
	XX59S6404BF-80	3.82E-16	1.25E+00	2.91E-03	8.24E-01	3.05E-03	8.91E-01	3.12E-03	9.43E-01
	XX59S6416BF-10	3.82E-16	1.00E+00	2.33E-03	6.59E-01	2.44E-03	7.13E-01	2.49E-03	7.54E-01
	XX59S6408BF-10	3.82E-16	1.00E+00	2.33E-03	6.59E-01	2.44E-03	7.13E-01	2.49E-03	7.54E-01
	XX59S6404BF-10	3.82E-16	1.00E+00	2.33E-03	6.59E-01	2.44E-03	7.13E-01	2.49E-03	7.54E-01
	XX59S6416CF-75	3.82E-16	1.33E+00	3.10E-03	8.77E-01	3.25E-03	9.48E-01	3.32E-03	1.00E+00
	XX59S6408CF-75	3.82E-16	1.33E+00	3.10E-03	8.77E-01	3.25E-03	9.48E-01	3.32E-03	1.00E+00
	XX59S6404CF-75	3.82E-16	1.33E+00	3.10E-03	8.77E-01	3.25E-03	9.48E-01	3.32E-03	1.00E+00
	XX59S6416CF-80	3.82E-16	1.25E+00	2.91E-03	8.24E-01	3.05E-03	8.91E-01	3.12E-03	9.43E-01
	XX59S6408CF-80	3.82E-16	1.25E+00	2.91E-03	8.24E-01	3.05E-03	8.91E-01	3.12E-03	9.43E-01
	XX59S6404CF-80	3.82E-16	1.25E+00	2.91E-03	8.24E-01	3.05E-03	8.91E-01	3.12E-03	9.43E-01
	XX59S6416CF-10	3.82E-16	1.00E+00	2.33E-03	6.59E-01	2.44E-03	7.13E-01	2.49E-03	7.54E-01
	XX59S6408CF-10	3.82E-16	1.00E+00	2.33E-03	6.59E-01	2.44E-03	7.13E-01	2.49E-03	7.54E-01
	XX59S6404CF-10	3.82E-16	1.00E+00	2.33E-03	6.59E-01	2.44E-03	7.13E-01	2.49E-03	7.54E-01
	XX59S6432CFT-54	3.82E-16	1.85E+00	4.32E-03	1.22E+00	4.52E-03	1.32E+00	4.62E-03	1.40E+00
	XX59S6432CFT-60	3.82E-16	1.67E+00	3.89E-03	1.10E+00	4.07E-03	1.19E+00	4.16E-03	1.26E+00
	XX59S6432CFT-70	3.82E-16	1.43E+00	3.33E-03	9.42E-01	3.49E-03	1.02E+00	3.56E-03	1.08E+00
	XX59S6432CFT-80	3.82E-16	1.25E+00	2.91E-03	8.24E-01	3.05E-03	8.91E-01	3.12E-03	9.43E-01
	XX59S6432CFT-10	3.82E-16	1.00E+00	2.33E-03	6.59E-01	2.44E-03	7.13E-01	2.49E-03	7.54E-01

Appendix D - Experimental Setup

Below is the equipment setup for the experiment attempted. With an alpha source and a DRAM in the evacuated vacuum chamber, the experiment would have detected any fluorescence produced by alpha particle interaction with the chip materials. The presence of fluorescence would provide important information about the alpha producing reactions which are known to occur in DRAMs. Due to equipment problems, the experiment was unsuccessful.

The experiment is discussed in chapter VI.

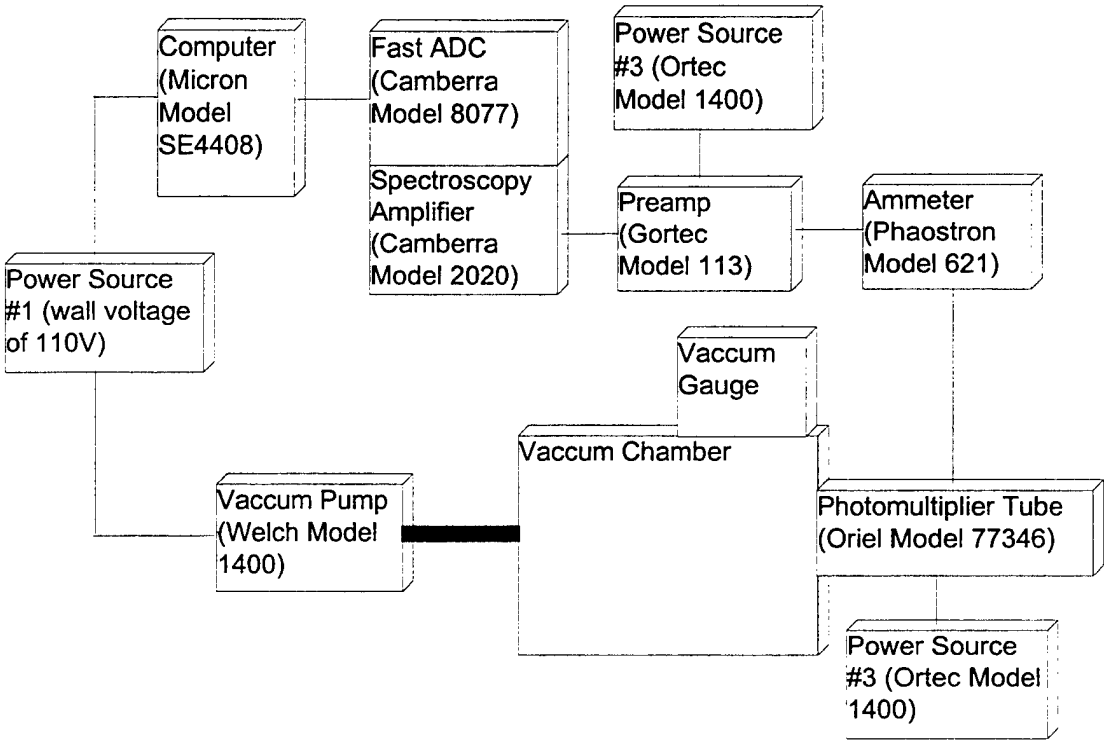

Appendix E - Figures and Tables

The following figures show the relationships between many of the different factors affecting the particle flux and the COTS DRAM SERs. The tables show data which was either obtained from outside sources for use in this project or obtained as a result of the work done in this project.

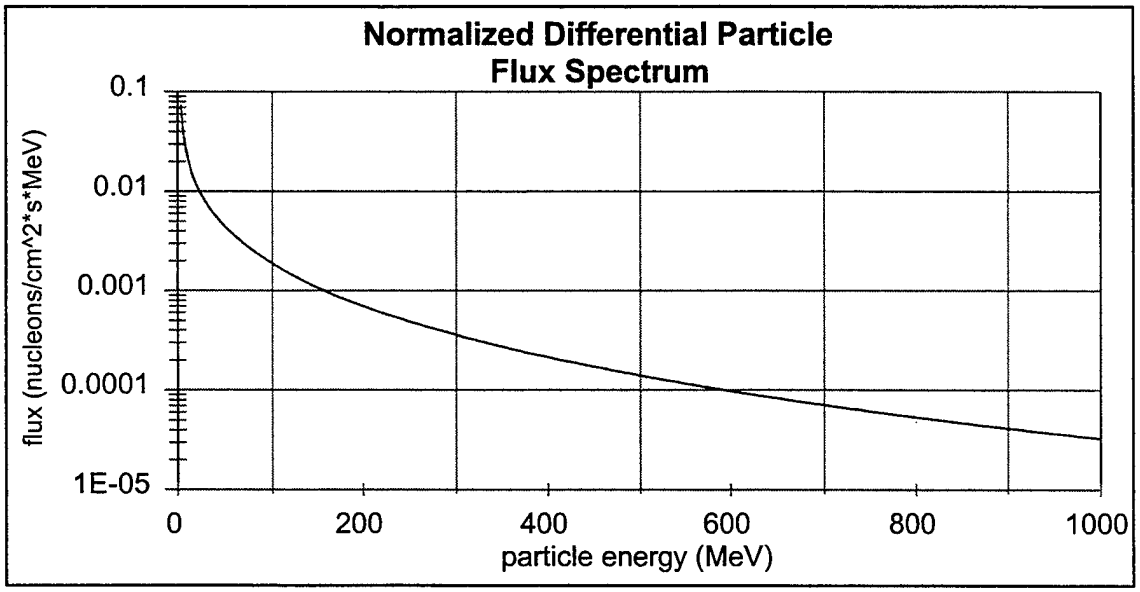

Figure E.1 - Normalized differential particle flux spectrum (eq. 2.1) for neutrons, protons, and pions in the earth's atmosphere [7]

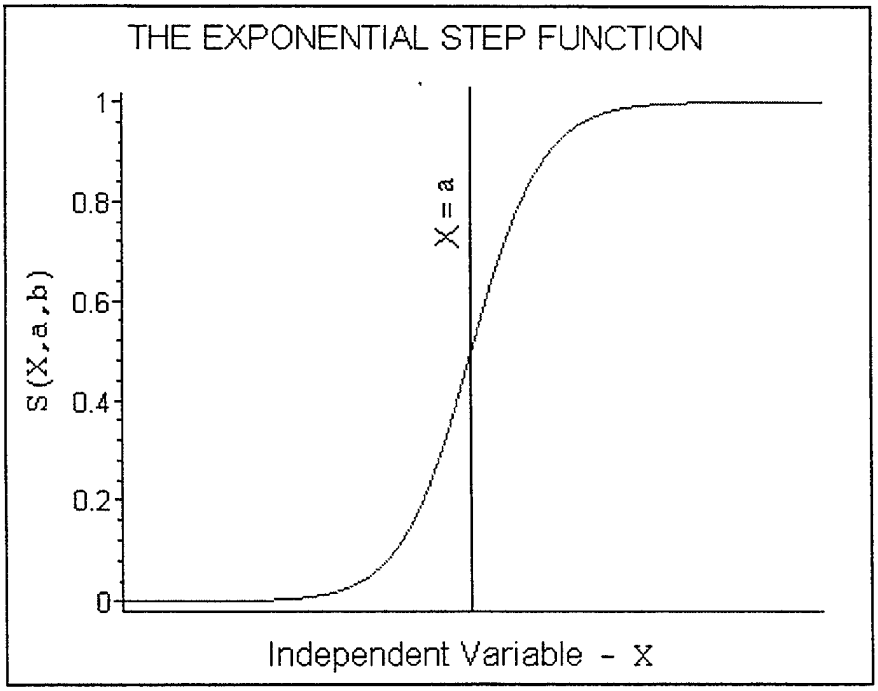

Figure E.2 - The exponential step function (eq. 2.2) used to combine functions valid over specific intervals.

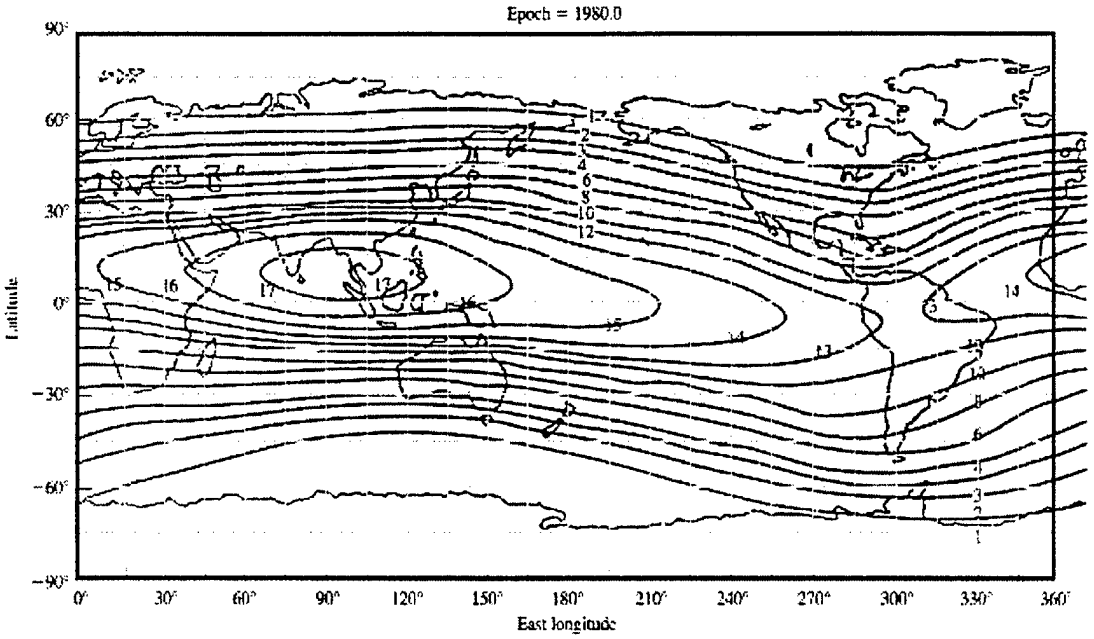

Figure E.3 - Reference map showing the 20km geomagnetic cutoff at various locations in the world [7]

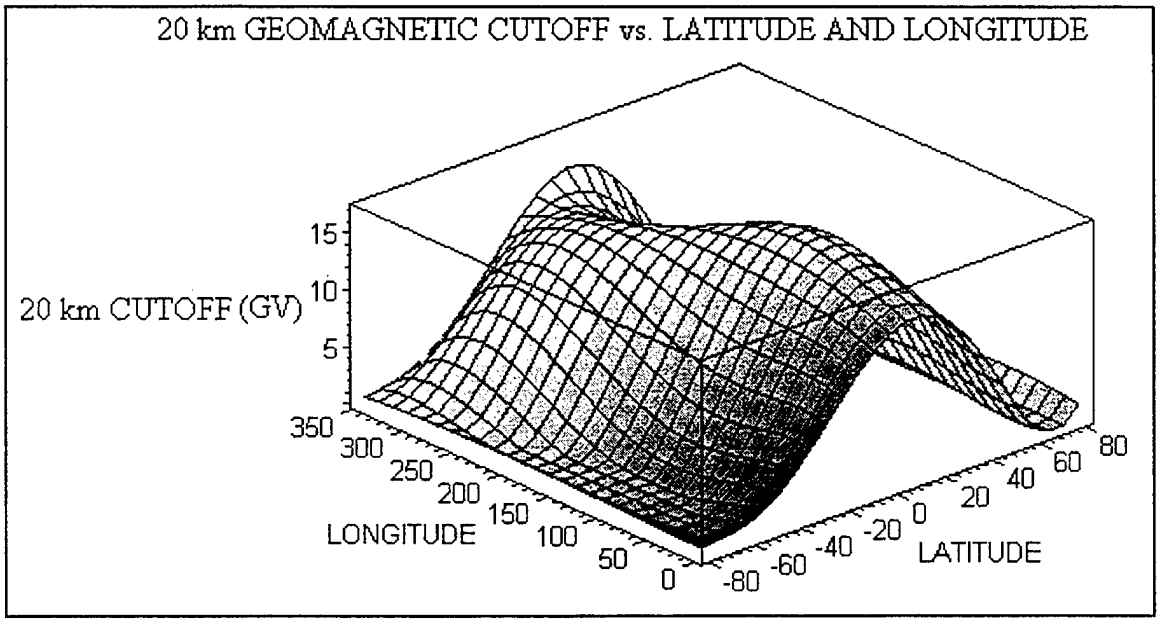

Figure E.4 - RIG, (eq. 2.3) which shows the 20km geomagnetic cutoff at various latitudes and easterly longitudes

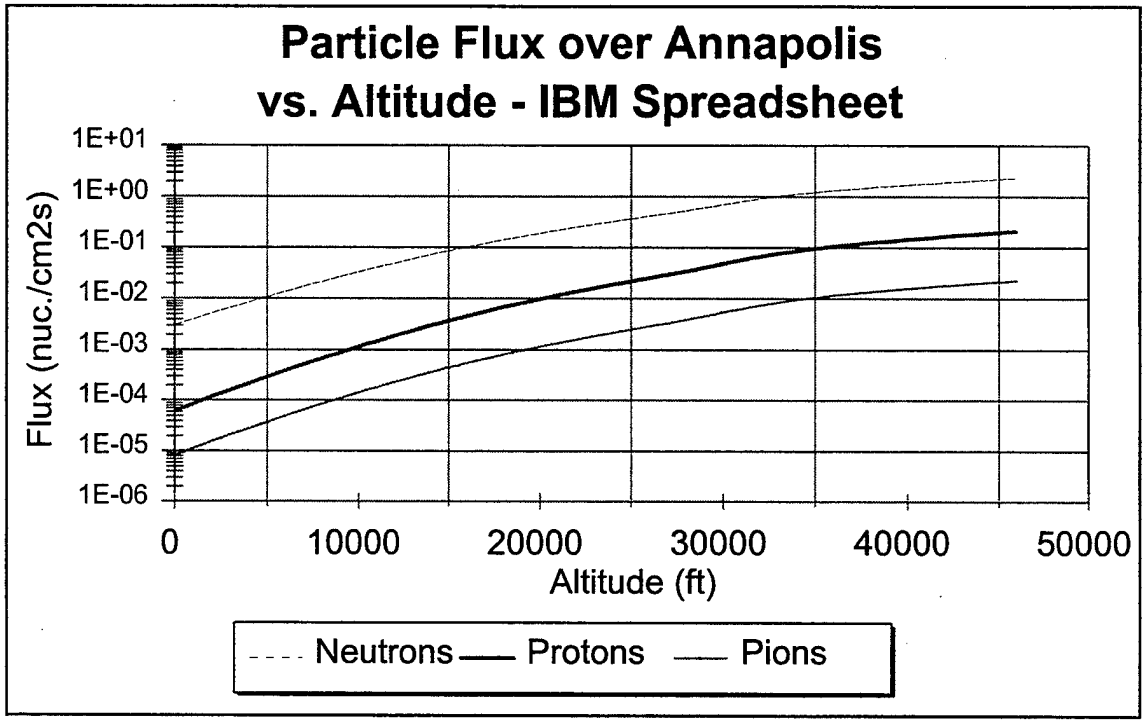

Figure E.5 - Pion, proton, and neutron fluxes over Annapolis based on information obtained in the IBM Model [7]

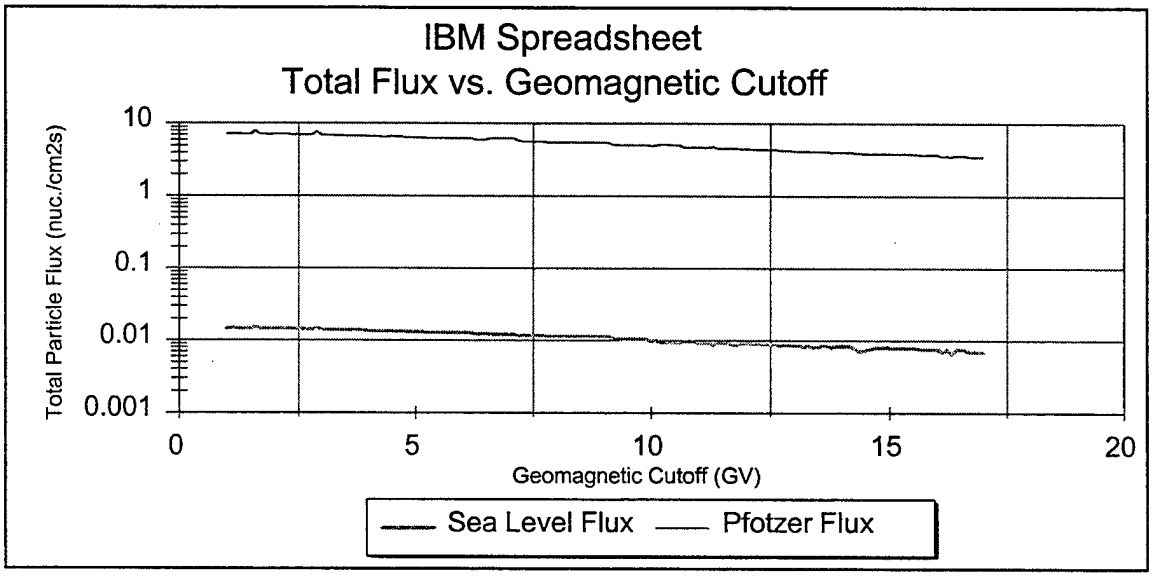

Figure E.6 - Sea level and Pfotzer point total particle fluxes at different geomagnetic cutoffs based on the IBM model [7]

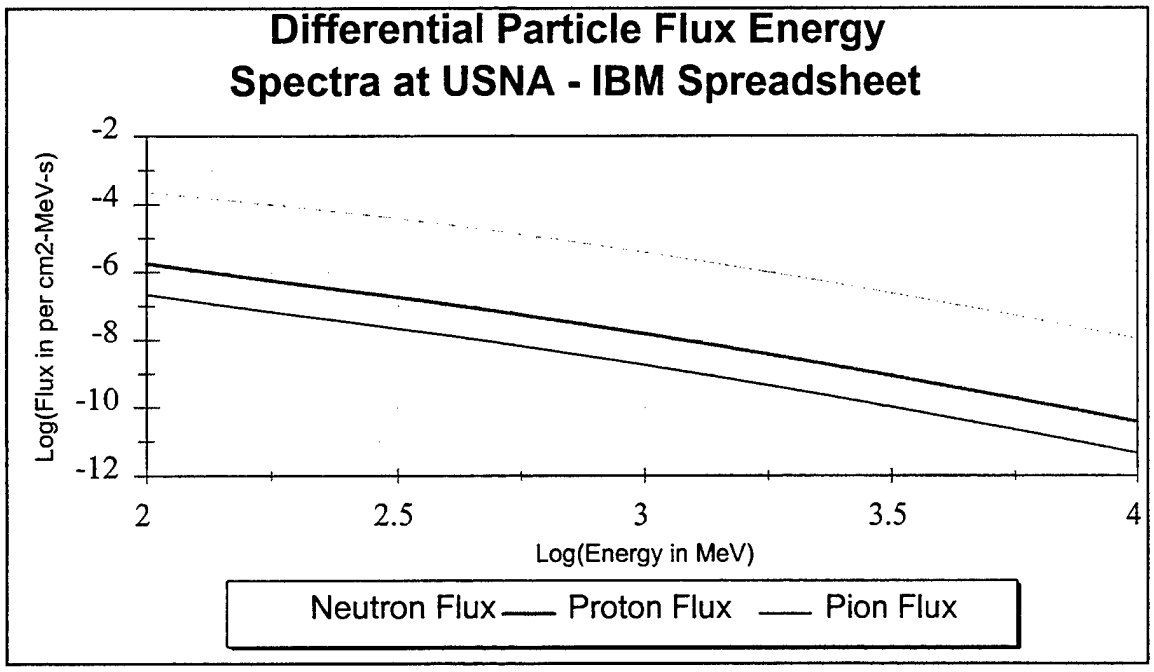

Figure E.7 - The pion, proton, and neutron differential flux energy spectra in Annapolis at sea level based on the IBM model [7], using equation 2.1 for the shape of the differential particle flux energy spectrum

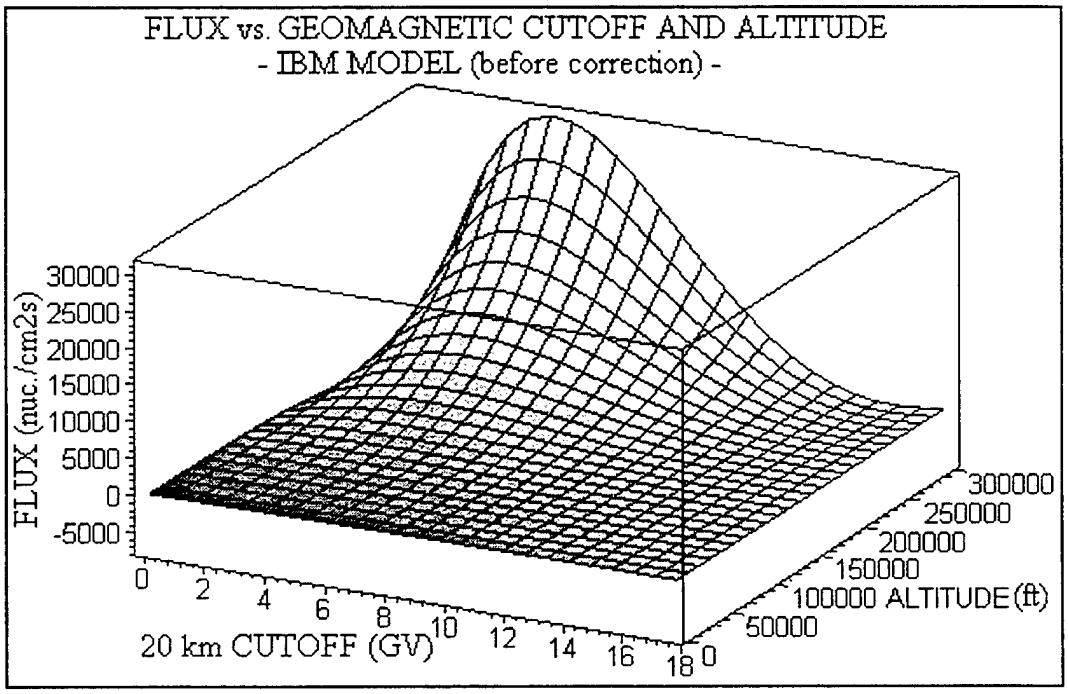

Figure E.8 - Flux as a function of altitude and 20km geomagnetic cutoff (eq. 2.6) using the data points from the IBM model [7]

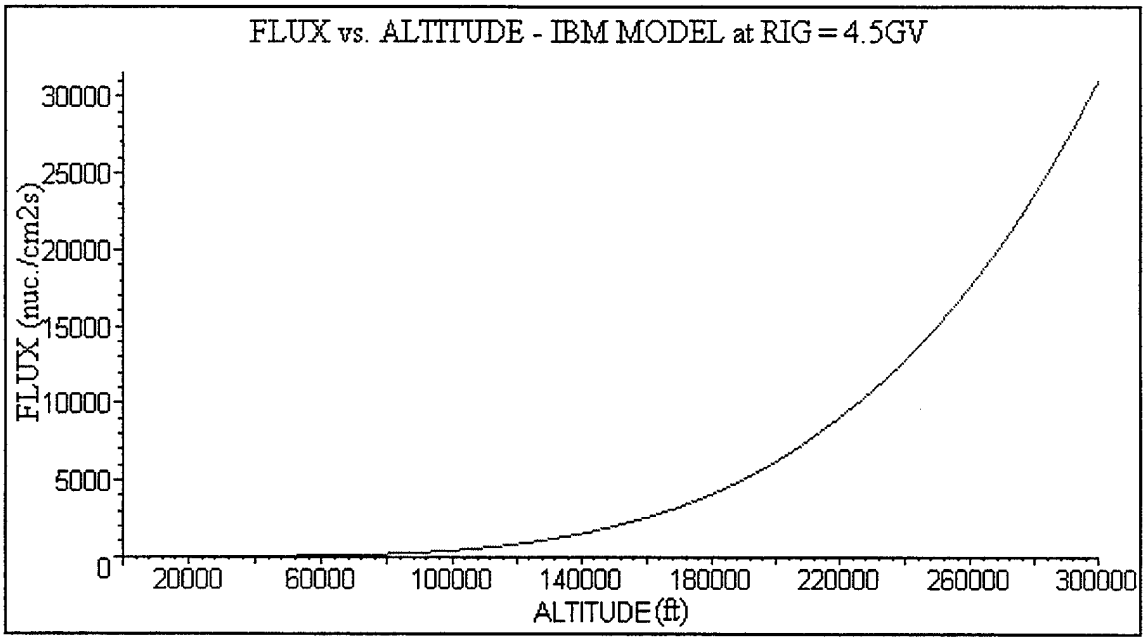

Figure E.9 - The flux as a function of altitude when the 20km geomagnetic cutoff is 4.5GV (eq. 2.7), based on the IBM model

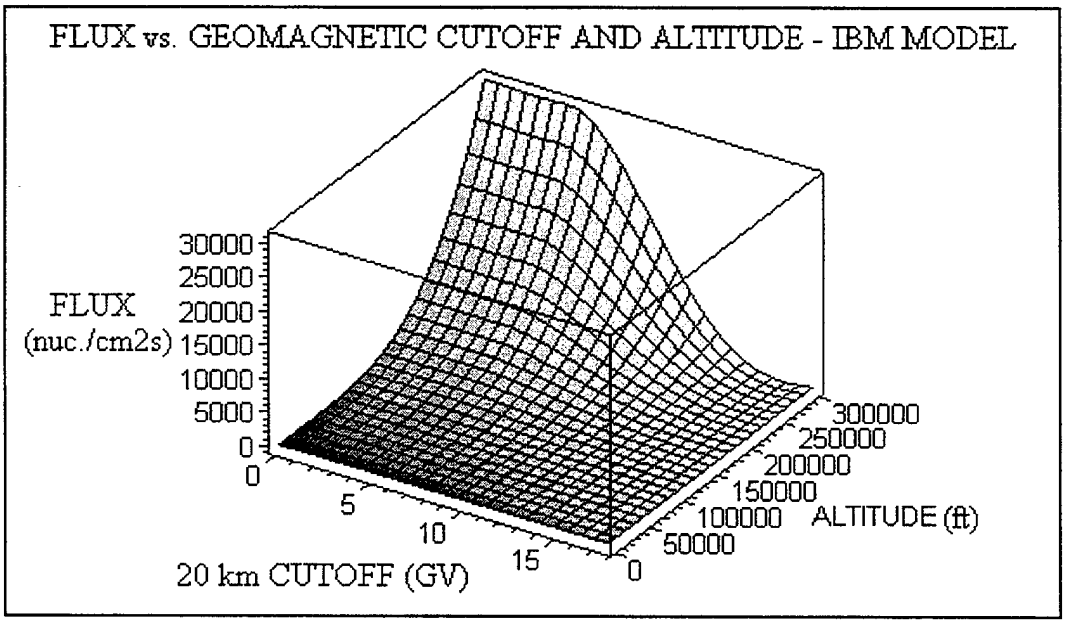

Figure E.10 - The flux as a function of altitude and 20 km geomagnetic cutoff after correction using the exponential step function (eq.2.8)

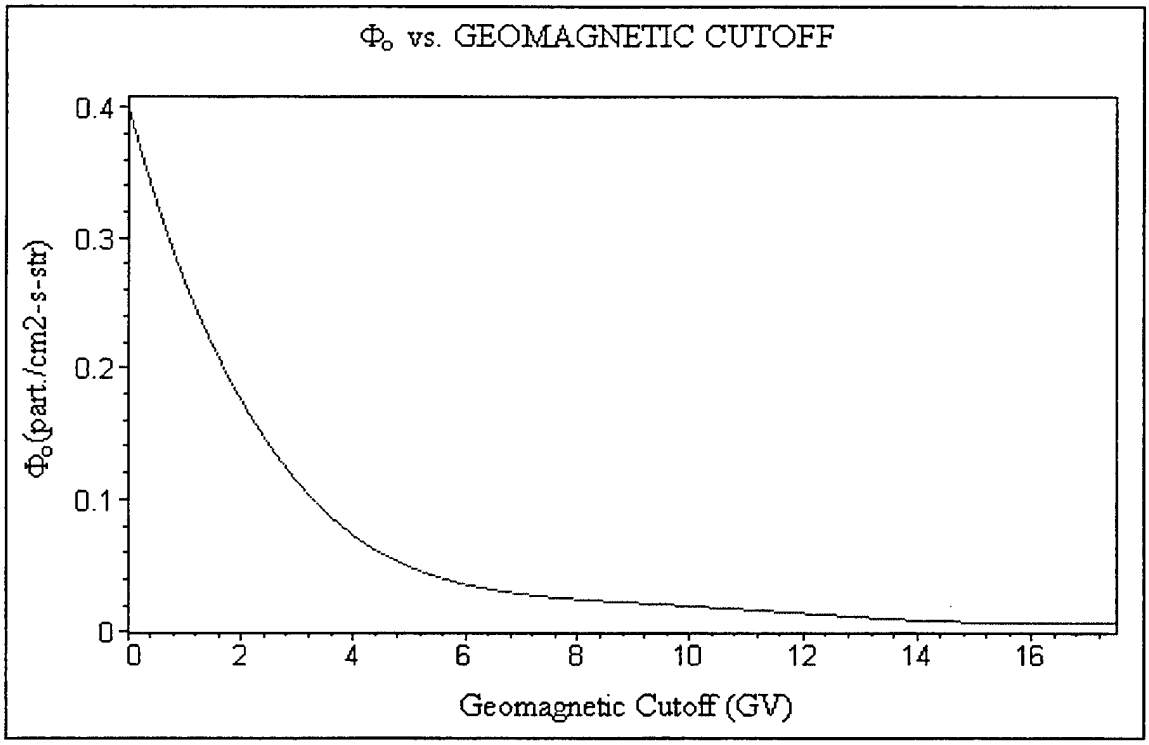

Figure E.11 - The flux of particles capable of making it to a specific location based on the geomagnetic rigidity at that location (eq. 2.9), based on CREME [16]

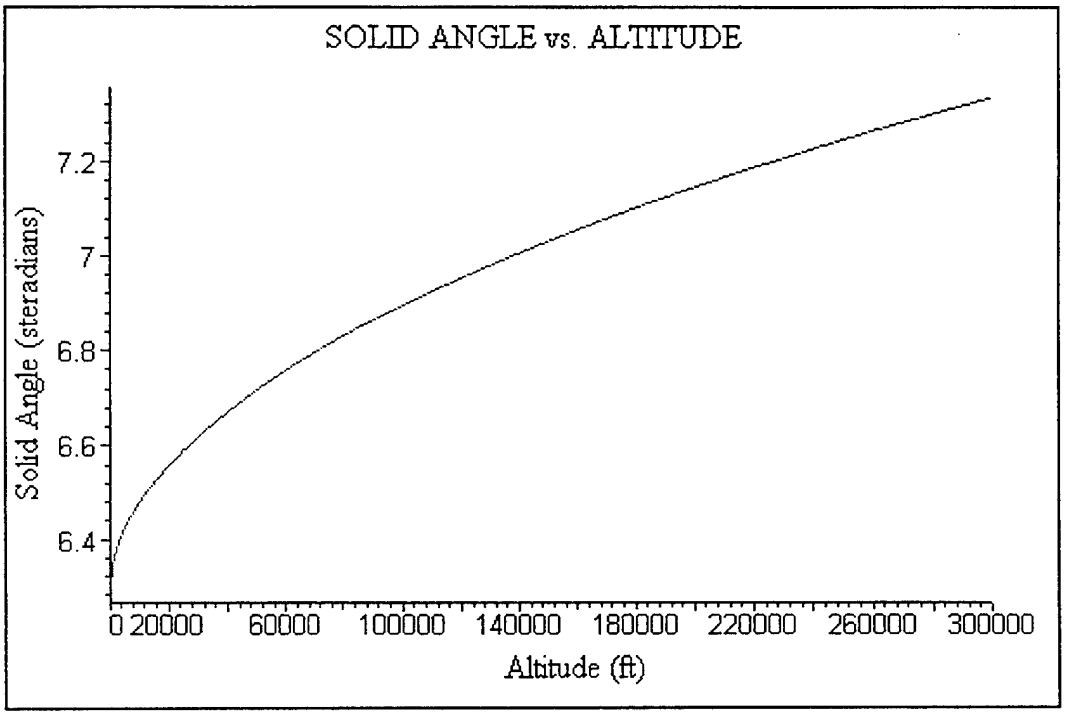

Figure E.12 - The portion of the solid angle not blocked by the earth, based on altitude (eq. 2.10), from [15]

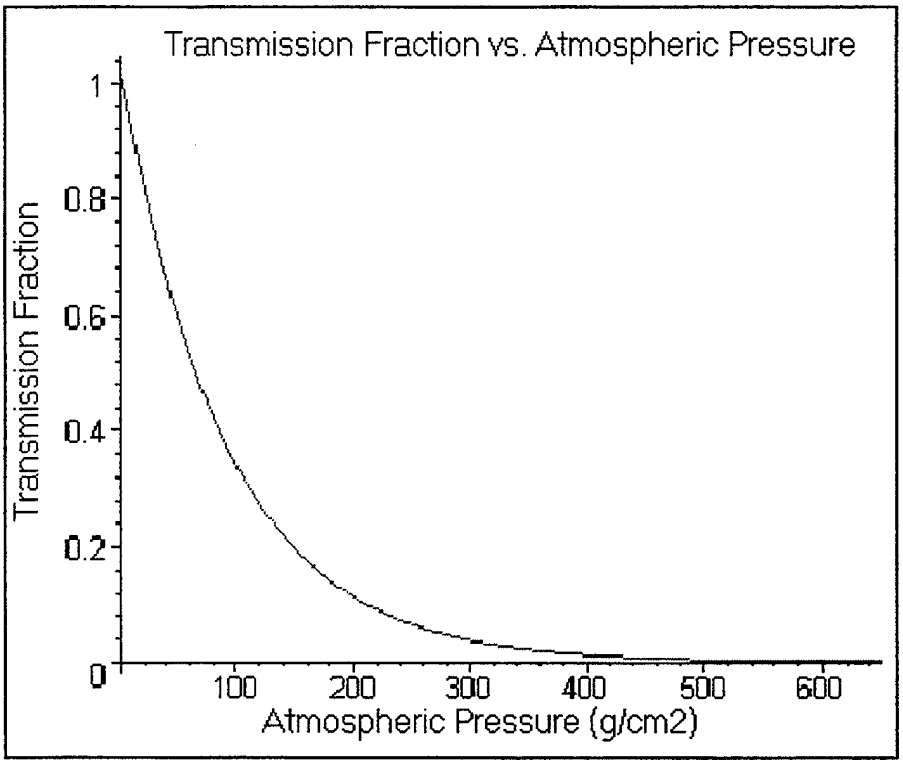

Figure E.13 - The fraction of particles transmitted to a specific location based on the atmospheric pressure at that location (eq. 2.11), obtained from CREME data [16]

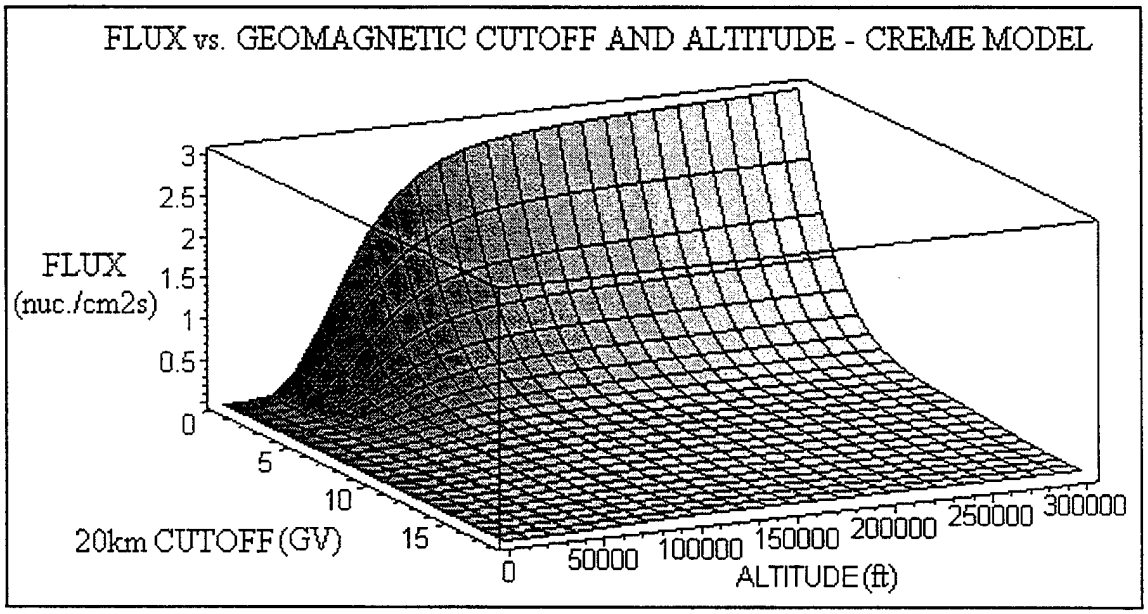

Figure E.14 - The flux as a function of 20km geomagnetic cutoff and altitude (eq. 2.13), based on CREME [11-14,16]

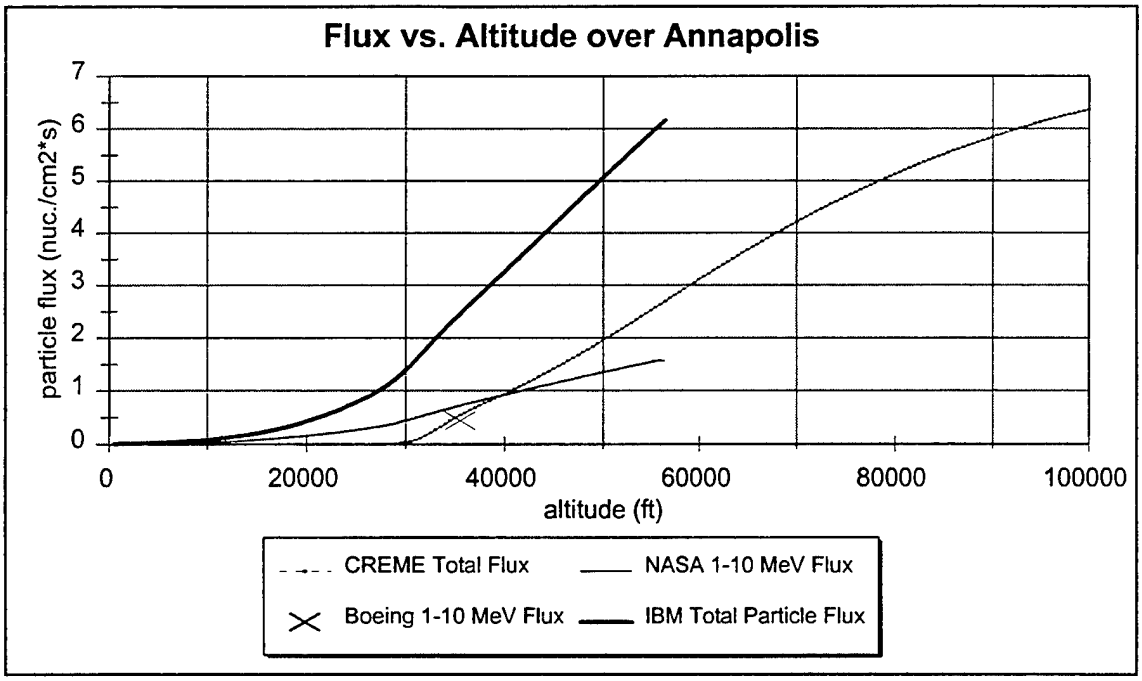

Figure E.15 - A comparison of the flux calculated by the IBM, NRL, Boeing, and NASA models above Annapolis from sea level to 100,000ft.

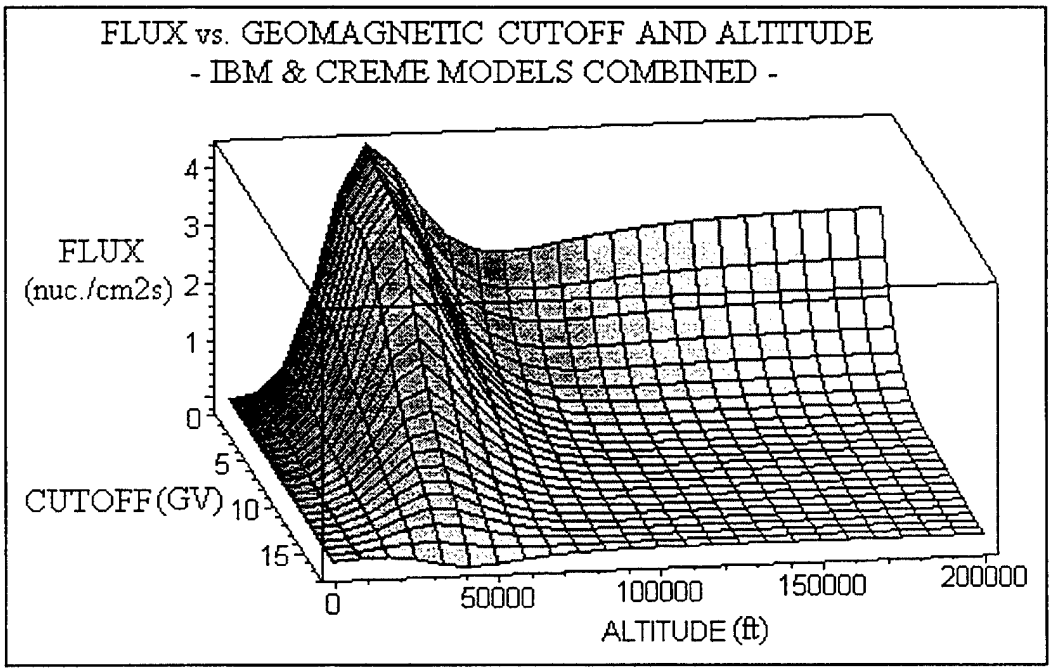

Figure E.16 - The flux as a function of 20km geomagnetic cutoff and altitude (eq.2.14), based on a combination of the functions in Figures E.10 (eq.2.8) and E.14 (eq. 2.13).

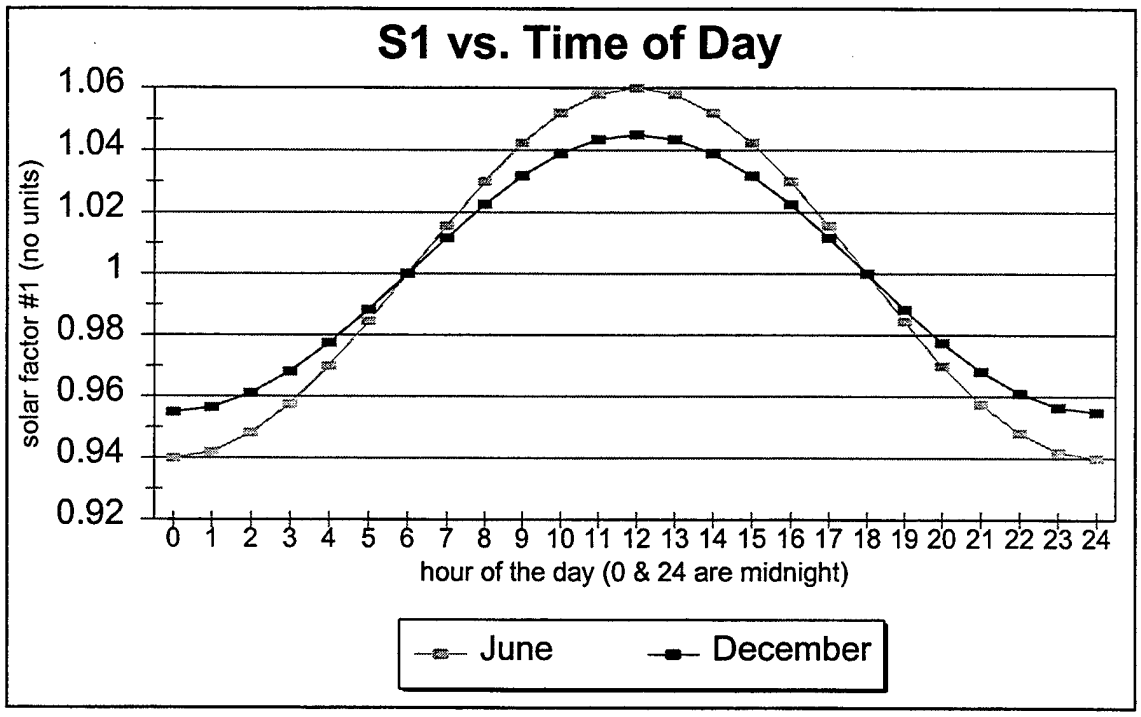

Figure E.17 - The first solar factor, which accounts for the small variations in atmospheric flux over different times of the day, plotted as a function of hour (eq. 2.15)

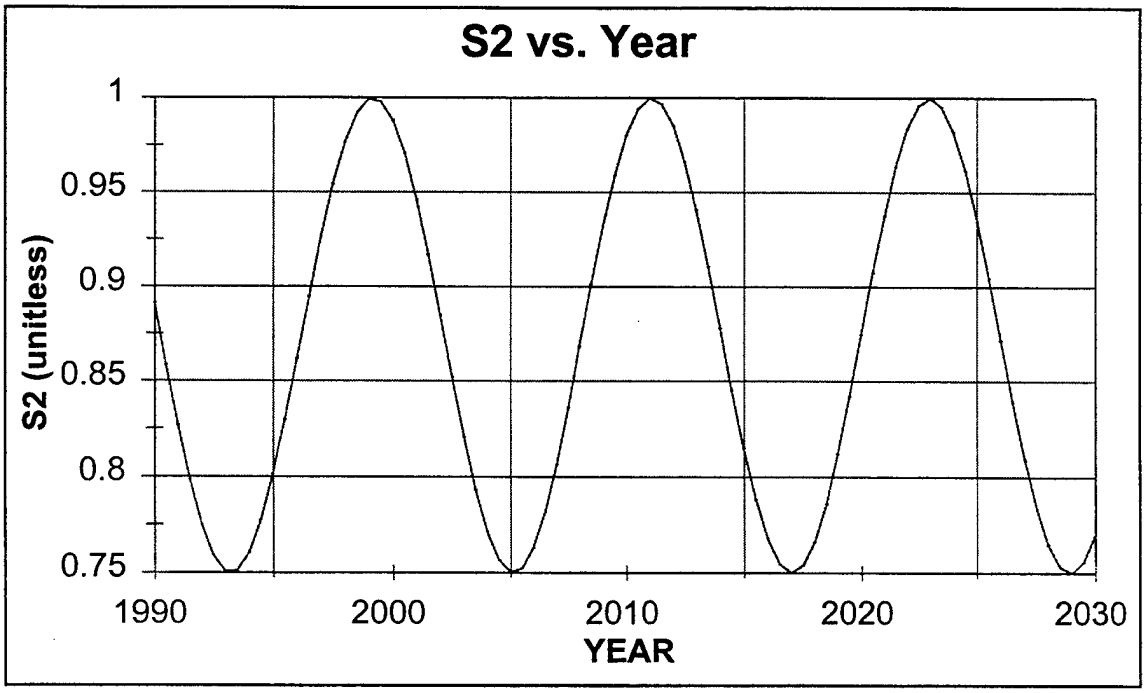

Figure E.18 - The second solar factor (eq. 2.16), which accounts for changes in the atmospheric flux due to the solar cycle, plotted as a function of year

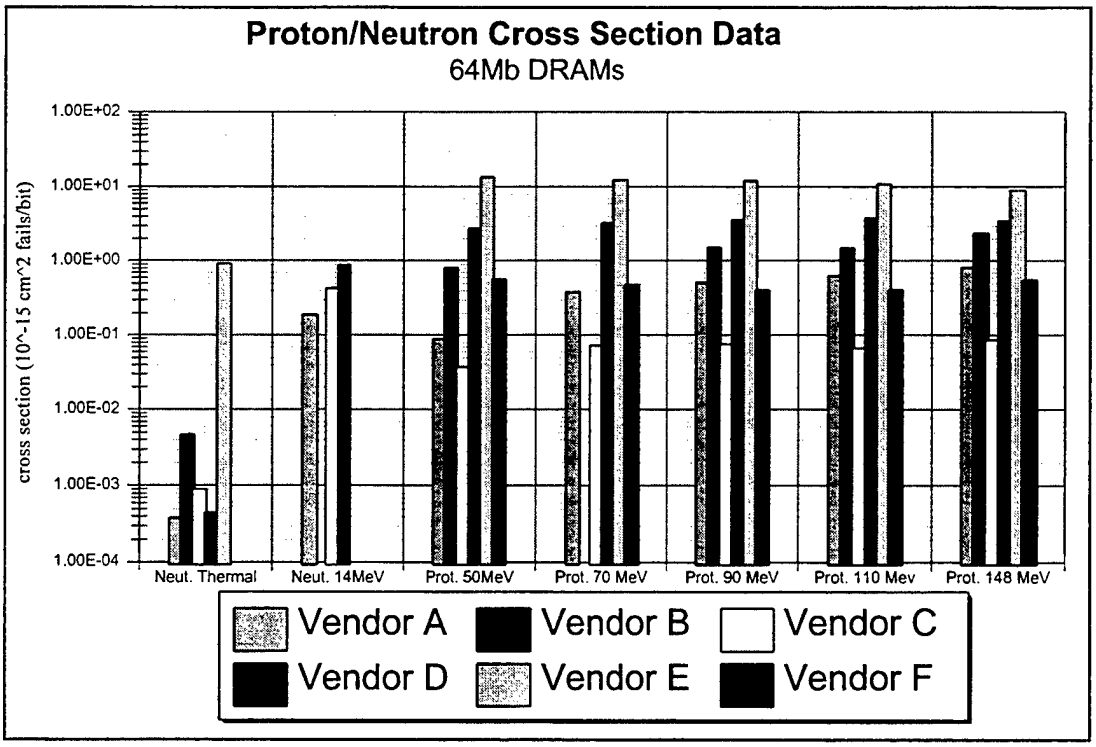

Figure E.19 - The experimental neutron and proton SEU cross-section data for the six different vendors [17]

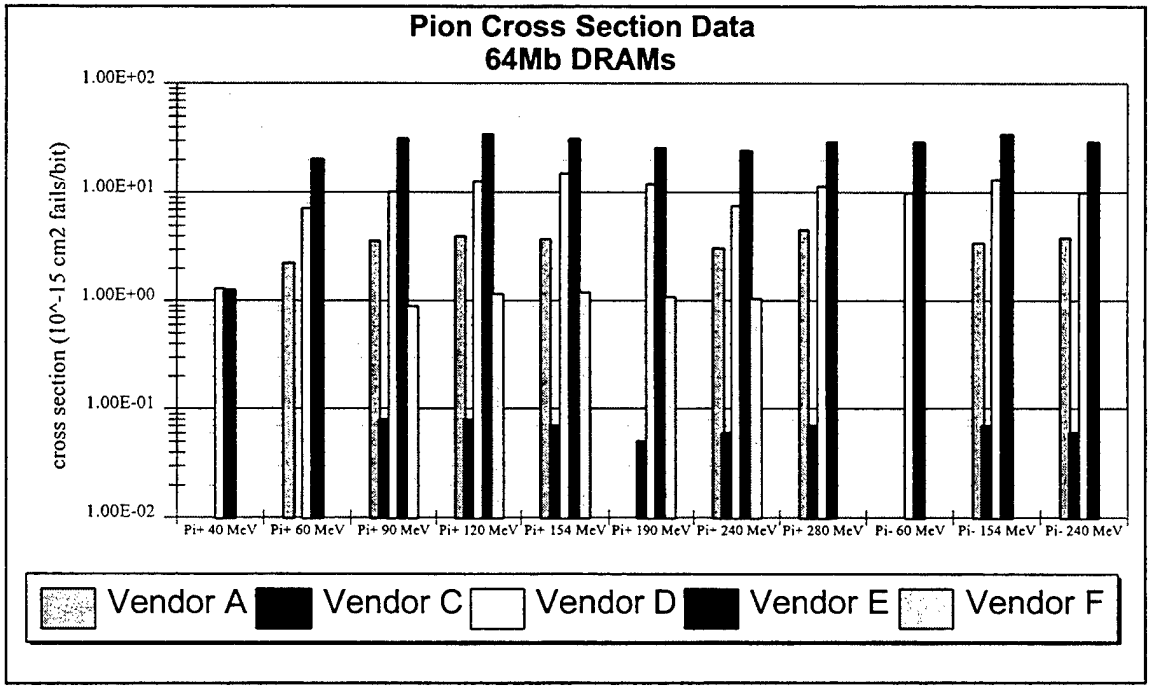

Figure E.20 - The experimental pion SEU cross-section data for the five different vendors

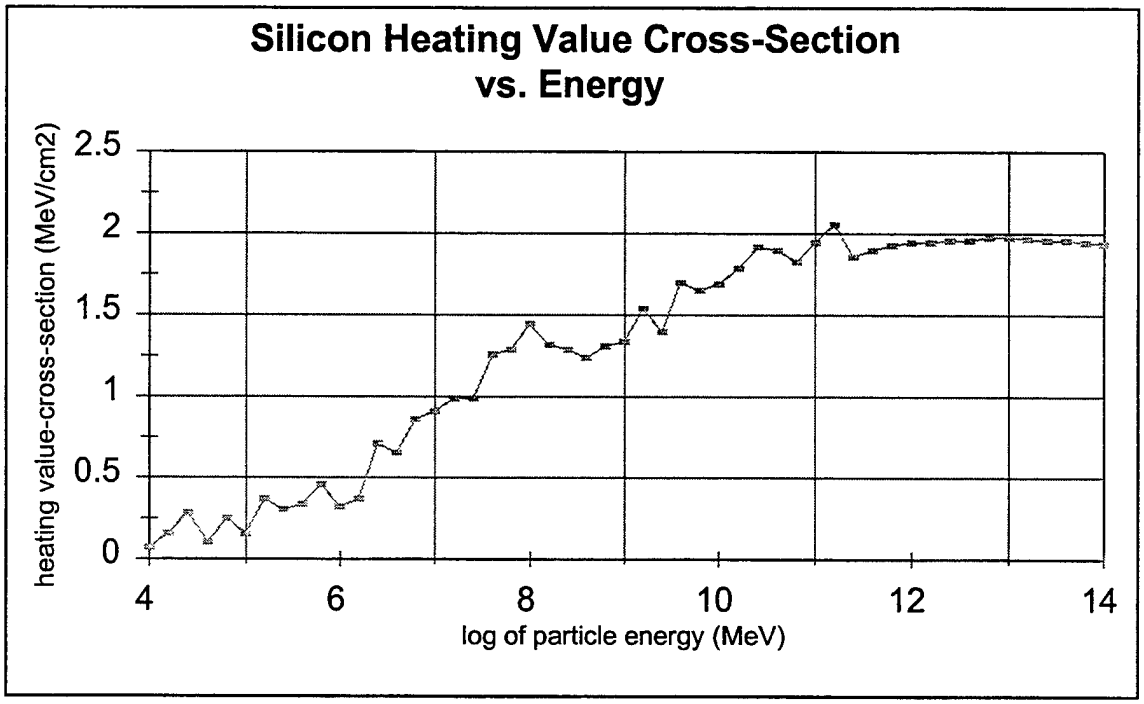

Figure E.21 - Heating value cross-sections at energies between 4MeV and 14MeV [32]

Vendor	α	β
A	0.741	-1.817
B	0.728	-1.308
C	-0.413	-0.391
D	0.639	-0.737
E	-0.0002	1.071
F	0.005	-0.349

Table E.22 - The α and β coefficients for eq. 3.3 for each vendor, describing the logarithmic fit used to find the SEU cross-sections between 14 and 150 MeV

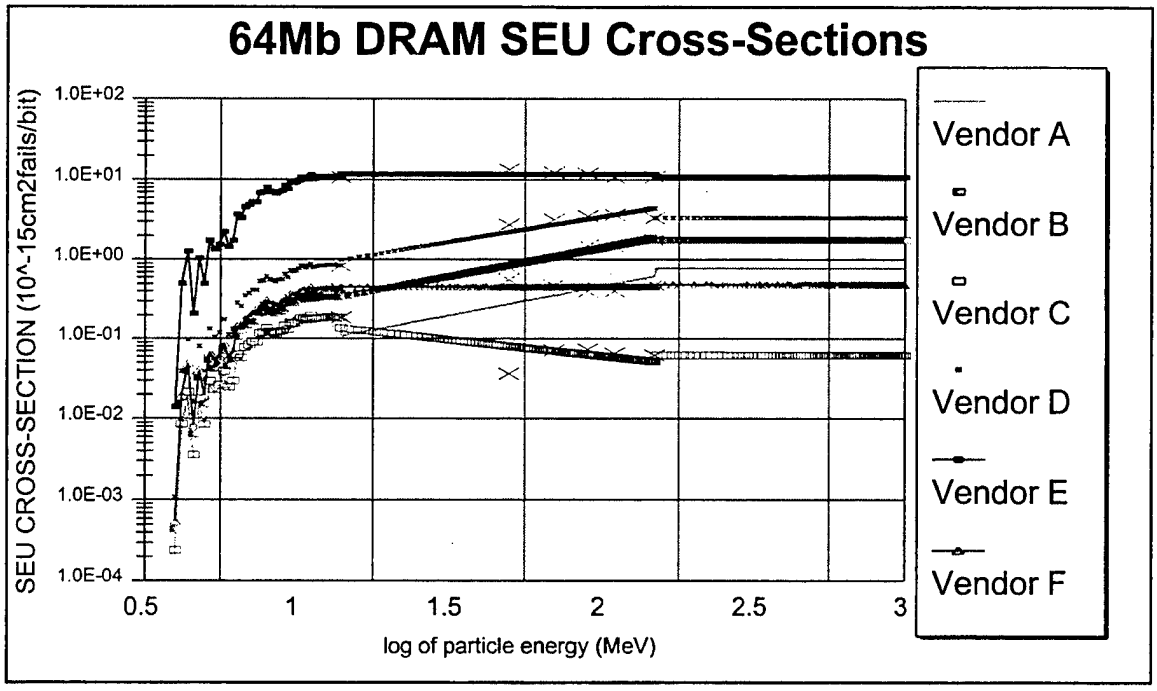

Figure E.23 - The experimental neutron and cross-section data (the X's) and the SEU cross-section spectra for the six vendors obtained through extrapolation and interpolation procedures (eqs. 3.2, 3.3 and 3.4)

Vendor	α'	β'
A	1.803	-0.392
C	-0.400	0.156
D	9.386	-9.995
E	22.936	-23.278
F	-0.125	1.314

Table E.24 - The $\alpha'$and β' coefficients for eq. 3.5 for each vendor, describing the logarithmic fit used to find the SEU cross-sections between 20 and 280 MeV

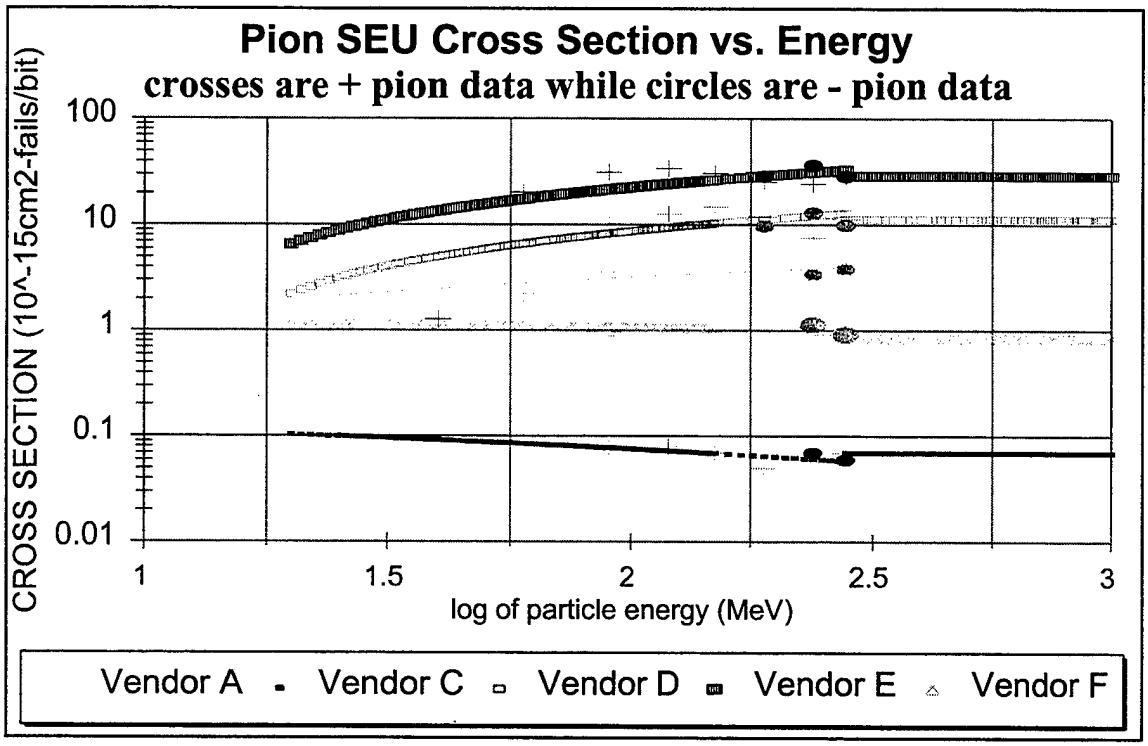

Figure E.25 - The experimental pion data (+'s and •'s) and the SEU cross-section spectra for the five vendors obtained through extrapolation and interpolation procedures (eqs. 3.5 and 3.6)

Vendor	neutrons and protons $\sum_i \{\sigma_{SEU}(E_{i+.5}) \cdot F(E_i, E_{i+1})\}$ (10^{-15} fails-cm^2/bit)	pions $\sum_i \{\sigma^{\pi}_{SEU}(E_{i+.5}) \cdot F(E_i, E_{i+1})\}$ (10^{-15} fails-cm^2/bit)
A	0.303	1.861
B	0.792	N/A
C	0.085	0.049
D	1.835	4.579
E	9.536	11.871
F	0.382	0.629

Table E.26 - The summation term in eq. 5.2 for the tested DRAM of each vendor

Appendix F - CALCULATION OF SERs IN MODERN DRAMS

$$SER(fails/s) = NS_1S_2\Phi_T(RIG(LAT,LONG), ALT)\{\sum_i \sigma_{SEU}(E_{i+\frac{1}{2}}, Vender)F(E_i, E_{i+1})\}\frac{(fA'e^{-V_{dd}})_{untested}}{(fA'e^{-V_{dd}})_{tested}}$$

Where:

I. Φ_T is the particle flux (particles/cm^{2}s) at a specific location, combined from the IBM and CREME models, based on the altitude and 20km geomagnetic cutoff at that location:

$$\Phi_T = \hat{S}(ALT, 35000, 15000)\Phi_{CREME} + \hat{S}(ALT, 35000, -15000)\Phi_{IBM}$$

where

$$\Phi_{IBM} = .0142\left\{\begin{array}{l}(.5+.5\tanh(RIG-4.5))[(.376e-7ALT^2)+(.145e-1RIG)+(.286e-3ALT)\\-(.192e-4RIG^4)-(.107e-1RIG^2)+(.796e-3RIG^3)+(.498e-11ALT^3)\\-(.806e-16ALT^4)+(1.02)+(.879e-5RIG\,ALT)-(.286e-19RIG^4ALT^4)\\-(.822e-13RIG^2ALT^3)+(.159e-8RIG^2ALT^2)-(.452e-8ALT^2RIG)\\-(.170e-7RIG^4ALT)-(.288e-16RIG^2ALT^4)+(.158e-17RIG^3ALT^4)\\-(.190e-9ALT^2RIG^3)+(.177e-15ALT^4RIG)-(.699e-12ALT^3RIG)\\+(.186e-13RIG^3ALT^3)-(.729e-15ALT^3RIG^4)-(.612e-5RIG^2ALT)\\+(.581e-6RIG^3ALT)+(.644e-11ALT^2RIG^4)]+(.5-.5\tanh(RIG-4.5))[.938\\+(.247e-3ALT)+(.349e-7ALT^2)+(.157e-11ALT^3)+(.265e-15ALT^4)]\end{array}\right\}$$

$$\Phi_{NRL} = \frac{\pi}{2500}\left[.5+.5\frac{\left((.209e8+ALT)^2-(.438e15)\right)^5}{.209e8+ALT}\right]*$$

$$\left[+4010-.670e18\frac{RIG}{(.209e8+ALT)^2}+.520e32\frac{RIG^2}{(.209e8+ALT)^4}-.191e46\frac{RIG^3}{(.209e8+ALT)^6}+.341e59\frac{RIG^4}{(.209e8+ALT)^8}-.236e72\frac{RIG^5}{(.209e8+ALT)^{10}}\right]*$$

$$e^{\left[\begin{array}{l}(-.00549(1033-.0365ALT+.426e-6ALT^2)(-\tanh(\frac{ALT}{3000}-10)+1)\\-5.67e^{(\frac{-ALT}{22700})}(\tanh(\frac{ALT}{3000}-10)+1)+.0245\end{array}\right]}$$

and $\hat{S}(X, a, b) = [.5 + .5(\tanh((X-a)/b)]$

II. RIG is the 20km geomagnetic cutoff (GV) at a location based on the latitude and easterly longitude:

$$
RIG = \left\{ \begin{array}{l}
(.130LONG) + (.494e-1LONG) - (.393e-6LAT\ LONG^3) + (.153e-9LAT^3LONG^3) \\
+(.608e-11LAT^2LONG^4) - (.160e-7LONG^2LAT^3) - (.150e-8LAT^2LONG^3) \\
-(.960e-14LAT^2LONG^5) + (.106e-8LONG^4LAT) + (.339e-6LAT^3LONG) \\
+(.428e-4LONG^2LAT) - (.698e-3LAT\ LONG) + (.178e-12LONG^3LAT^4) \\
-(.696e-15LAT^4LONG^4) + (.292e-6LAT^2LONG^2) - (.364e-4LAT^2LONG) \\
-(.343e-10LAT^5LONG) - (.410e-19LAT^5LONG^5) + (.110e-17LAT^4LONG^5) \\
-(.369e-10LONG^2LAT^4) + (.462e-8LAT^4LONG) - (.143e-13LONG^3LAT^5) \\
-(.776e-12LONG^5LAT) + (13.5) + (.448e-12LAT^3LONG^4) - (.537e-2LAT^2) \\
+(.381e-15LAT^3LONG^5) + (.444e-16LONG^4LAT^5) + (.143e-11LONG^2LAT^5) \\
-(.603e-4LAT^3) + (.534e-6LAT^4) + (.637e-8LAT^5) - (.333e-3LONG^2) \\
+(.159e-5LONG^3) - (.728e-8LONG^4) + (.125e-10LONG^5)
\end{array} \right\}
$$

III. N is the number of bits in the DRAM while S_1 and S_2 are unitless solar factors which account for changes in the flux caused by changes in the solar wind:

$$S_1 = 1 - Acosine[(2\pi/24\pi)(h+m/60)]$$

$$S_2 = 0.875 + 0.125sine\{[2\pi/10.9][y+((M-1)/12)-1960.5]\}$$

where

$A = [.00525 + .00075cosine[(2\pi/12)(M-6)]$
m is the minute of the hour
h is the hour of the day
M is the month of the year
y is the year

IV. f, V_{dd}, and A′ are the frequency (MHz), operating Voltage (V), and area (mm^2) of the experimentally tested DRAM for a specific vendor (*tested*) and of the DRAM being analyzed (*untested*).

V. $\sigma_{SEU}(E_{i+1/2}, Vendor)$ is the SEU cross-section ($10^{-15} cm^2$/particle) of a DRAM based on the Vendor and Energy (MeV) of the incident neutrons and protons. $F(E_i, E_{i+i})$ is the fraction of the total particle flux made up by particles with energies between E_i and E_{i+1}.